THERMAL ANALYSIS OF VASCULAR REACTIVITY

A Thesis

by

CHINMAY DESHPANDE

Submitted to the Office of Graduate Studies of
Texas A&M University
in partial fulfillment of the requirements for the degree of

MASTER OF SCIENCE

May 2007

Major Subject: Mechanical Engineering

THERMAL ANALYSIS OF VASCULAR REACTIVITY

A Thesis

by

CHINMAY DESHPANDE

Submitted to the Office of Graduate Studies of
Texas A&M University
in partial fulfillment of the requirements for the degree of

MASTER OF SCIENCE

Approved by:

Chair of Committee,	Obdulia Ley
Committee Members,	Debjyoti Banerjee
	Hamn-Ching Chen
Head of Department,	Dennis O'Neal

May 2007

Major Subject: Mechanical Engineering

ABSTRACT

Thermal Analysis of Vascular Reactivity. (May 2007)
Chinmay Deshpande, B.E., University of Pune, India
Chair of Advisory Committee: Dr. Obdulia Ley

Cardiovascular disease (CVD) is the leading cause of death in the United States. Analysis of vascular reactivity (VR) in response to brachial artery occlusion is used to estimate arterial health and to determine the likelihood of future cardiovascular complications. Development of a sensitive technique to assess VR is fundamental to the field of preventive cardiology. The conventional technique to study VR is by monitoring arterial diameter changes during hyperemia following occlusion using ultrasound based methods.

Such measurements require highly qualified technicians and expensive equipment; and are complicated by signal noise introduced by motion and posture among others. It is well known that tissue temperature changes are a direct response to variations in blood flow, and it has been observed in small clinical studies that variations in fingertip temperature during brachial artery occlusion and subsequent hyperemia is a simple surrogate for the measurement of vascular reactivity and endothelial dysfunction. Given the promising nature of thermal monitoring to study VR, this thesis focuses on the analysis of the underlying physics affecting fingertip temperature during vascular occlusion and subsequent hyperemia. I will quantify the contribution of hemodynamic, anatomical and environmental factors over digit temperature changes, which will serve to determine the sensitivity of the digital thermal monitoring (DTM) technique.

I have quantified the effect of several contributing factors to fingertip temperature and DTM results. The aims of this thesis focus on: (1) creation of a mathematical

model of heat transfer at baseline, during, and after a reactive hyperemia test; and (2) validation of the model and experimental analysis of thermal and flow parameters in healthy volunteers.

The proposed project is an innovative study that intends to show and quantify the relationship between VR and digital thermal reactivity , translating mathematical models based on the physics of heat transfer and fluid mechanics to clinical application. The parametric studies performed with the zeroth order model served to separate the contribution of environment and blood flow over the temperature curves measured during brachial artery occlusion. The thermal models developed were able to reproduce the trend of the temperature response observed experimentally at the fingertip.

ACKNOWLEDGMENTS

I would like to take this opportunity to express my honest gratitude to my advisor, Dr. Obdulia Ley for encouraging me through out the graduate studies for guiding me to perform better. Discussions with her always inspired me. I appreciate the different opportunities that she gave me to explore my true potential.

I would like to thank Dr. M. Naghavi and the Endothelix team for extending their cooperation, resources and valuable comments during the research work. This project was inspired by Endothelix Inc, the company that pioneered fingertip temperature monitoring for vascular reactivity. I greatly appreciate and would like to thank Balaji Prapancham and Cristina de la Paz for their time and effort in conducting the experiments.

Last, but not least, I would like to thank all my friends and family for being there whenever I needed them the most, and without whom I may have lacked the encouragement required to do this work.

TABLE OF CONTENTS

CHAPTER Page

LIST OF TABLES

TABLE Page

LIST OF FIGURES

FIGURE Page

FIGURE Page

FIGURE Page

FIGURE Page

FIGURE Page

CHAPTER I

INTRODUCTION

A. Endothelial Dysfunction, Vascular Reactivity and CVD

Cardiovascular disease (CVD) is known to be the leading cause of death in the US and other developed countries. The prediction of cardiovascular events remains a difficult and expensive problem given the large asymptomatic population. Cardiovascular disease encompasses complications produced by coronary artery disease, myocardial infarction and atherosclerosis. These are complications that start developing when the integrity of the arterial walls is compromised as seen in Fig. 1 [1, 2, 3, 4]. Arteries are lined by endothelial cells (Fig. 1(A)), which are known to respond to blood shear stress by changing their geometry. Such changes produce clear alterations in the transport of cells and macromolecules through the arterial wall, favoring the formation of atherosclerotic plaques; and affecting the elastic properties of the arteries and their response to stimuli that controls arterial diameter changes. The healthy endothelium is a metabolically active tissue that regulates vascular tone via release of the vasodilators like nitric oxide among others. The complex molecular biology underlying endothelial release of constricting and dilating substances has been reviewed by Luscher and Noll [5] and by Vogel *et al.* [6]. Significant evidence shows that most of the traditional risk factors for CVD, such as smoking, high blood pressure, hypercholesterolemia obesity and diabetes, are associated with impaired endothelial function or EDF (endothelial dysfunction) [7, 8, 9, 1, 2, 10]. Given the unpredictable nature of cardiovascular disease, a non-destructive, cost-effective large-scale screening technique for EDF is needed.

The journal model is *IEEE Transactions of Automatic Control.*

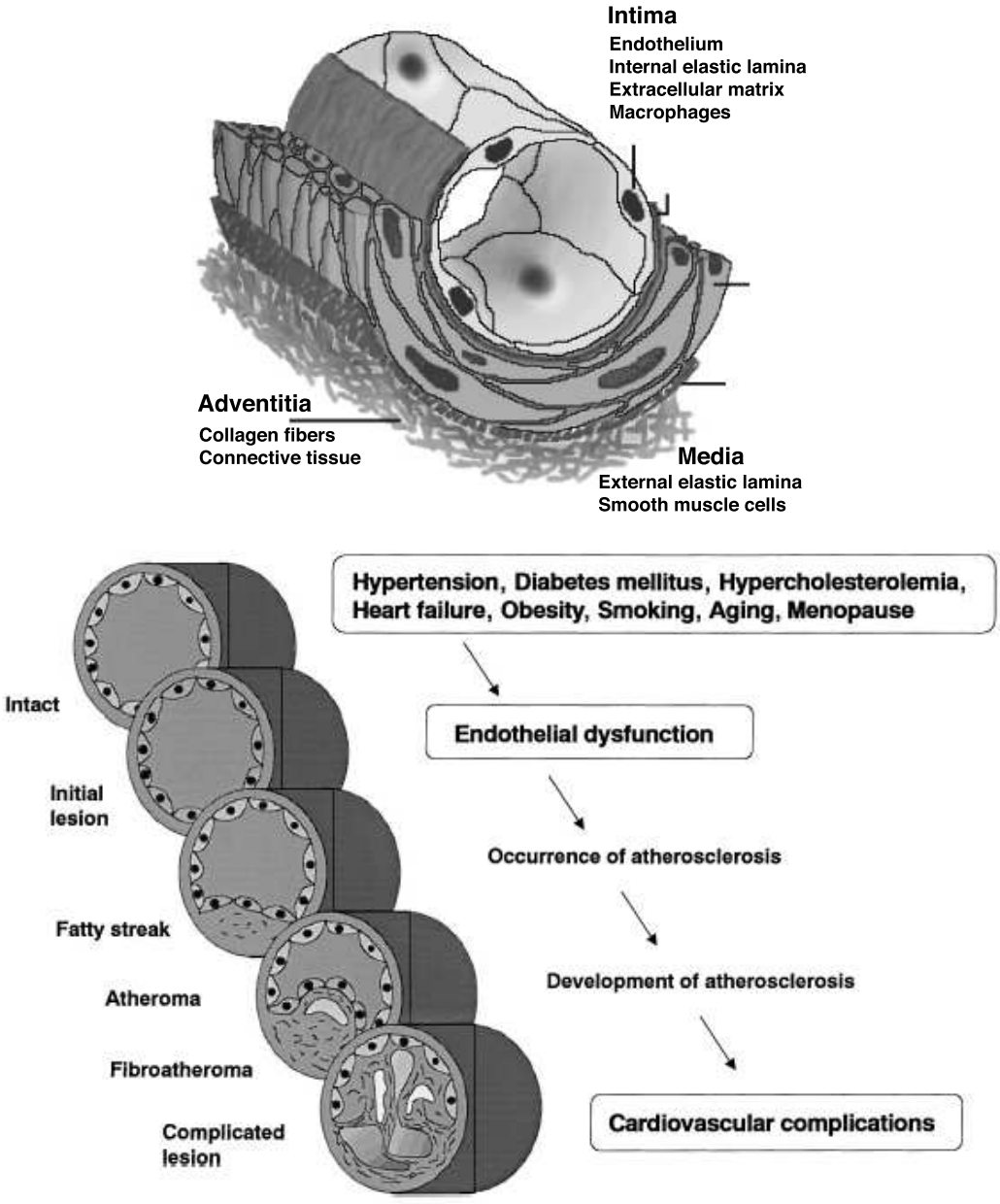

Fig. 1. **(A)** Cross section of an artery showing the arterial wall composition and the location of the endothelial cell layer. **(B)** Progression of atherosclerosis in cardiovascular disease and its relationship to endothelial dysfunction (ED) from [11].

A common method for studying endothelial function or vascular reactivity (VR) (*i.e.* how blood vessels react to stimuli affecting vascular tone or vessel diameter) involves measuring arterial diameter responses to pharmacological agents that affect vascular tone. The use of pharmacological agents (acetylcholine, angiotensin II, norepinephrine, adrenergic antagonists) requires arterial cannulation which is associated with some discomfort and risk, and limits one's ability to study large numbers of patients or assess serial changes in vascular reactivity.

Recently, a noninvasive technique, called *Flow mediated dilation* or FMD has been used to study EDf or VR. This technique is based upon producing an increase in shear stress in the selected artery. Increased shear stress stimulates the release of nitric oxide, a vasodilator substance [12]. The method through which blood flow and shear stress is increased in the selected artery is by arterial occlusion (4 to 5 minutes). FMD is performed in the main arteries of arms and legs, such as brachial artery and superficial femoral artery, respectively. A review of the considerable technical challenges involved in measuring FMD is given in Ref. [13, 11]. FMD is diminished in patients with atherosclerosis and with coronary risk factors, and improves with risk-reduction therapy. Therefore, the measurement of FMD can be a good prognostic instrument in preventive cardiology [13, 1].

The resulting increase in blood flow observed after ischemic periods is referred as reactive hyperemia. In healthy arteries, reactive hyperemia is correlated to increases in the arterial diameter. Fig. 2 shows the change in vessel diameter in a healthy individual, as determined by high-resolution ultrasound imaging. Endothelium-dependent FMD of the brachial artery is quantified as the maximum percent change in arterial diameter (8.4% in this example). Brachial arterial flow-mediated dilation (FMD), assessed by high-resolution ultrasonography, reflects endothelium-dependent vasodilator function.

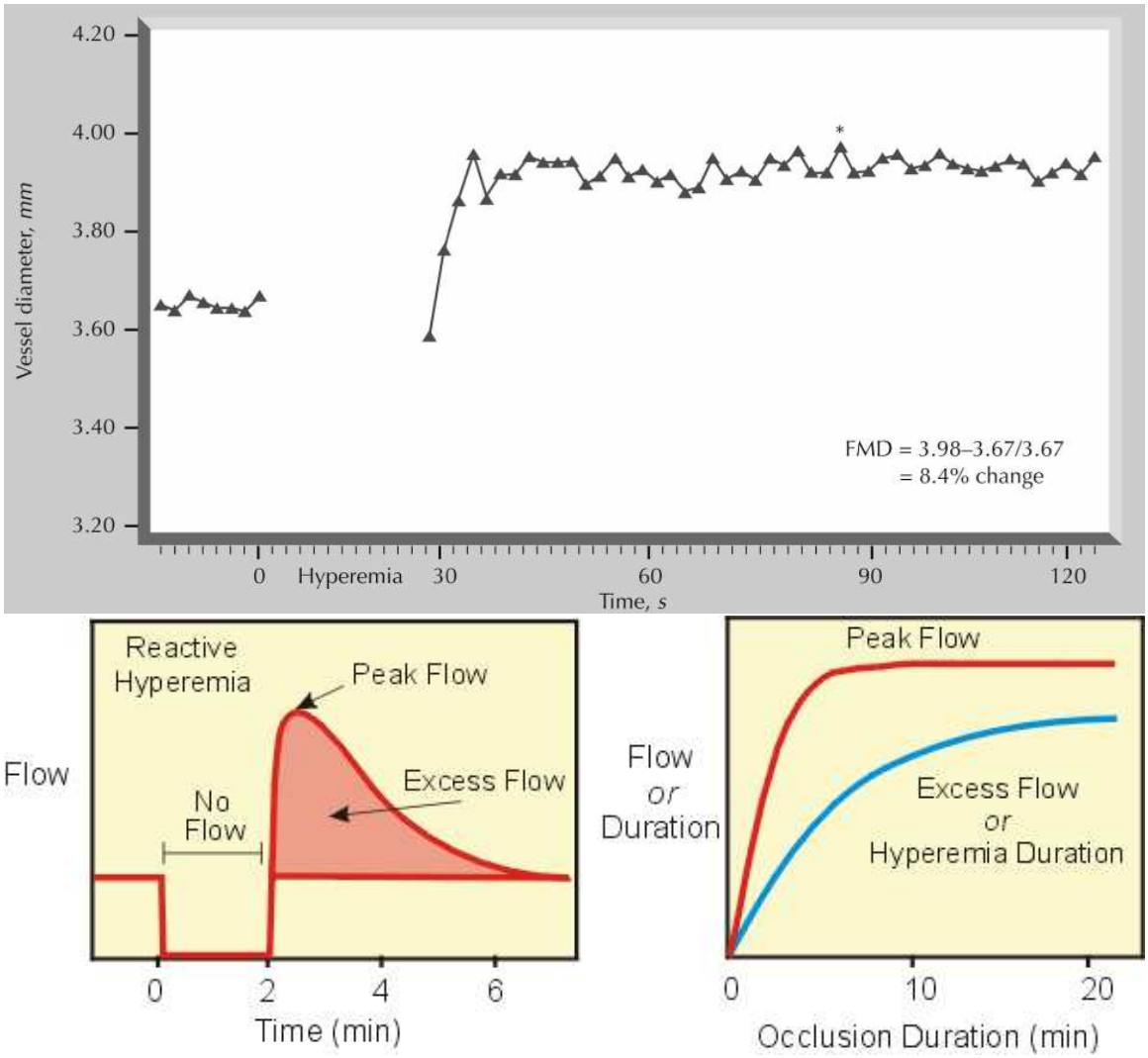

Fig. 2. **(Top)** The flow-mediated dilation (FMD) response in a single patient from the Vascular Health Interventions Laboratory. The y-axis depicts change in brachial artery diameter following deflation of the ischemic cuff. Asterisk indicates that FMD is measured as the percent change in arterial diameter at peak response. Taken from [14]. **(Bottom)** Schematics showing reactive hyperemia following a brief period of ischemia produced by 2 minutes of arterial occlusion; the hyperemic blood flow lasts for several minutes and occurs in response to tissue ischemia. The magnitude of hyperemic response depends on occlusion time and occlusion pressure.

Given the strong correlation between endothelial dysfunction and CVD, significant effort has been devoted to study vascular reactivity (VR), as it relates to endothelial function, and serves to predict risks as well as to track changes in response to therapy. Several techniques are available to monitor VR, such as high-resolution ultrasound [15, 16, 17, 18] and plethysmography [11]; however, there is no accepted method in routine clinical practice. Technical limitations of the ultrasound method (sensitivity to probe positioning, artifact, low repeatability, need for skilled technicians, observer dependence and bias), and high cost, limit its use to research centers and research applications. In contrast, digit temperature monitoring (DTM) during brachial artery occlusion and hyperemia presents a sensitive, low-cost and reliable technique to assess VR that can be used on large-scale populations and for continuous personal monitoring [7].

B. Digital Thermal Monitoring and Vascular Reactivity

Fingertip temperature is affected during brachial artery occlusion and subsequent hyperemia, such temperature change is the direct result of variations in tissue blood flow and other parameters, such as environmental conditions and anthropometric factors as shown in Fig. 3. The time required for the fingers to return to normal temperature, as well as the temperature change experienced, depends largely on the hyperemic response (*i.e.* endothelial function) [8, 9]. Thermal monitoring of vascular reactivity (VR) during and after vessel occlusion is a novel and simple method for EDF monitoring that has been investigated in small patient studies [7], but further research is necessary to assess the potential of this technique and to analyze the various factors impacting accurate diagnosis via thermal measurement.

Preliminary studies have shown the ability of the DTM test to discriminate indi-

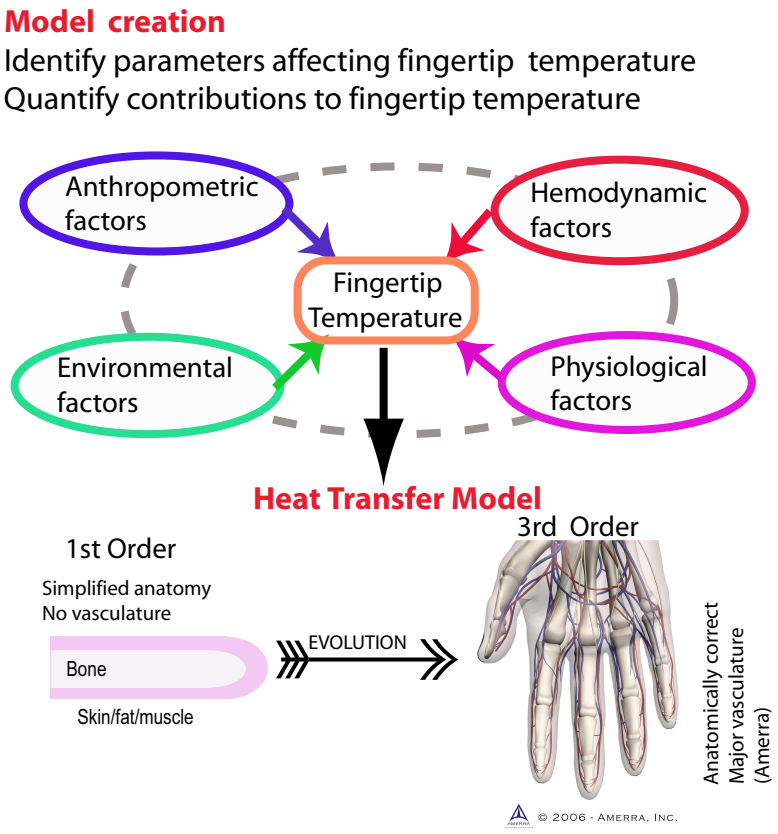

Fig. 3. List of factors affecting fingertip temperature and indication of the modeling efforts.

viduals with established CVD or high risk of future CVD (as measured by Framingham Risk Score) from normal and low-risk individuals [7, 19] (Fig. 4(D)). A graphical description of the DTM technique, and an illustration of the temperature changes is given Fig. 4(A). During DTM test, a rapid temperature increase in the fingertips following arterial occlusion is observed (Fig. 4(B)); the magnitude of such temperature change TR or temperature rebound is reduced due to endothelial dysfunction (Fig. 4(C)). The temperature change is directly correlated to the magnitude of the hyperemic response and vascular reactivity of the conduit arteries in the limbs.

It is well known that tissue temperature is a direct result of blood perfusion, but

other parameters also contribute. These parameters can be classified as:

- Anthropometric factors, such as tissue composition, skin thickness, fat content, surface area, tissue volume, and body mass index.
- Environmental factors, such as ambient temperature, the presence of natural and forced air currents, unequal radiation, and air humidity.
- Hemodynamic factors, such as blood pressure, blood viscosity, and hematocrit.
- Vascular factors, related to the presence of artery vein pairs and different vascular beds that act as countercurrent heat exchangers, and have different thermal contributions due to vessel size
- Physiological factors, such as body temperature, skin temperature, response of conduit vessel diameter to hypoxia and ischemia, microvasculature response, and the activation of arteriovenous anastomoses.
- Metabolic factors, related to tissue oxygen consumption and its relationship with to blood perfusion.

The main goal of this research is to analyze theoretically and experimentally the underlying physics of digit temperature transients and the influence of hemodynamic, anatomical and environmental factors. Analysis and quantification of such relationships are necessary to establish digit temperature change during arterial occlusion and hyperemia as a significant marker in assessing the risk of coronary heart disease (CHD), and to determine the optimal set of experimental parameters for performing digit temperature tests. This research is motivated by preliminary clinical studies demonstrating the feasibility of thermal monitoring as a diagnostic tool for endothelial dysfunction.

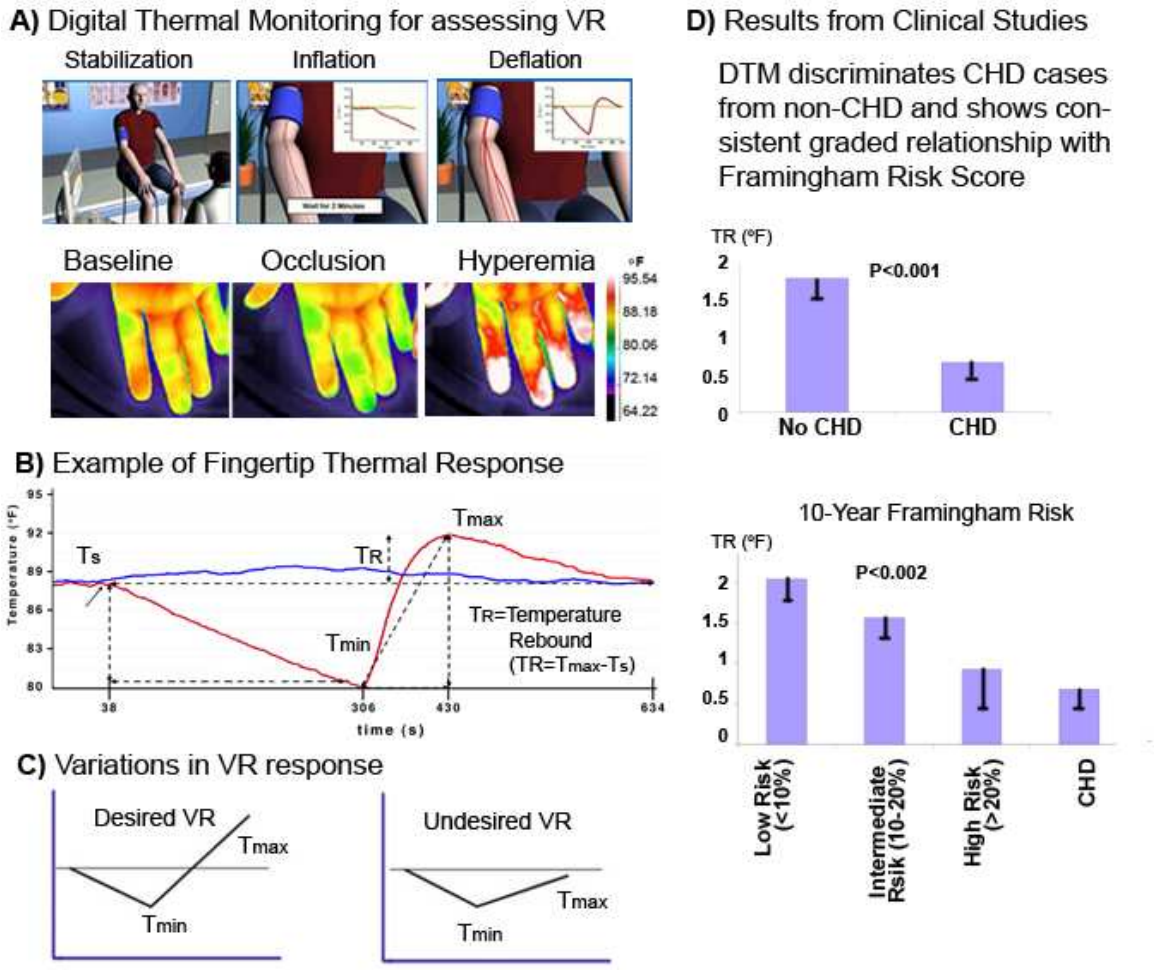

Fig. 4. **(A)** Digital thermal response during and after brachial artery occlusion, the infrared thermographs indicate temperature changes during the procedure. **(B)** Parameters measured with a DTM device (VENDYS^{TM}). Blue line shows temperature of the control finger. **(C)** An schematic example of desired and undesired VR observed on healthy and CVD volunteers. **(D)** Findings from clinical studies comparing TR in coronary heart disease (CHD) vs non-CHD [7, 19, 20].

The proposed analysis will help quantify the patient variability introduced by anthropometric, environmental, and hemodynamic factors. This study will examine the underlying physical factors that affect temperature, and will help improve sensitivity of thermal measurements for future advanced studies of vascular reactivity and endothelial dysfunction involving biochemical and physiological factors.

1. Significance of Mathematical and Numerical Analysis

To relate temperature changes in arm, hand and finger with blood flow, thermal analysis using a mathematical model is proposed. Mathematical models for tissue temperature determination and analysis are desirable to further understand the underlying physics. As realistic geometries can be introduced in the system using tomographic data, temperatures can be calculated in highly resolved data sets, and parametric and sensitivity studies can be performed rapidly. Mathematical analysis can be used to perform sensitivity and optimization studies that help improve experiment design.

C. Thesis Overview and Importance of the Study

This work is based on the premise that fingertip temperature variation during blood flow occlusion can be used as an indirect measurement of vascular health. Temperature of the fingers drops during blood flow occlusion, increases during reperfusion due to the hyperemic response, and finally it returns to normal value a short time after circulation is reestablished. The time required to return to normal temperature and the temperature change experienced depend on the capacity of the occluded arteries to dilate and restore normal circulation among other things. Analysis of the relationship between blood flow and temperature, will allow to quantify vascular reactivity and will serve to establish the importance of digital thermal monitoring DTM as an

economic screening technique for vascular health.

The analysis presented herein shows the relationship between endothelial dysfunction or vascular reactivity and changes in fingertip temperature during vascular occlusion. The study is based on a mathematical model of heat transfer, that incorporates the contribution of the factors described in Fig. 3. This thesis is the first study that intends to show such relationship. Validation of the heat transfer model is also provided using string gauge plethysmography studies, were the blood volume to the limbs and finger is calculated during normal and hyperemic conditions.

Two different mathematical models to determine fingertip temperature are created and presented in this study: a zeroth order model or lumped parameter model, and a first order model considering simplified anatomy. The proposed lumped model will allow to analyze the dynamic response of fingertip temperature to blood flow changes and environmental effects. Given its simplicity it will allow us to determine basic relationships between blood flow and heat loss to the environment. On the other hand, analysis of heat transfer in a the finger considering a simplified anatomy, will help create parametric studies where temperature variations in the skin at different regions can be analyzed. This first order model will also offer a simplified system to analyze the effect of anthropometric factors, such as skin thickness, surface area and physiological factors such as thermoregulatory response of the skin, which cannot be addressed with the lumped system. This study will provide the basis for future models considering realistic anatomy, will help establish and prove the connection between VR and DTM, which will increase the interest of the clinical community in DTM versus brachial artery ultrasound (BAUS) and other techniques that cannot be performed with easy in the physician's office.

This thesis is divided in 9 chapters; chapter II presents a description of heat transfer in tissues, as well as a summary of the heat transfer studies performed in

limbs. Chapter III presents the fundamentals of circulation, and indicates the relationship between vascular reactivity, temperature control, and flow control in the microvasculature. Chapter IV presents the anatomy of the finger to be modeled, the modeling of blood perfusion during reactive hyperemia. Chapters V and VI present the proposed models (zeroth order and first oder), boundary and initial conditions, as well as the calculated results. Chapter VII presents the Inverse Heat Conduction Problem (IHCP). Chapter VIII describes model validation using string gauge plethysmography as well as, the direct determination of skin heat flux and fingertip temperature using the VENDYS apparatus. The studies performed for the model validation were subjected to the Texas A&M University review board. Finally, chapter IX indicates the conclusions and shows future work related to model improvements and further validation studies.

CHAPTER II

HEAT TRANSFER IN TISSUES

Tissue temperature is directly impacted by blood flow, metabolic heat production, and the heat lost to or gained from the environment. Tissues are anisotropic materials characterized by the presence of a vascular structure and local heat generation due to metabolism. Several mathematical models have been proposed to determine tissue temperature and to quantify the contribution of various physiological and environmental parameters [21, 22, 23, 24, 25, 26, 27, 28, 29, 30]. These models have been used to understand the thermoregulatory mechanisms in living organisms [31, 32, 33]; to develop temperature control during hypothermia and hyperthermia; to estimate the temperature distributions in core organs where direct temperature measurement is highly invasive [34, 35]; to determine changes in organ temperature due to energy deposition of electromagnetic waves [36, 37]; and, more recently, to determine blood perfusion [38, 39].

Among the factors to be considered when developing a basic model to describe the thermal state of a biological system are:

1. Geometry of the organ or tissue in consideration
2. Heat capacity or thermal inertia of the tissues involved
3. Conduction of heat due to temperature gradients in the tissue
4. Heat production due to metabolic processes
5. Role of blood flow in the transfer of heat between tissues and between tissue and environment

6. Thermoregulatory mechanisms and physiological responses of an organism to different thermal stresses

7. Thermo-physical properties of tissues and their variations with the temperature

8. The interaction with the environment

A. Model Classification

These models are based on the energy conservation at the tissue level, and the application of constitutive laws. Thermal energy transport in living tissue is extremely difficult to model due to tissue heterogeneity; convective effect added by the vasculature; species to species variability of tissue thermal properties; as well as the difficulty encountered in the in-vivo measurement of tissue thermal properties. Consideration of organ anatomy and physiology are essential characteristics in the development of thermal models, as these define blood flow and metabolic activity. Finally, the consideration of thermoregulatory mechanisms, such as sweating, shivering, panting, vasoconstriction and vasodilation are also important and require determination of empirical relationships.

Circulatory system adds convective heat transport to the other thermal characteristics governing tissue heat transfer, such as conduction and heat capacitance. Blood circulation is strongly dependent on physiology, organ anatomy and vasculature, and when including the effects of blood flow in the thermal modeling of tissue, two different factors should be considered: blood vessels change its diameter size as they branch out; and second, there are fundamental vascular structures which appear in tissues or organs. Depending on its diameter, blood vessels are classified as arteries, arterioles, capillaries, venules and veins (Table I). Arteries and veins have diameters of the order of millimeters, and after several branching generations reduce

their diameter to hundreds of micrometers to become arterioles and venules, respectively; finally, when arterioles and venules branch out they form what is called the capillary bed, which is a complex network of blood vessels that have a diameter of few micrometers. Table I shows the vessel radius, thermal equilibration length x_{e_j} and the ratio between vessel length l_j and x_{e_j}. The thermal equilibration is complete when the temperature difference between blood and tissue is reduced to $\frac{1}{e}$ of its initial value. The thermal equilibration begins at the terminal arteries and veins, and it is widely accepted that equilibration takes place at the arteriole and venule levels (precapillary beds).

Because blood in vessels of diameters greater than $300\mu m$ flows at high velocities $(13 - 8\ cm/s)$ and requires to travel long distances before reaching thermal equilibration; then blood flow in the large vessels is treated as a Newtonian fluid in a tube buried in a solid interchanging heat with its surroundings. To deal with the thermal effects of the microvasculature, several thermal models refereed as bioheat equations have been proposed, some of these are presented in Table II. The main difference between these models is the required knowledge of geometrical properties of the vessel network. The distinction between macro and micro vasculature is important depending on the tissue of interest. For instance, structures like limbs, or neck contain countercurrent artery vein pairs. Highly perfused tissues, such as liver, kidney or brain, have dense capillary beds as their main structure. Structures like fingers also show high capillary concentration and the presence of shunts (anastomoses) able to control the volume of blood entering the capillary bed and that play an important role in the environmental energy exchange. The presence of these structures and the response to local and global temperature changes has never been introduced in theoretical models. Only empirical relationships have been created to analyze the relationship between skin, air and body temperature, which is the result of such vascular

Table I. Properties of vascular compartments.

Generation	Vessel	r_i (μm)	x_{e_j} (m)	l_j/x_{e_j}
1	Aorta	5000	190	0.002
2	Large artery	1500	4	0.05
3	Arterial branch	500	0.3	0.3
4	Terminal branch	300	0.08	0.1
5	Arteriole	10	$5X10^{-6}$	400
6	Capillary	4	$2X10^{-8}$	6000
7	Venules	15	$2X10^{-6}$	800
8	Terminal vein	750	0.1	0.1
9	Venous branch	1200	0.3	0.3
10	Large vein	3000	5	0.04
11	Vena Cava	6250	190	0.002

For a blood vessel in the j-th branching generation, r_j and $l_j$represent the vessel radius and length, respectively; and x_{e_j} denotes the thermal equilibration length. [25]

Table II. Bioheat transfer models.

Model	Description	Applicability (vessel diameter mm)
Pennes [21]	Single equation, Capillary diffusion depicted by source like term	0.3
Chen and Holmes [25]	Single Equation Modified perfusion term + convective term + perfusion conduction term	0.5-1.0
WJL Model [27]	3-layer model 6 coupled equations, Incomplete countercurrent equilibration	0.3
WJ Model [26]	Single equation, Effective tensor conductivity dependent on vascular geometry	0.15

control, these relationships have been used in whole body thermoregulation models [40] and during the 80's when liquid crystals were used to monitor body temperature.

1. Bioheat Equation

One of the oldest tissue thermal models, but the most widely used due to its simplicity was developed by Pennes in 1948 [21]. To determine the average tissue temperature (T), the tissue is modeled as an isotropic homogeneous conductor with constant thermal conductivity (k_t), which has two heat generation sources, one due to the metabolic heat (q_m) produced by the tissue and assumed constant, and the other due to the heat transfered from blood to tissue (q_b). So the energy equation had the form

$$\rho_t C_t \frac{\partial T}{\partial t} = k_t \nabla^2 T + q_b + q_m, \tag{2.1}$$

where ρ_t and C_t represent the density and heat capacity of the solid tissue.

Using Fick's law, Pennes proposed that the rate of heat transfered from blood to tissue q_b can be represented by a non-directional heat source term of the form:

$$q_b = \rho_b C_b \omega_b (T_a - T_v), \tag{2.2}$$

where T_a and T_b correspond to the arterial and venous temperatures, and ω_b is a constant representing the blood perfusion or the rate at which the quantity of blood in a given mass or volume is replenished, and is a free parameter which can be determined by curve fitting with the experimental temperature measurements.

Pennes's primary premise was that the energy exchange between blood vessels and surrounding tissue occurs across the capillary bed, where the blood velocity is very low; therefore, one approximates that

$$T_v = T,$$

at the capillary level, this assumption physically implies that the arriving blood undergoes a nearly instantaneous thermal equilibration, and that the venous blood is at the average tissue temperature.

The Pennes bioheat equation was commonly used until the 70's and 80's when several authors ([23, 24, 25, 41]) pointed out that the capillary perfusion is not isotropic, the arterial temperature varies during vessel branching; and that Pennes equation does not account for artery-vein counter-current heat exchange, or the directional convective mechanism of heat transfer due to blood flow. Nowadays it is recognized that the main thermal equilibration occurs in the pre- and post- capillary vessels instead of the capillary bed. However, as log as temperature measurements are performed far away of large vessels, Eq. (2.1) gives reasonable results.

B. Previous Studies in Human Limbs

Limbs and fingers are major sites of heat loss due to their large surface area in comparison with their tissue volume. Early analysis indicate that the most influential factor to limb temperature is blood flow [42]. Arms and fingers provide a tissue structure, where temperature can be easily measured; environmental boundary conditions can be extracted from the theory of natural and forced convection outside finite length cylinders; finally, limbs offer a tissue where blood flow can be easily interrupted for several minutes without significant danger of necrosis. Interest in limb heat transfer was based in comfort studies [43], to further understand thermoregulation in humans [40], and to gain insight into the role of blood flow on tissue temperature [21] or during cold induced vasodilation (CIVD) [44].

Mathematical models analyzing thermal characteristics of limbs can be classified depending on the anatomical and vascular complexity considered in their develop-

ment. Early heat transfer studies in limbs or zeroth order models [21] neglect tissue composition and vascular structure. First order models consider simplified anatomy [45, 46]; models that introduce the thermal effects of countercurrent vessels [45, 46, 47] are referred as second order models.

The first study of heat transfer analysis on human limbs was by Pennes [21]; this study corresponds to the first analysis and prediction of the tissue temperature distribution using a mathematical model of heat transfer. In this study skin and deep tissue temperature are measured in all surfaces in the arm (*inferior, superior, medial and lateral*) from the elbow to the hand. This work assumes radial temperature variation only and presents an analytical solution for the steady state case. In this work, tissue blood perfusion is approximated to match the experimental measurements.

The study performed by Pennes [21] neglects arm length, tissue composition and vascular structure. To account for these parameters and to determine their effect on the temperature distribution of the arm and hand tissues, other authors have studied the presence of countercurrent macro-vessels embedded in the tissue cylinder with surface convection [45, 46]. The local micro-vascular temperature field is described by a 'hybrid' model which applies the Weinbaum-Jiji [26] and Pennes [21] equations in the peripheral and deeper tissue layers, respectively.

The model proposed by Zhu *et al* [46] considers three main regions that correspond to: core, deep muscle layer and outer muscle layer or skin (Fig. 5). The core region hosts the axial vessels, which have been combined into single artery-vein countercurrent pair places in a tapered tissue cylinder of finite length; three main temperatures are distinguished in this region that correspond to: tissue, arterial blood and venous blood. It assumes that blood velocity profiles are parabolic and the model neglects axial conduction. The muscle layers are described by a hybrid model. Finally, tissue metabolism is proportional to blood flow in the deep tissue

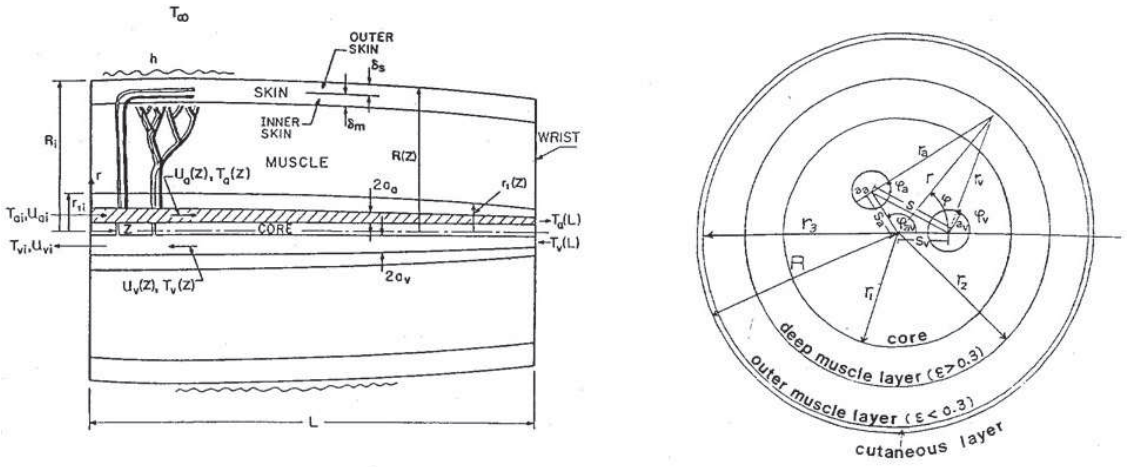

Fig. 5. Limb schematic and cross-section tissue distribution used by Zhu *et al* in [46].

layer. The predictions of the model show good agreement with measurements for the axial surface temperature distribution in the arm and confirm the minimum in the axial temperature variation first observed by Pennes.

More recent work, has presented a theoretical framework to investigate temperature variations along countercurrent blood vessels with diameters from 300 to 1000 μm in skeletal muscle [47]. The thermal interaction between the blood vessel pair and surrounding tissue is investigated for two vascular branching patterns. This paper shows that temperature variations along large thermally significant vessels depend strongly on the vascular geometry and local blood perfusion rate.

The fingers are considered a thermal window, that is a tissue structure whose potential rate of heat dissipation is determined by local peripheral or skin blood flow. Other thermal windows are wings, flippers, ears and tails. In these structures a conservation principle between the external heat flow from the skin to the surroundings and the internal heat flow due to the skin blood flow can be established, as follows

$$h_e \left(T_{skin} - T_{air}\right) = h_i \left(T_a - T_{skin}\right) \tag{2.3}$$

h_e is the external convection coefficient due to natural and forced convection, and can be determined from empirical relationships derived for cylinders; and h_i is a convective coefficient proportional to the volumetric blood flow rate permeating the skin tissue.

To analyze heat transfer through the fingers, a lumped parameter model of a finger tip has been developed by Shitzer *et al* [44] to analyze cold induced vasodilation CIVD and the effectiveness of different types of gloves. The semi-spherical model includes the effects of thermal inertia, heat exchange with the environment and heat transport by blood perfusion. The overall heat transfer coefficient of the insulation layer is calculated by common engineering formulae. The effects CIVD are modeled by symmetrical triangular wave forms as these were found to best depict the behavior of fingers exposed to cold environments.

C. Body Temperature Control and Skin Temperature

Body temperature in mammals and other homeotherms is maintained within a fairly constant range that is compatible with other regulatory systems and cellular physiology. Temperature regulation in animals implies the presence of mechanisms capable of level the rate of heat production to the rate of heat transfer to the environment. In mammals, chemical energy obtained from foods is converted into heat to support cellular processes and maintain body temperature. Analogously, heat can be lost to the environment by conduction, convection, radiation and evaporation. The rate of heat transfered by each one of these modes depends on the tissue volume, surface area, and the temperature difference between skin and the external medium.

The heat balance equation for the case of constant mean body temperature for

a resting subject is

$$S = MR - W - E - C - K - R, \tag{2.4}$$

where S corresponds to the rate of storage of heat in the organism, MR is the rate of metabolic energy transformed in heat, W is the rate of work done by the organism, E, C, K and R denote the rate of evaporative, convective, conductive and radiant heat transfer from the organism to the environment, respectively. The quantities in equation (2.4) are commonly expressed in terms of body surface area Wm^{-2} or body mass Wkg^{-1}.

Temperature regulation is the result of evolution, and it helps to optimize organ function, some thermoregulatory mechanisms observed in homeotherms are shivering, sweating, and panting. These thermoregulatory mechanisms are the result of metabolic and blood flow changes controlled by the thermostatic region of the hypothalamus. Shivering increases heat production in muscle tissue by producing involuntary muscular contractions, as a result the skeletal muscle temperature raises. During sweating and panting, heat is lost by evaporative heat transfer. Conversion of water from liquid to vapor is an endothermic process, evaporation occurs when the water vapor pressure on the skin is greater than that of the surrounding air. In sweating vasodilatation of the cutaneous vessels is observed, and the blood volume supplying the skin is cooled by surface evaporation; the sweating rate of humans is of the order of 10 to 15 grams of $H_2O/$ min m^2, and the latent heat of vaporization is approximately 40 W for 1 gram of H_2O per minute.

1. Skin Temperature and Blood Flow

In thermoregulation, control of skin blood flow is vital to the maintenance of normal body temperatures during challenges to thermal homeostasis, such as hypothermia

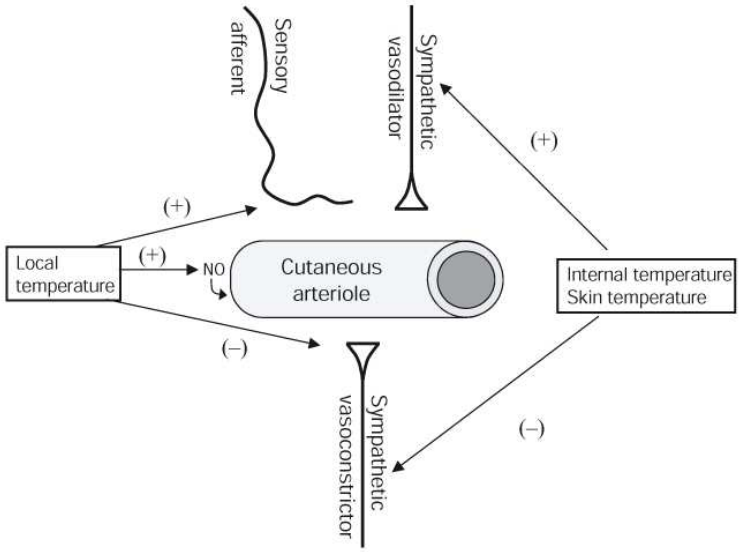

Fig. 6. Overview of thermoregulatory control of skin blood flow. Reflex innervation includes sympathetic vasoconstrictor nerves, and active vasodilator nerves. Local increases in temperature cause vasodilation by stimulating local neuropeptide release from sensory nerves and by non-neural local vasodilation caused by nitric oxide (NO). Local cooling stimulates localized neurotransmission from noradrenergic nerves to cause vasoconstriction. Plus signs refer to positive relationships: increases in temperature cause increases in activity and vice versa. Minus signs refer to inverse relationships: increases in temperature cause decreases in activity and vice versa. Taken from [48].

or hyperthermia. The human cutaneous circulation is controlled by two populations of sympathetic nerves: adrenergic vasoconstrictor nerves and vasodilator nerves, activated during hypothermia and hyperthermia, respectively. In addition to the sympathetic nerves, arteriovenous anastomoses (AVA), mostly located on glabrous skin (palms, soles and lips), provide low-resistance conduits that allow blood to flow directly from arterioles to venules affecting the rate of environmental heat exchange.

Small changes in skin blood flow can cause relatively large changes in heat dissipation. Resting skin blood flow in thermo-neutral environments is approximately

250 mL/min, which results in a heat dissipation of approximately 80 to 90 kcal/h, about the level of resting metabolic heat production. A change in skin blood flow from resting neutral levels of as little as 8 mL per 100 mL/min over the entire body surface results in a doubling of heat transfer to the environment [49]. During exercise or heat exposure, increases in body temperature trigger cutaneous vasodilation and sweating. Cutaneous vasodilation increases blood flow to the skin severalfold, substantially increasing convective transfer of heat from the core to the periphery. In humans, skin blood flow can increase up to 6 to 8 L/min.

Concurrent with cutaneous vasodilation, the evaporation of sweat decreases skin temperature, thereby cooling the blood in the dilated skin vessels before it returns to the core. In general, skin blood flow and sweating continue to increase in proportion to internal temperature until a steady state is reached at which heat dissipation and heat generation are equal, and therefore body temperature is constant, or until maximal responsiveness is reached.

The increase in skin blood volume during hyperthermia requires increased cardiac output and redistribution of blood flow from areas. These adjustments are usually sufficient to match the demand for increased skin blood flow, such that oxygen supply to organs like heart and brain are not compromised. Control of cutaneous vasoconstriction during hyperthermia is baroreflex-mediated, as the cardiac output can change up to 60%.

The local and reflex thermoregulatory control mechanisms in skin are summarized in Figure 6, which shows how skin blood flow control depends on both reflex (whole body) and locally mediated cutaneous vasodilation and vasoconstriction. Mechanisms for reflex control of skin blood flow include sympathetic adrenergic vasoconstrictor nerves and sympathetic vasodilator nerves, the latter of which are responsible for 80% to 90% of the substantial cutaneous vasodilation during whole body

heat stress. Cutaneous sympathetic vasoconstrictor and active vasodilator systems also participate in blood pressure regulation via the baroreflex, such that the participation of one or the other system depends on the thermal status of the subject, and the presence and alterations on hormone concentration, like in menopause, or diseases impairing microvascular responsiveness, like diabetes mellitus, Reynaud's disease, scleroderma and erythromelagia.

Currently, the presence of AVA's and its response to local and global temperature changes or regulatory mechanisms of cutaneous blood perfusion have never been introduced in theoretical models of heat transfer. Only empirical relationships have been created to analyze the relationship between skin, air and body temperature; these relationships have been used in whole body thermoregulation models [40] and during the 80's when liquid crystals were used to monitor body temperature. Other projects in our laboratory focus on this analysis and intend to introduce neural reflex into a mathematical model [50]. However, in this thesis such regulatory mechanisms will not be considered lumped in the skin blood perfusion term, which is measured for the finger as indicated in Chapter VIII.

CHAPTER III

CONTROL OF BLOOD FLOW AND PERFUSION

This thesis deals with the analysis of factors affecting fingertip temperature. The human finger is highly adaptive to environmental changes in temperature and posture as well as physical and /or emotional stimuli. Fingers play an important part in body temperature control, this occurs through alterations in skin perfusion. The functional and morphological aspects of digital circulation are still inadequately understood after more than 100 years of study. In the previous chapter the relationship between skin temperature and blood perfusion was discussed. Since we are interested in analyzing the thermal effect of vascular reactivity (VR), it is necessary to account for the variations of skin perfusion at the finger level. About 95% of the finger tissue is skin [51, 52, 53], as a result, we will discuss the characteristic of the circulatory system at the skin level.

Skin is a large organ that can weight about 2 kilograms or 5% of the total body weight, in an average size individual and have a surface area of 1.8 m^2. Given its location and vasculature, it works as an insulator and heat exchanger. Skin is characterized by a dense system of capillary loops and that is connected to a venous plexus capable of storing a significant volume of blood. The blood in the skin travels at very low velocities and its proximity to the external environment allows rapid heat dissipation. Finally, changes in the venous blood volume allows different levels of heat dissipation. In this chapter, details about circulatory system and the factors controlling blood perfusion in arms and fingers are discussed.

A. Cutaneous Circulation and Controlling Factors

Circulation can be classified depending on the nature of the organs feed (regional circulation); it is divided into circulation to the organs that are very active during exercise, and those that do not show an increase in oxygen uptake during exercise. These last group of organs are referred as non-muscular or non-contracting organs, and correspond to splanchnic circulation (liver, gastrointestinal tract, pancreas, spleen), cutaneous circulation (skin), cerebral and renal circulation.

The function of cutaneous blood flow is nutrition of the skin and thermoregulation. In a hot environment, skin blood flow may approach 8 l/min. This increased skin blood flow is met by an increased cardiac output and by redistribution of blood flow from other regions. In this setting the cutaneous circulation can comprise over 60% of the total vascular conductance [54]. The cutaneous circulation contains three major types of blood vessels: **(1)** arteries, capillaries, and veins that serve mainly nutrition needs; **(2)** subcutaneous venous plexus that plays a major role in the conduction of heat, as it provides a large surface area for heat exchange and contains a major fraction of the cutaneous blood volume; and **(3)** arteriovenous anastomoses (AVAs) that connect cutaneous arterioles and venules directly, playing an important role in the reduction of blood flow in a cold environment. The vasculature in the skin is one of the most compliant vascular regions, the other is the splanchnic circulation.

AVA's have a low level of basal tone and are innervated exclusively by sympathetic fibers, to which they are very responsive. Blood flow in AVA's is controlled by temperature changes (body or environmental). Some responses are mediated by nerves, while others are direct effects on the vasculature itself. AVA's action affect blood volume in the venous plexus. If the venous plexus is full, then the amount and rate of heat exchange increases(i.e. more heat is lost to the environment and at a

higher rate), as a result of the increased heat loss, the skin temperature drops.

B. Measurement of Blood Perfusion

Measurement of blood perfusion at the skin level can be measured by laser doppler flowmetry (LDF), and laser doppler imaging (LDI); it is also determined indirectly through infrared imaging (IR). In techniques involving laser doppler signals, moving blood in the microvasculature causes a Doppler shift of the scattered laser light, which is photodetected; LDI uses a beam that scans the area and then the information is processed to build a colour coded map of blood flow; IR imaging is based on the fact that regions with high perfusion are at a higher temperature. The limitations of these technique are the penetration depth of the laser light, and the fact that these techniques render measurements that indicate only relative changes of blood perfusion. Another highly used technique to determine blood volume is plethysmography; this technique has been used to determine blood volume in limbs and fingers for almost a hundred years; however the sensitivity of the technique has increased considerably during this time. Plethysmography is based on the principle that when veins draining an organ are occluded, then the arterial inflow will increase the volume of the organ in consideration, the difference between the initial and final volume gives a relationship for the blood volume entering the organ during the study time.

Currently the two plethysmographyc techniques that are performed in clinical and research setting are Photoplethysmography (PPG) and Strain Gauge Plethysmography or SGP. In PPG an infrared sensor that detects skin color changes during each heartbeat is placed at the skin. SGP monitors volume changes using a strain gauge around the finger or limb and more details about the technique, as well as the common errors and problems associated to it are described in Chapter VIII.

C. The Circulatory System: Vessel Classification

The circulatory system is divided in three main parts: pulmonary circulation that feeds lungs, coronary circulation in charge of feeding heart tissue, and systemic circulation that perfused the rest of the body; it carries oxygenated blood away from the heart, to the body, and returns oxygen-depleted blood back to the heart. Fig. 7 shows how oxygenated blood leaves the lungs and enters the Left Atrium (LA) of the heart via the pulmonary veins. This oxygenated blood is then pumped from the Left Atrium (LA) of the heart to the Left Ventricle (LV) of the heart, and then out of the heart to the body tissues via the aorta, which is the major artery leaving the heart. The aorta divides into other arteries that serve different parts of the body, namely upper-body or arms and head, and lower-body or legs. Blood is deoxygenated when it leaves the tissues and organs it has supplied with oxygen and other nutrients, to return back to the pulmonary circulatory system. From the upper body, blood returns from the head via the jugular veins, and from the arms via the subclavian veins. All of the blood in the major veins of the upper body flows into the superior vena cava, which returns the blood to the right ventricle of the heart.

Depending of their size, blood vessels are classified in conduit vessels, resistance vessels, exchange vessels and capacitance vessels. Conduit arteries have diameters in the order of mm and lengths that go from $4 \times 10^{-2}m$ in the aorta to $10^{-2}m$ in main arterial branches; these arteries are characterized by a rather small intravascular pressure drop along the arterial length. Exchange vessels correspond to capillaries where nutrient and oxygen transport take place. Capacitance vessels represent venous vessels which constitute a major blood reservoir capable of storing about 80% of the blood volume; in these vessels the intravascular pressure is very small and varies between 15 to 5 mmHg in comparison with conduit arteries where the intravascular

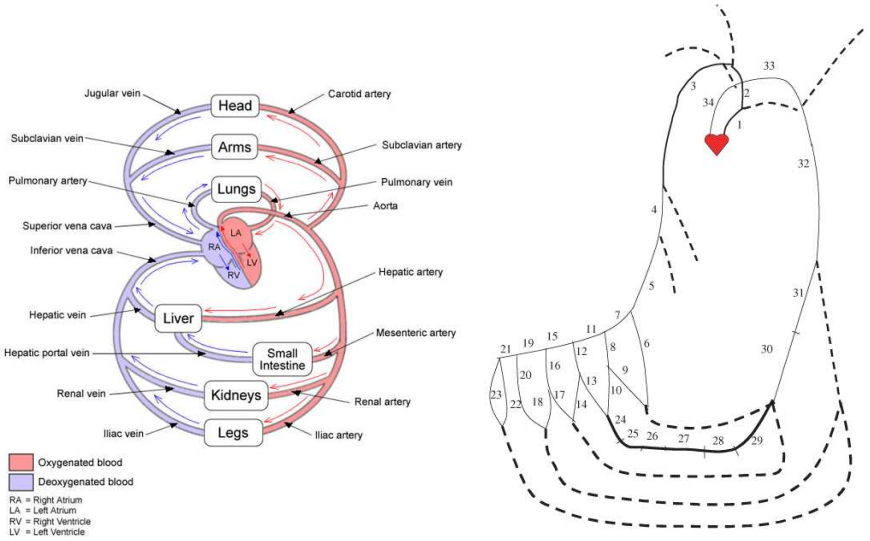

Fig. 7. **(A)** Diagram of the circulatory system, **(B)** Diagram showing blood vessels from heart to finger, vessel number and sizes are indicated in Fig. 8, adapted from [55].

pressure is between 100 and 90 mmHg. Finally, resistance vessels are medium to small arteries that have a thick layer of smooth muscle cells (SMC), and are responsible of the control of blood flow.

Variations in organ blood flow are produced by changes in the vascular resistance, which is the result of variations in vascular geometry such as vessel diameter. Variations in vessel diameter are produced by: **1)** active mechanisms due to the response of SMC to alterations in chemical, metabolic and intravascular pressure changes; and **2)** passive mechanisms produced by the viscoelastic properties of the arteries. Because of the vessel size and SMC content in the different arteries from aorta to arterioles, vascular resistance is strongly controlled by medium to small arteries or resistance vessels. Figures 7 and 8, show blood vessels from heart to fingertip and its corresponding length and radius; comparing Fig. 8 with Table I, we observed that thermal equilibration is achieved after generation 23.

Segment number	Vessels	Length (m)	Proximal radius (m)	Distal radius (m)	Number of vessels
1	Ascending aorta	0.07	1.25e−2	1.14e−2	1
2	Anonyma artery	0.035	0.7e−2	0.7e−2	1
3	Subclavian artery	0.43	0.44e−2	0.28e−2	1
4	Ulnar artery	0.067	0.215e−2	0.215e−2	1
5	Ulnar artery	0.171	0.203e−2	0.184e−2	1
6	Proper palmar digital artery	0.14	0.055e−2	0.045e−2	1
7	Superficial palmar arch	0.01	0.18e−2	0.18e−2	1
8	Common palmar digital artery	0.08	0.68e−2	0.68e−2	1
9	Proper palmar digital artery	0.08	0.05e−2	0.05e−2	1
10	Proper palmar digital artery	0.08	0.05e−2	0.05e−2	1
11	Superficial palmar arch	0.006	0.16e−2	0.16e−2	1
12	Common palmar digital artery	0.08	0.068e−2	0.068e−2	1
13	Proper palmar digital artery	0.08	0.05e−2	0.05e−2	1
14	Proper palmar digital artery	0.08	0.05e−2	0.05e−2	1
15	Superficial palmar arch	0.006	0.144e−2	0.144e−2	1
16	Common palmar digital artery	0.08	0.068e−2	0.068e−2	1
17	Proper palmar digital artery	0.08	0.05e−2	0.05e−2	1
18	Proper palmar digital artery	0.08	0.05e−2	0.05e−2	1
19	Common palmar digital artery	0.006	0.13e−2	0.13e−2	1
20	Proper palmar digital artery	0.15	0.06e−2	0.05e−2	1
21	Principal artery of thumb	0.02	0.1e−2	0.1e−2	1
22	Proper palmar digital artery	0.06	0.066e−2	0.066e−2	1
23	Proper palmar digital artery	0.06	0.066e−2	0.066e−2	1

Segment number	Vessels	Length (m)	Area (m^2)	Number of vessels
24	Terminal arteries	0.08	0.063e−4	32
25	Arterioles	0.018	0.75e−4	2.4e+5
26	Capillaries	0.002	7.5e−4	1.0e+6
27	Venules	0.02	2.55e−4	0.36e+6
28	Terminal veins	0.08	0.42e−4	36
29	Dorsal venous network of hand	0.08	0.43e−4	2
30	Ulnar veins	0.3	1e−4	2
31	Brachial vein	0.15	0.85e−4	1
32	Subclavian vein	0.2	0.9e−4	1
33	Anonyma vein	0.065	2.5e−4	1
34	Superior vena cava	0.045	4.5e−4	1

Fig. 8. Physiological data of arteries and veins in upper limbs from heart to fingertip. Adapted from [55].

The mathematical model proposed and studied in this thesis does not include vasculature detail; but future studies require the analysis of the countercurrent heat transfer occurring at the arm and finger level due to deep vessels, as well as their elastic response during hyperemic experiments. The fact skin is the dominant tissue in fingers, we are confident that the studied performed herein will provide significant knowledge to latter consider the significance of countercurrent artery-vein pairs.

CHAPTER IV

ANATOMICAL AND PHYSIOLOGICAL CONSIDERATIONS

This chapter describes the anatomical and physiological consideration required to develop a thermal model for the finger. Given the description of the tissue thermal models and the importance of system anatomy and physiology in Chapters II and III, this chapter describes the finger anatomy and blood perfusion characteristics that will be latter incorporated in the thermal models proposed. It further introduces the classification scheme adopted to describe the mathematical models. The models were created to study the thermal behavior of the human finger during the DTM test that induces a hyperemic response in the fingers as a result of vascular occlusion that can be performed at different levels: upper arm (brachial artery), wrist (radial artery), finger base. To simplify the thermal analysis of the limb during DTM and because the method only measures fingertip temperature, the proposed models predict the tissue temperature on just the finger.

A. Anatomy of the Finger

It is important to consider the anatomy and physiology of the finger, as it directly impacts the proposed thermal models. A human finger is a highly complex three-dimensional structure composed of different layers as seen in Fig.9(A). At the center of the finger is the bone structure. There are three bones in each finger called the proximal phalanx, the middle phalanx and the distal phalanx, which are held together by tendons. The figure also shows the dense distribution of arterioles in the finger. Further, the arteriogram as seen in Fig. 9(B) shows a higher density of capillaries at the finger tip than in the rest of the finger; which influences the temperature distribution along the finger length. This can be observed from the infra-red (IR)

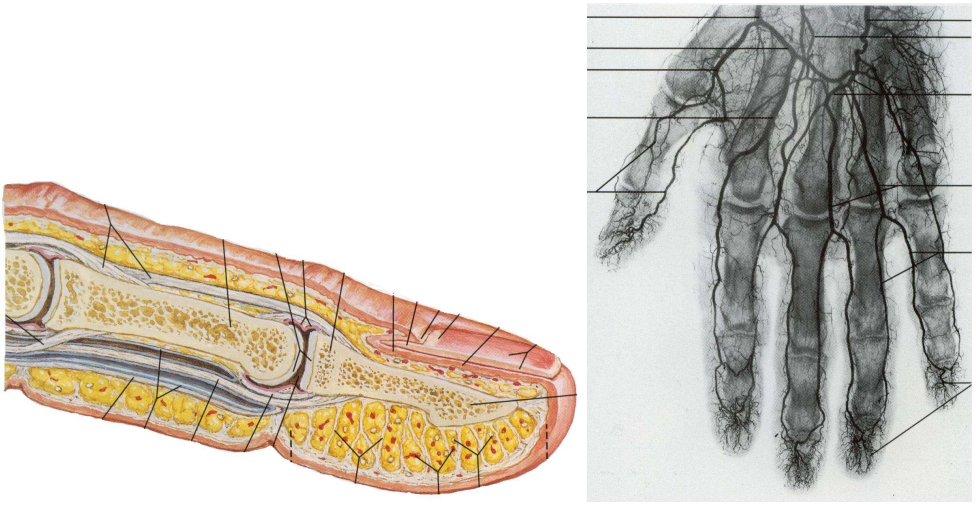

Fig. 9. **(A)** Sagittal section of the human finger showing the tissue structure and the distribution of the arteries (adapted from [56]). **(B)** Arteriogram of the right hand (palmer aspect). Taken from [57].

images of hand (Fig. 10), the temperature was found to vary along the length of the finger. The thermo-physical properties of the different tissues [33] within the finger vary significantly and thus the size of the layers will affect the temperature distribution in the finger. It should be noted that blood perfusion in the hand and the fingers particularly takes place predominantly through the skin [58]. As can be seen in this sample IR image, the maximum temperature distribution was found to be 0.75 ^oC, which is significant considering that the rise in temperature due to reactive hyperemia is of the order of 1-2 ^oC. Thus for the proposed models (the ones which consider the anatomy of the finger), the blood perfusion in the skin cannot be assumed uniform as was assumed in [33].

B. Modeling of Reactive Hyperemia

The blood perfusion during hyperemia varies with time. A model developed by Ley for stroke [59] was used for modeling the temporal variation of blood perfusion and

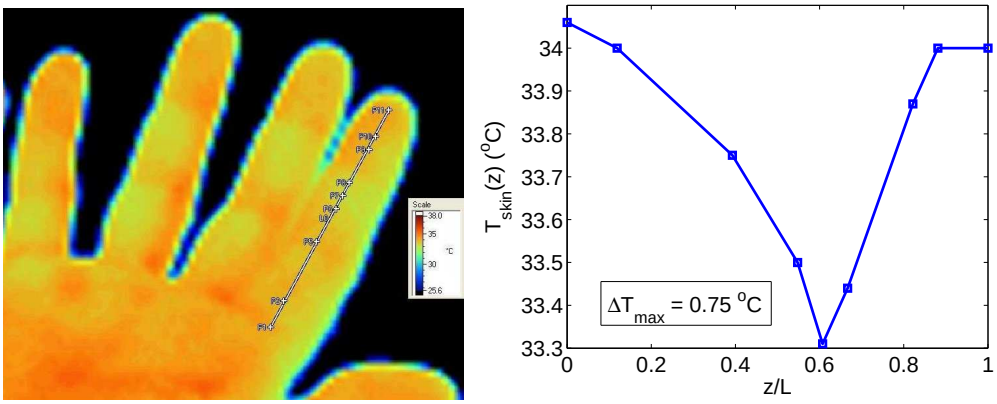

Fig. 10. **(A)** A representative IR image of right hand showing the points on the index finger used for plotting the skin temperature variation along the axial direction of the index finger. The IR image was obtained using a VENDYS^{TM} Infra-red camera and then converted into a temperature map using a software called, FlexView 1.2.2 from Infrared Solutions. **(B)** Variation in the temperature along the skin obtained from the IR image. The temperature at the tips and the base of the finger is significantly higher than the rest of the finger.

was optimized for modeling reactive hyperemia. During regional ischemia due to blood flow occlusion, two different stages are identified which correspond to: vascular occlusion (Stage I) and reperfusion (Stage II) as can be seen in Fig. 11. During EDF studies, vascular occlusion can last between 2 to 5 minutes [60]; and blood flow is reduced completely during the first minute. Reperfusion starts with hyperemia or abnormally high regional blood flow, then the blood flow is reduced and returns to the normal value in the following minutes [61]. For every tissue, during *Stage I* or vascular occlusion, the blood flow falls exponentially, following a relationship of the form:

$$\omega_b^I(t) \;=\; (\omega_0 - \omega_s)\exp\left(-t/\tau_0\right) + \omega_s, \;\; \text{for} \;\; t \leq t_{occ}, \tag{4.1}$$

where, ω_0 represent the initial blood flow and have the same values as the healthy tissue; τ_0 is a constant related to the time in which the blood flow falls during vascular

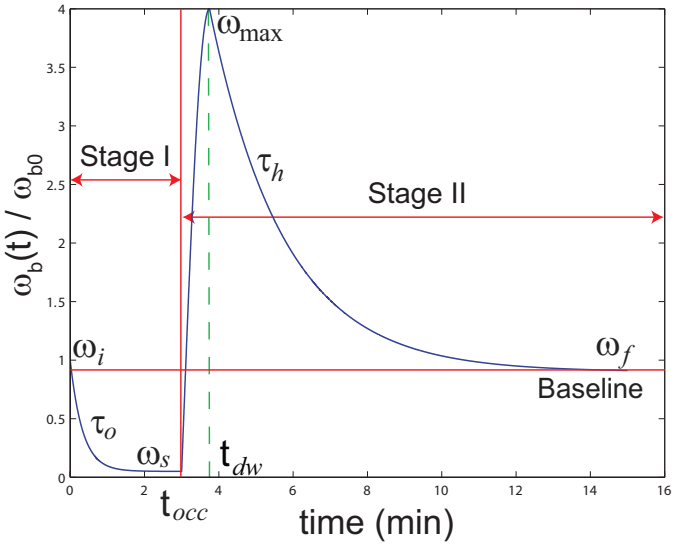

Fig. 11. Representative graph showing the modeled variation of blood perfusion with time during reactive hyperemia.

occlusion, and it was assigned a value of 3 minutes. ω_s is the value of the blood perfusion during the vascular occlusion, and generally has a value of 0 to 5 percent of the initial blood perfusion ω_0. The values of blood flow and metabolic heat during vessel occlusion are defined as: $\omega_s = \alpha\omega_0$where the parameter α is such that $0.1 \geq s \geq 0.05$ and denotes the reduction of the blood flow during vascular occlusion.

During reperfusion (*Stage II*), experiments show that the blood flow can surpass the basal blood flow value by 200 to 400 percent (hyperemia) [60] during hyperemia and then return to the ischemic value after several minutes. The variations in the blood flow and metabolic rate in the reperfusion stage are approximated by the following relationships:

$$\omega_b^{II}(t) = \begin{cases} (\omega_{max} - \omega_s)\sin^2(\pi t/2t_{dw}) + \omega_s, & \text{for } t_{occ} < t \leq (t_{occ} + t_{dw}) \\ (\omega_{max} - \omega_f)\exp\left(-(t - t_{occ} - t_{dw})/(\tau_h)\right) + \omega_f, & \text{for } t > (t_{occ} + t_{dw}), \end{cases} \tag{4.2}$$

where, the parameters ω_0, ω_s, represent the same quantities described before; ω_{max}

Table III. Base case values for the parameters defined in the reactive hyperemia model.

Parameters	Units	Basal values
$\alpha = \omega_s/\omega_i$	-	0.05
$\beta = \omega_{max}/\omega_i$	-	4
$\zeta = \omega_f/\omega_i$	-	1
τ_0	s	5
τ_h	s	120
t_{dw}	s	45
t_{occ}	s	180

represents the maximum hyperemic blood flow, occlusion time among other parameters; the hyperemic blood flow is defined as $\omega_{max} = \beta\omega_0$, where β is found to be in the range of 2 to 4. t_{dw} is the time required to reach the hyperemic blood flow. τ_h indicates the rate at which blood flow returns to its normal value during reperfusion. $\omega_f = \zeta(\omega_0)$ is the final value of blood flow after hyperemia and is assumed equal to the basal values *i.e.* $\zeta = 1$.

The model for reactive hyperemia contains a lot of parameters that can be varied to simulate the temporal history of blood perfusion and the fingertip temperature observed after occluding the brachial artery of a healthy or an unhealthy patient. However to perform a parametric study, a need was felt to establish certain base value, so that while doing a sensitivity analysis by varying one parameter all the other parameters will be assume their basal values. The basal values of the parameters of reactive hyperemia were decided by a trial and error process of matching the temporal history of temperature at the fingertip calculated from the zero-order with a representative graph of a healthy person and can be summarized in Table III.

C. Classification of Proposed Thermal Models

To get a preliminary understanding for the effect of the factors affecting the fingertip temperature, two models are created: a zero-order model and a first-order model, where the finger geometry is approximated by 2D axis-symmetric simplified geometry considering four layers viz. skin, fat, muscle and bone. The details and results for these models are presented in the following chapters. These models use the transient blood perfusion function described in the previous section and predict the finger temperature during the DTM test.

The classification was decided based on the complexity of the model. Higher the order of the model, the better the modeling of the anatomy as well as the heat transfer phenomena within the finger. A zero-order model is a lumped model and neglects the heat conduction within the finger. A first-order model consider a two dimensional cylindrical finger geometry, and considers the heat conduction within the tissue, but the vascular structure within the finger is approximated by a volumetric blood perfusion term. A second-order (subject of future research) will consider a more anatomically correct finger and also the vascular structure within the tissue.

CHAPTER V

ZERO-ORDER MODEL

This chapter describes a simplified mathematical model of heat transfer within the finger; the model is created to analyze the sensitivity of the fingertip temperature to parameters, such as maximal hyperemic flow, body temperature, ambient conditions and anthropometric measurements. This model, referred as a zero-order model, is based on a lumped parameter model of a fingertip developed by Shitzer *et al.* [44] to study cold induced vasodilation (CIVD).

In the zero-order model,the heat production in the tissue is a result of the incoming blood flow which is distributed to the capillary bed in the tip of the finger and is assumed to equilibrate with the temperature of tissue. Blood in the fingertip is assumed to be supplied and drained by a single artery-vein pair. Finally, heat loss to the environment takes place as a result of convection at the skin surface.

A. Assumptions

The zero-order model is based on the following assumptions:

(i) The finger is assumed as a dimensionless mass system, neglecting the spatial variation in temperature of the fingertip (lumped model).

(ii) Metabolic heat generation is neglected in this analysis, as it is a constant and small, because finger and skin are not metabolically active, and no significant movement or exercise is performed during the procedure.

(iii) The thermo-physical properties of the tissue are assumed to be uniform, isotropic and independent of fingertip temperature.

(iv) Blood flow is assumed to be independent of temperature; this is a valid approximation, given the small temperature variation that the skin naturally experiences. However, in reality, blood flow will be affected by temperature following the Arrhenius equation [62], which indicates the presence of mechanisms that increase blood flow when temperature increases. The Arrhenius relation is commonly used for metabolically active organs like brain, heart and liver.

Thermoregulatory mechanisms present in the skin are responsible for variation in the cutaneous blood flow are neglected; this is done because a time dependent perfusion term is introduced that should account for these effects is introduced in the model. A more realistic description, where many of these assumptions will be removed, will be included in the second order model which is the subject of future studies.

B. Governing Equation

The governing equation for modeling the basic heat transfer in the lumped model is based on the energy conservation principle *i.e.*

$$Stored\ \ Energy = (Energy\ \ Generated - Energy\ \ Lost)$$

The lumped equation for the fingertip temperature considers heat delivered by blood flow to the tissue and the heat loss due convective heat transfer experienced at the skin surface and is expressed as:

$$\rho C_p V \frac{dT}{dt} \ = \ h_{air} A(T - T_{air}) + \rho_b C_{p_b} \omega_b(t)(T_A - T), \tag{5.1}$$

where, ρ indicates the tissue density, C_p is the tissue specific heat, V represents the fingertip volume, approximated as a semisphere, ($V = \pi D^3/12$), A is the fingertip

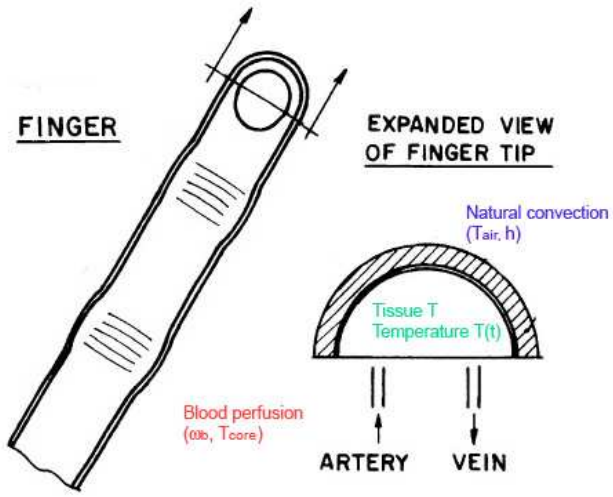

Fig. 12. Illustration for zero-order model (adapted from Shitzer [44]).

surface area ($A = \pi D^2/2$), ρ_b and C_{p_b} indicate the density and specific heat of blood, and ω_b indicates the volumetric blood flow or perfusion; and its temporal variation is given by Eq. 4.1 and Eq. 4.2 for blood perfusion in reactive hyperemia described in the previous chapter and measured in Chapter VIII. T_A is the arterial temperature, assumed to be constant and equal to core or body temperature; finally T_{air} represents the temperature of the surrounding air. For this model, the base case value for initial blood perfusion, $\omega_0 = \omega_{b(t=0)}$ was defined as the value satisfying the governing equation at steady state, where the tissue temperature was set to T_i. The expression for ω_0 was found to be:

$$\omega_0 = \frac{h_{air} A (T_{air} - T_i)}{\rho_b C_{p_b} (T_A - T_i)}. \tag{5.2}$$

C. Model Geometry and Tissue Properties

In the zero-order model illustrated in Fig. 12, the geometry of the model is essentially zero dimensional, and described wholly by the mass of the fingertip. The fingertip is approximated by a hemisphere, having a surface area of, $A = \frac{\pi D^2}{2}$ and the volume

Table IV. Thermo-physical properties used for zero-order model.

Properties	Tissue	Blood
$\rho, (kg/m^3)$	1085	1069
$C_p, (J/kg.^oK)$	3680	3650
$k, (W/m.^oK)$	0.47	-
$\omega_0, (m^3/s)$	3.768×10^{-10}	-

given by, $V = \frac{\pi D^3}{12}$, where D, is the average fingertip diameter. The cross section area of the fingertip resembles more of an ellipse than a cylinder; therefore, the radius R, is calculated as an average of the fingertip radius in the direction parallel to the nail (R_1), and the fingertip radius perpendicular to the nail (R_2). For the calculations, the average fingertip diameter is given by $D = 2R = (R_1 + R_2) * size_{fac}$, where $size_{fac} = 0.8, 1, 1.2$, is defined as a size factor, used to vary the fingertip dimensions. For most of the calculations presented next $R_1 = 0.55cm$ and $R_2 = 0.65cm$ are the base case values used. The base case thermo-physical, geometric, environmental and physiological properties used in the model are given in Table IV and Table V.

Lumped analysis is valid if the Biot number[1] of the system, ($Bi = hL_c/k$) is less than or equal to 0.1. For this problem, with the characteristic dimension L_c given by $V/A = D/6$; the tissue thermal conductivity (k), the convection coefficient, (h_{air}), at their respective base case values give a Biot number of ($Bi = 0.0176$) < 0.1.

[1]Biot number is the ratio between convection at the surface of the body and conduction within the body.

Table V. Base case values for geometric, environmental and physiological parameters in the zero-order model.

Properties	Base case Value
R_1	0.55 cm
R_2	0.65 cm
$size_{fac}$	1
h_{air}	6 $W/m^2.^oK$
T_{air}	25 ^oC
T_A	37.5 ^oC
T_i	31.5 ^oC

D. Initial Condition

The zero-order model of Eq. 5.1 represents a initial condition problem, thus requires an initial starting condition for obtaining the solution to the Eq. 5.1. The initial condition is given by:

$$T \ = \ T_i, \ \text{ at } \ t = 0, \tag{5.3}$$

where, T_i is the initial temperature. The temperature at the skin surface of a finger was found to vary significantly among subjects during validation studies. In a young adult, it can be as low as 28^oC and as high as 36^oC, with the normal average being around $31 - 33^oC$; this value depends on air temperature and posture among other things. For the calculations of this chapter, the base case initial temperature was assumed to be 31.5^oC.

Table VI. List of parameters varied to study their effect on finger temperature during hyperemia in the zero-order model.

Parameter	Base case Value	Variation
β	3	2, 3, 4
τ_h	120 s	60, 120, 180
t_{dw}	45 s	25, 35, 45
h_{air}	6 $W/m^2.^oK$	3, 6, 9
T_{air}	25 ^oC	21, 23, 25
T_A	37.5 ^oC	37, 37.5, 38
T_i	31.5 ^oC	30, 31.5, 33

E. Model Results

The zero-order model was solved numerically using a fourth order Runge-Kutta algorithm implemented in MATLAB, as a closed form solution is not available for time varying blood perfusion term $\omega_b(t)$. Details regarding the experimental validation for the zero-order model can be seen in Chapter VIII. The zero-order model was useful in studying the effect of different parameters on the temperature response of the finger during hyperemia. The parameters varied during the study and the variation in their values is summarized in Table VI.

The factors affecting the fingertip temperature are classified into 3 groups *v.i.z*: hemodynamic factors (β, τ_h, t_{dw}), environmental factors (h_{air}, T_{air}), physiological factors (T_A, T_i) (see Table. VI). In this study, each parameter was varied in turn, keeping all the other parameters constant at their base case values as indicated in Tables III and V.

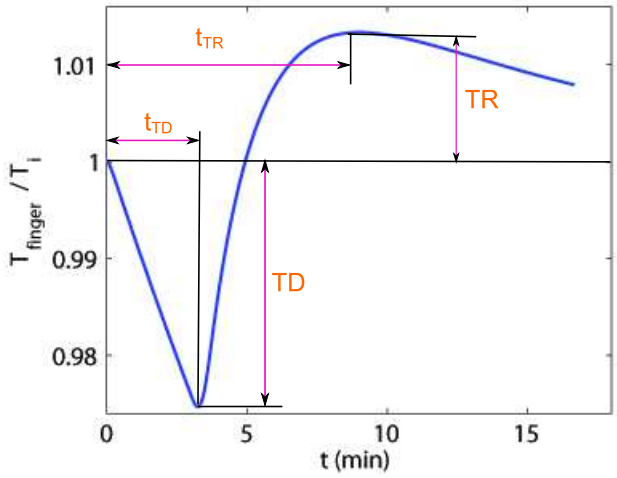

Fig. 13. Representative plot for the thermal response of the finger. TR: Maximum rebound temperature; TD: Maximum drop in temperature; t_{TR}: time required to attain TR; t_{TD}: time required to attain TD.

It is important to note that, though in reality a change in some of the above factors will cause a change in the blood perfusion in the finger as a result of the thermoregulatory and feedback mechanism of the body, the initial blood perfusion (ω_0) was maintained constant, to see only the effect of the varying parameter on the model. For future studies we intend to look at these correlations experimentally and produce empirical relationships that can be incorporated in more complex models.

It should be noted here that, the thermal response of the finger was characterized by 4 terms: the maximum rebound temperature, (TR), the time required to achieve TR, (t_{TR}), the maximum drop in temperature (TD), the time required to achieve TD, (t_{TD}) and are illustrated in Fig. 13.

The effect of factors affecting the fingertip temperature can be summarized as follows:

(i) Effect of hemodynamic factors:

(a) Maximum hyperemic blood flow (β): The maximum hyperemic blood

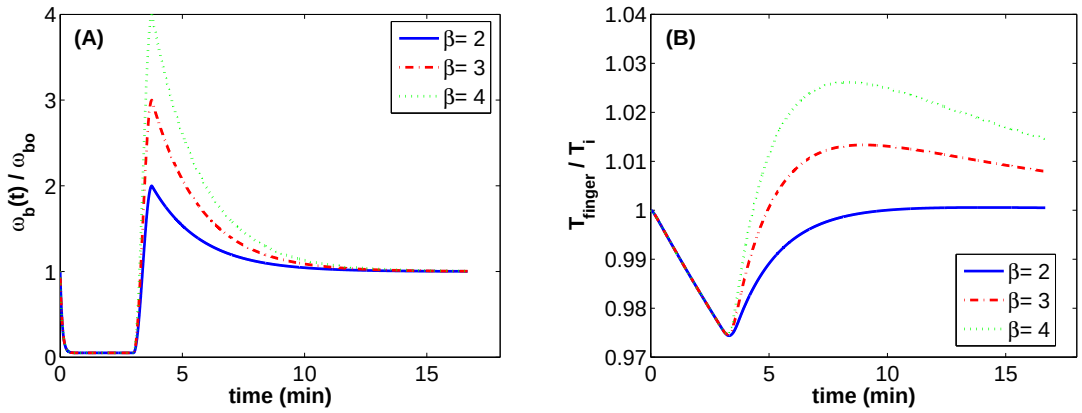

Fig. 14. **(A)** Blood perfusion due to variation in β during reactive hyperemia, **(B)** Effect of variation in β on temperature during reactive hyperemia, calculated using the zero-order model.

reached due to hyperemia depends on the vascular health of the arteries. Higher β values are correlated to healthier arteries, that are capable of experiencing large vasodilation. In healthy persons, the maximum hyperemic blood flow reached is up to 4 times the baseline blood flow. The temperature response was calculated for $\beta = 2, 3, 4$ and shown in Fig. 14. It is seen that maximum rebound temperature (TR) is directly proportional to β.

(b) Rate at which blood flow drops to baseline after hyperemia (τ_h): Increase in τ_h, decreases the rate at which blood drops, which consequently increases the maximum rebound temperature (TR) observed as can be seen in Fig. 15.

(c) Time required to reach maximum hyperemic blood flow (t_{dw}): t_{dw} indicates the responsiveness of the arteries to stimulus (here arterial occlusion). A increase in t_{dw} produces the following alterations in fingertip temperature: **(1)** decrease in the maximum drop in temperature (TD) observed, and **(2)**

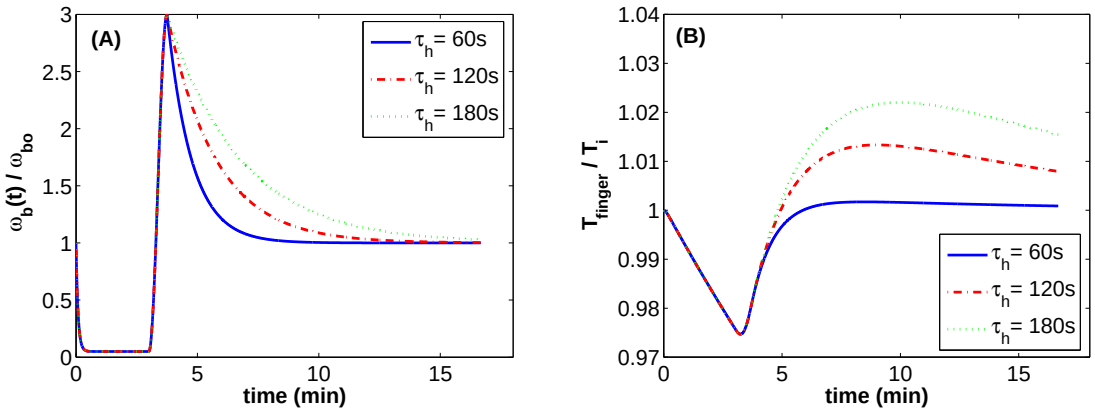

Fig. 15. **(A)** Blood perfusion due to variation in τ_h during reactive hyperemia, **(B)** Effect of variation in τ_h on temperature during reactive hyperemia, calculated using the zero-order model.

increase in the time, (t_{TD}) in which TD is attained, and, **(3)** increase in the maximum rebound temperature (TR). These behaviors can be observed in Fig. 16. If t_{dw} is large then the temperature drop observed in finger continues beyond occlusion time.

(ii) Effect of environmental factors:

(a) External heat convection coefficient (h_{air}): The external heat convection coefficient is found to have a pronounced effect on the temperature response observed as a whole, both during occlusion and during reactive hyperemia. h_{air} is found to be inversely proportional to the initial temperature (T_i). This indicates that the environment within the room should be controlled and the subject should not be subjected to any sort of drafts from a air conditioning unit or other sources. The values of h_{air} = 3, 6, 9 considered in the numerical study are well within the range of natural convection. A higher heat convection coefficient has a cooling effect on the finger and decreases the hyperemic temperature response or TR value as

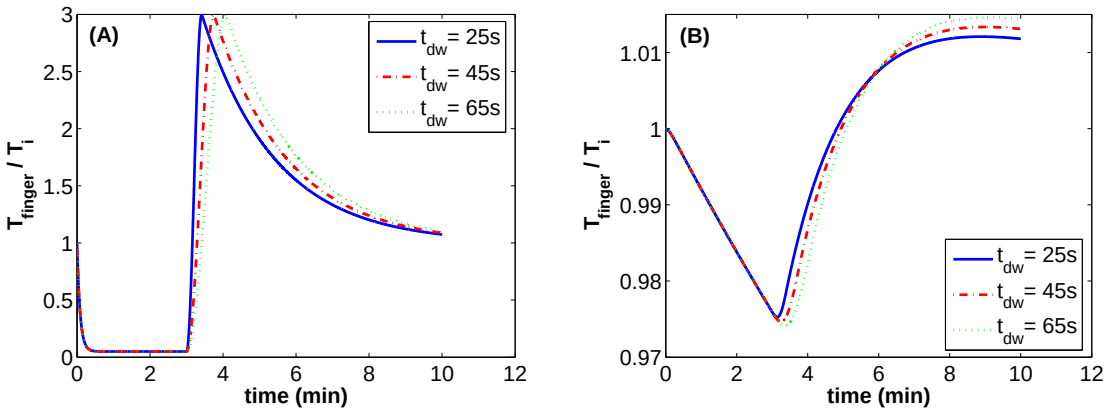

Fig. 16. **(A)** Blood perfusion due to variation in t_{dw} during reactive hyperemia. **(B)** Effect of variation in t_{dw} on temperature during reactive hyperemia, calculated using the zero-order model.

can be seen in Fig. 17. The experiments performed, presented in Chapter VIII, show that thermal response of the finger to reactive hyperemia is inversely proportional to the heat transfer coefficient observed in Fig. 17.

(b) Surrounding air temperature (T_{air}): The effect of surrounding air temperature can be seen in Fig. 18. T_{air} is found to be directly proportional to the initial temperature (T_i). The lower the surrounding temperature, the higher is the heat loss from the finger, and, smaller is the thermal response or the rebound temperature (TR). Although, this model does not include the thermoregulatory response of the body, calculations show that, the surrounding temperature should be maintained high enough (greater than 24 ^oC according to the model) to see the sole effect of reactive hyperemia on the thermal response. It was observed in the experiments performed, that a room temperature has to be maintained above 23 ^oC to perform the DTM test, otherwise the TR value registered is negative and test might predict a false positive.

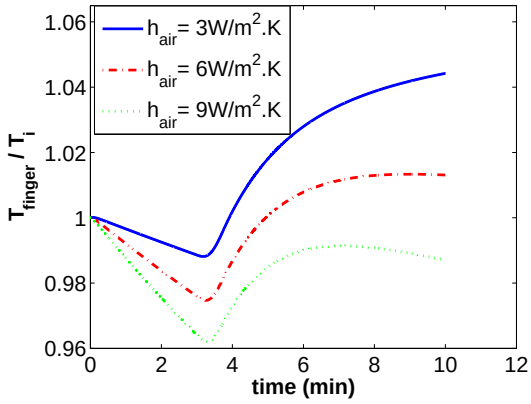

Fig. 17. Effect of variation in h_{air} on temperature during reactive hyperemia, calculated using the zero-order model.

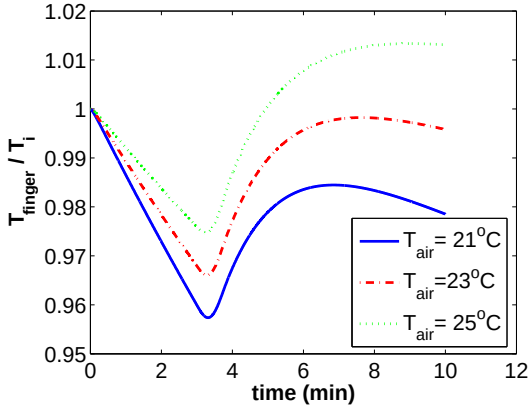

Fig. 18. Effect of variation in T_{air} on temperature during reactive hyperemia, calculated using the zero-order model.

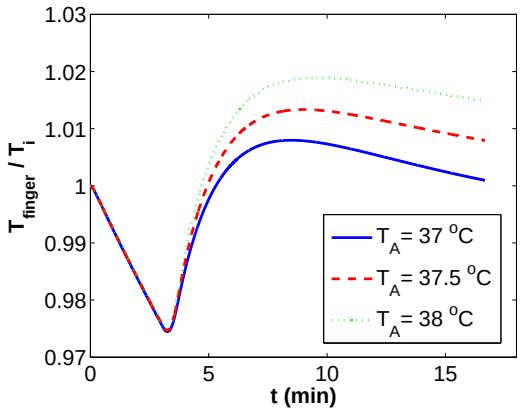

Fig. 19. Effect of variation in T_A on temperature during reactive hyperemia, calculated using the zero-order model.

(iii) Effect of physiological factors:

(a) Body temperature (T_A): The thermal response of the finger can be seen in Fig. 19. T_A is found to be directly proportional to the initial temperature (T_i). A higher T_A indicates a higher temperature at the skin of the finger (T_{skin}), meaning less vasoconstriction in peripheral vasculature. A higher body temperature is found to increase the maximum thermal response observed due to hyperemia and vice-versa.

(b) Initial finger temperature (T_i): The initial temperature of the finger, (T_i) before the onset of occlusion and subsequent hyperemia is supposed to be almost constant or oscillating closely about a central value. This value should represent steady state if sufficient time for thermal equilibration is allowed. It is seen that the lower the temperature of the finger, better is the rebound temperature (TR) observed due to hyperemia as can be seen in Fig. 20. It was not possible to experimentally to see the effect of T_i, as a change in the initial temperature of the finger will produce a proportionate change in the blood perfusion in the finger as a result of the

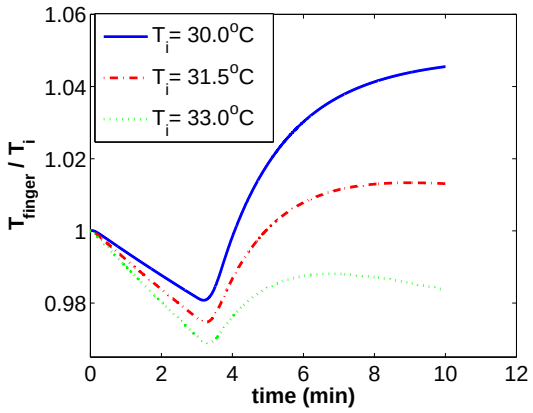

Fig. 20. Effect of variation in T_i on temperature during reactive hyperemia, calculated using the zero-order model.

thermoregulatory mechanism of the human body. More detailed analysis is needed to look at the case of low initial temperature in the finger or also referred as "cold finger"; however, this analysis will be performed in the future.

It is observed, from Figs. 14-20, that all the parameters considered above (β, τ_h, t_{dw}, $h_{air}, T_{air}, T_A, T_i$) have significant effect over TR and TD. A summary of the main relationships observed from the calculations is given in Table VII.

It should be noted that in reality, the initial fingertip temperature T_i, is affected by h_{air}, T_{air}, as well as T_A. Such relationships are expected as an increase in h_{air} will have a cooling effect on the skin surface temperature; at the same time, heat transfer coefficients are known to depend on surface temperature [63, 64]. Further, skin temperature is known to decrease as T_A and T_{air} decrease, as indicated by thermoregulatory studies [40].

Table VII. Proportionality relation for variation of fingertip temperature during parametric studies using zero-order model. The superscript indicates the model used.

Parameter	Proportionality	Plot
β^0	$\beta^0 \propto \left[\mathrm{TR}^0, \frac{1}{t^0_{\mathrm{TR}}}\right]$	Fig. 14
τ_h^0	$\tau_h^0 \propto \left[\mathrm{TR}^0, t^0_{\mathrm{TR}}\right]$	Fig. 15
t^0_{dw}	$t^0_{dw} \propto \left[\mathrm{TR}^0, \mathrm{TD}^0, \frac{1}{t^0_{\mathrm{TR}}}, \frac{1}{t^0_{\mathrm{TD}}}\right]$	Fig. 16
h^0_{air}	$h^0_{air} \propto \left[\frac{1}{\mathrm{TR}^0}, \mathrm{TD}^0, \frac{1}{t^0_{\mathrm{TR}}}\right]$	Fig. 17
T^0_{air}	$T^0_{air} \propto \left[\mathrm{TR}^0, \frac{1}{\mathrm{TD}^0}, t^0_{\mathrm{TR}}\right]$	Fig. 18
T^0_A	$T^0_A \propto \left[\mathrm{TR}^0, \frac{1}{t^0_{TR}}\right]$	Fig. 19
T^0_i	$T^0_i \propto \left[\frac{1}{\mathrm{TR}^0}, \mathrm{TD}^0, \frac{1}{t^0_{\mathrm{TR}}}\right]$	Fig. 20

Table VIII. Dependence of initial temperature, (T_i) on parameters in the zero-order model. The superscript indicates the model used.

Parameter	Proportionality	Plot
h^0_{air}	$h^0_{air} \propto \left[\frac{1}{T^0_i}\right]$	Fig. 21(A)
T^0_{air}	$T^0_{air} \propto [T^0_i]$	Fig. 22(A)
T^0_A	$T^0_A \propto [T^0_i]$	Fig. 23(A)

1. Coupled Zero-Order Model

To illustrate this relationship between T_i and parameters h_{air}, T_{air}, and T_A illustrated in the previous paragraph; the zero-order model was modified and coupling between T_i and the aforementioned parameters was introduced by the following relation:

$$Ti \;=\; \frac{h_{air}AT_{air} + \rho_b C_{p_b} w_0 T_A}{h_{air}A + \rho_b C_{p_b} w_0}, \tag{5.4}$$

which was obtained by solving Eq. 5.1 at steady state. In this modified or coupled zero-order model, T_i was allowed to change as the above parameters (h_{air}, T_{air}, T_A) change. Using Eq. 5.4 the variation of T_i with the above parameters was plotted. It can be seen from Figures 21(A), 22(A) and 23(A) that T_i is inversely proportional to h_{air}; and directly proportional to both T_{air} and T_A. These proportionality relationships are summarized in Table VIII.

The thermal response or variations in TR and TD calculated in response to changes in: **(1)** h_{air} and T_i **(2)** T_{air} and T_i **(3)** T_A and T_i are shown in Figures 21(B), 22(B) and 23(B). The proportionality relationships observed among these coupled

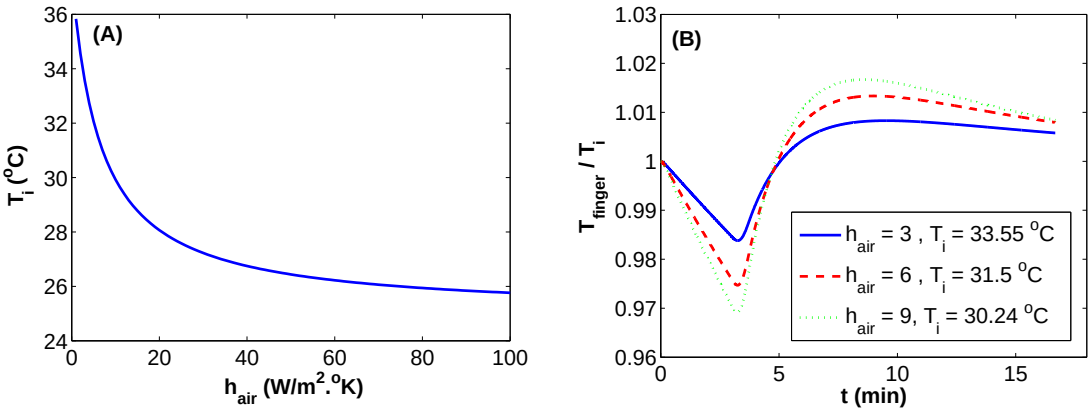

Fig. 21. **(A)** Dependence of T_i on h_{air}, **(B)**Effect of variation in h_{air} on temperature during reactive hyperemia including the variation in T_i, calculated using the coupled zero-order model.

parameters are then summarized in Table IX.

Comparing the proportionality relations for h_{air}, T_i, T_A, and T_i obtained from the zero-order model (see Table VII), with the proportionality relations obtained after considering the coupling between them (see Table IX), we can make the following observations:

(i) Coupling between h_{air} and T_i: From Fig. 21(B), it can be concluded that T_i enforces a greater influence on the maximum rebound temperature (TR) than h_{air}; whereas the maximum temperature drop TD, is strongly influenced by h_{air} as compared to T_i.

(ii) Coupling between T_{air} and T_i: From Fig. 22(B), it can be noted that T_i enforces a greater influence on the rebound temperature (TR) than T_{air}; whereas maximum temperature drop TD, is strongly influenced by T_{air} as compared to T_i.

(iii) Coupling between T_A and T_i: From Fig. 23(B), it can be noted that the effects

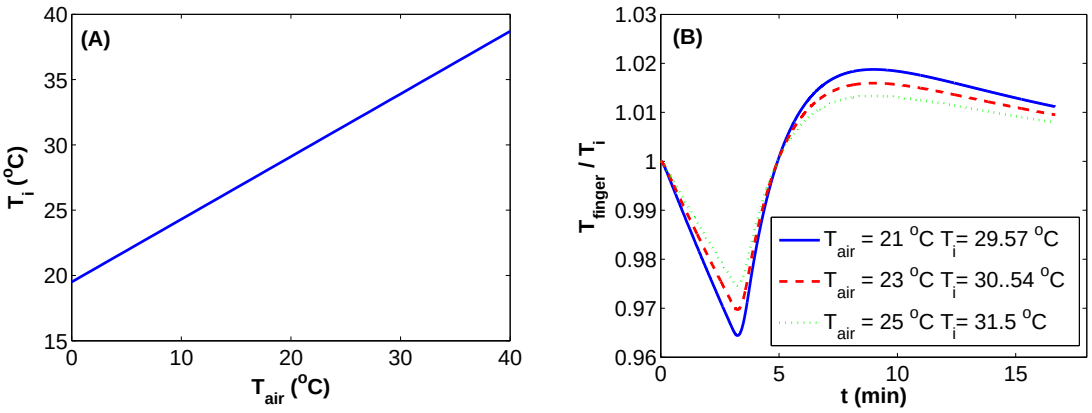

Fig. 22. **(A)** Dependence of T_i on T_{air}, **(B)** Effect of variation in T_{air} on temperature during reactive hyperemia including the variation in T_i, calculated using the coupled zero-order model.

of T_i and T_A almost cancel each other and the resulting thermal response is very less sensitive to minor changes in body temperature T_A.

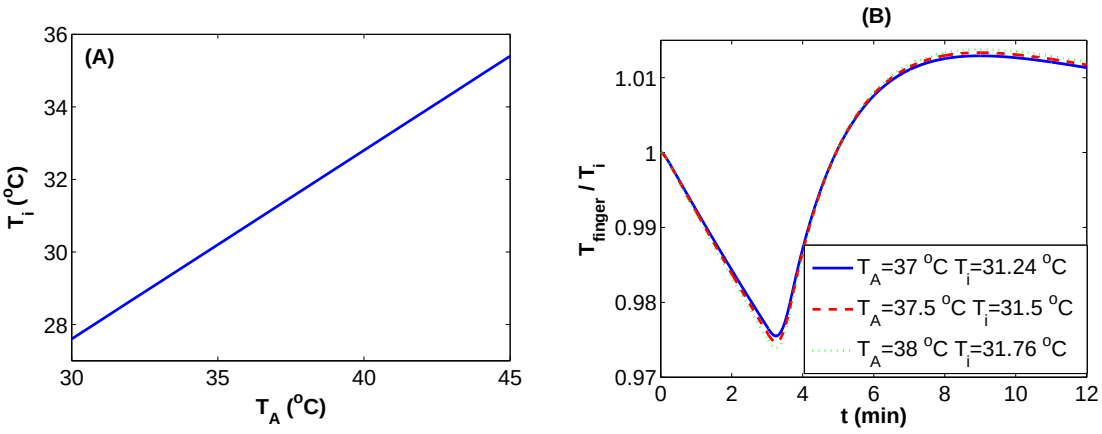

Fig. 23. **(A)** Dependence of T_i on T_A, **(B)**Effect of variation in T_A on temperature during reactive hyperemia including the variation in T_i, calculated using the coupled zero-order model.

Table IX. Proportionality relations considering coupling between T_i and the parameters h_{air}, T_{air}, T_A on thermal response of the finger using coupled zero-order model. The superscript indicates the model used.

Parameter	Proportionality	Plot
h^0_{air}	$h^0_{air} \propto \left[\mathrm{TR}^0, \mathrm{TD}^0, \frac{1}{T_i^0}\right]$	Fig. 21(B)
T^0_{air}	$T^0_{air} \propto \left[\frac{1}{\mathrm{TR}^0}, \frac{1}{\mathrm{TD}^0}, T_i^0\right]$	Fig. 22(B)
T^0_A	$T^0_A \propto \left[\mathrm{TR}^0, \mathrm{TD}^0, T_i^0\right]$	Fig. 23(B)

CHAPTER VI

FIRST ORDER MODEL

The zero-order model has proved to be useful for carrying out a parametric analysis of the effect of various factors such as $\beta, \tau_h, t_{dw}, h_{air}, T_{air}, T_A, T_i$, on the temperature variation at the fingertip. However as already mentioned, the zero-order model does not take into account: (1) temperature variations within the tissue, (2) metabolic heat generation within the tissue, (3) the influence of the different tissues such as skin, fat, muscle, and, bone present in the finger, (4) size and shape of finger. The first order model was therefore developed to take into account and analyze the effect of these factors on fingertip temperature.

A. Assumptions

The first order model addresses some of the assumptions made in the zero-order model, however because of the complexity of modeling tissue heat transfer, it is still based on some acceptable assumptions which are used to simplify the model. The assumptions made in the first order model are summarized as follows:

(i) The skin, fat, and, muscle tissue layers are assumed to be of uniform thickness throughout the finger. The finger consists of bone at the center, which is enveloped by layers of muscle, fat, and skin of uniform thickness throughout the length of the finger.

(ii) The anatomical geometry of the finger is very complex and three dimensional in nature. To simplify the modeling process in the first order model, finger geometry is assumed to be an axis-symmetric tapered cylinder.

(iii) The thermo-physical properties of the tissues considered are assumed to be

isotropic within each layer and independent of temperature. The thermophysical properties for hand tissue layers given in [33] were used for the respective layers for a finger in the first-order model and are shown in Table. XI.

(iv) The metabolic heat generation within all the layers is assumed to be uniform and constant[33]. As the source term due to metabolic heat generation is orders of magnitude smaller than the source term due to blood perfusion, metabolic heat generation was assumed constant during the DTM experiment.

(v) Blood perfusion within bone is neglected and that within the fat and muscle tissue is assumed non-zero and uniform throughout the finger [33].

(vi) Skin tissue of human finger has an abundant distribution network of blood capillaries and the fingertips have a large concentration of blood capillaries and nerve endings as observed from the arteriograms [57]. Also the blood flow in the hand is predominantly through the skin [58]. On this basis the blood perfusion (ω_{01}), in the skin is assumed to vary along the axial direction i.e. $\omega_{01} = G(z)$.

(vii) The function $G(z)$ was not available in the literature and is unknown. It was assumed to be a quadratic function of z (as a first approximation) after a trial and error process of trying to match the skin surface temperature obtained from the model with that of from IR image available for the finger and is given by $G(z) = (93.469x^2 - 5.266x + 0.5665)\omega_{01}$. Determination of a precise function for G(z) using inverse heat conduction formulation is the subject of the next chapter.

(viii) Blood perfusion and metabolic heat generation are assumed to be independent of temperature. In reality, blood perfusion and metabolic heat generation will be affected by temperature following the Arrhenius equations [62], and also because

of thermoregulatory feedback mechanism present in the body. As mentioned in the previous chapter, these aspects will be included in the second order models which are the subject of future studies.

(ix) Continuity of temperature and heat flux was assumed between the layers of tissue. This is a common approximation in biological systems, when dealing with layered type models [65].

B. Governing Equation

In the first order model, heat transfer phenomena in the finger was modeled by the Pennes bioheat equation. This governing equation, Eq. (6.1), was solved simultaneously for the four layers of tissue coupled by temperature and heat flux continuity at the interface of two layers. In the first order model, for compactness and convenience, a tensor notation is used for the different symbols, with skin as (j=1), fat as (j=2), muscle as (j=3), and, bone as (j=4) where appropriate. The governing equation can be given by:

$$\rho_j C_{p_j} \frac{\partial T_j}{\partial t} \;=\; k_j \nabla^2 T_j \;+\; \rho_b C_{p_b} \omega_{bj}(t)(T_A - T_j) \;+\; q_{mj}, \;\text{ at } \Omega_j \tag{6.1}$$

where, $k_j, \rho_j, C_{p_j}, \omega_{bj}, q_{mj}$ represent the thermal conductivity, density, specific heat, blood perfusion and metabolic heat generation of the respective tissue layers (Ω_j). ρ_b, C_{p_b} is density and specific heat of blood. T_A is the body or core temperature and is assumed to be a constant, its base case value being 37.5 ^oC . The base case values of the above properties are summarized in Table XI.

The Laplace operator in axis-symmetric coordinate system is given by Eq. (6.2).

$$\nabla^2(\cdot) \;=\; \left(\frac{\partial^2}{\partial r^2} \;+\; \frac{1}{r}\frac{\partial}{\partial r} \;+\; \frac{\partial^2}{\partial z^2} \right)(\cdot) \tag{6.2}$$

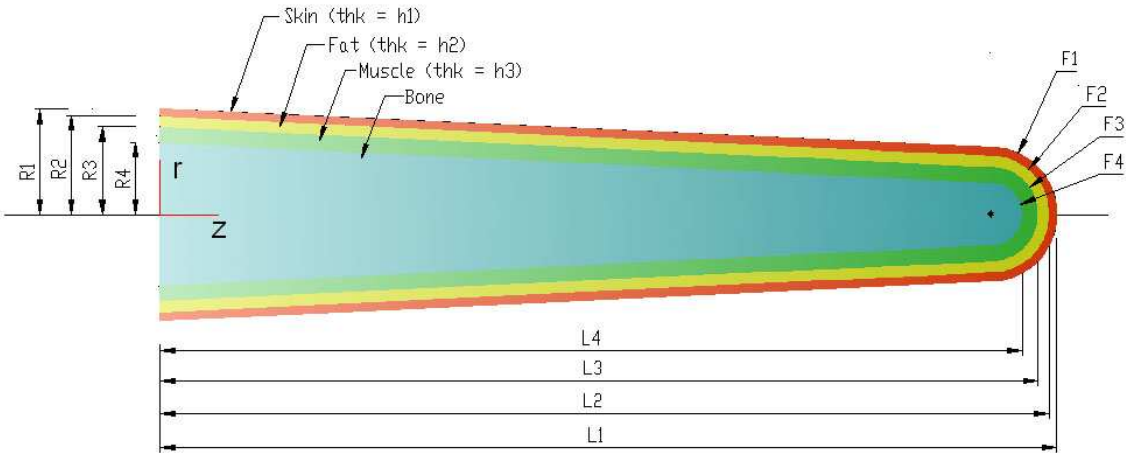

Fig. 24. First order model geometry illustrating the nomenclature for the dimensions.

Table X. Base case geometrical dimensions used for first order model.

Dimension	Symbol	Skin	Fat	Muscle	Bone
Length,(mm)	L_j	73	72.4	71.5	70.2
Base radius,(mm)	R_j	8.6	8.0	7.1	5.8
Fingertip curvature radius,(mm)	F_j	5.4	4.8	3.9	2.6
Layer thickness,(mm)	h_j	0.6	0.9	1.3	-

C. Model Geometry and Tissue Properties

In this model, the shape of the finger is approximated by a 2D axis-symmetric tapered cylinder with a hemispherical end as seen in Fig. 24; r and z being the radial and axial coordinates respectively. The finger tissue structure is assumed to formed by four discrete layers (Ω_j), viz. skin, fat, muscle and bone. The detailed base case dimensions used for the model can be seen in Fig. 24 and are provided in Table. X. The numerical values for the base case thermo-physical properties are given in XI.

Table XI. Thermo-physical properties [33] used for first order model.

Properties	Skin	Fat	Muscle	Bone	Blood
$\rho_j, (kg/m^3)$	1085	850	1085	1357	1069
$C_{p_j}, (J/kg.K)$	3680	2300	3768	1700	3659
$k_j, (W/m.K)$	0.47	0.16	0.42	0.75	-
$\omega_{0j}, (m^3/s.m^3)$	$4.54e^{-3}$	$3.6e^{-6}$	$5.38e^{-4}$	0	-
$q_{mj}, (W/m^3)$	368	58	684	368.3	-

D. Initial and Boundary Conditions

The governing equation given by Eq. (6.1) is solved for each of the four layers simultaneously using appropriate boundary and initial conditions.

1. The external surface of the skin layer is exposed to air at a temperature of T_{air} with a convection coefficient of (h_{air}). h_{air} is assumed constant during the calculation and at every point at the surface.

$$\vec{n} \cdot (k_1 \nabla T_1)\Big|_{\Gamma_{12}} = h_{air}(T_{air} - T_1)\Big|_{\Gamma_{12}}, \tag{6.3}$$

   where, T_1 represents the temperature in the skin layer (Ω_1); and Γ_{12} represents the outer surface of the skin exposed to air. A better approximation for h_{air} will involve considering its dependence on T_{air} and the skin surface temperature [63, 64].

2. Each one of the four layers of tissue at the base of the finger are subjected to a heat flux, (q_{flux}) due to temperature gradient between the hand and the respective layers. The numerical value for q_{flux} is not available in the literature, therefore a trial and error process was used to come up with a first approxima-

tion for q_{flux}, such that the temperature at the surface of the skin is similar to that obtained from the IR images. q_{flux_j} was assumed constant and equal to 5 $W/m^2.^oK$ A precise approximation for q_{flux} can be obtained by setting up a inverse heat conduction problem, which will be conducted in future studies.

$$\vec{n} \cdot (k_j \nabla T_j)\Big|_{\Gamma_{j1}} = q_{flux_j}, \tag{6.4}$$

where, Γ_{j1}, $(j = 1, 2, 3, 4)$ represents the interface between hand and respective layer at the base of the finger.

3. The interfaces between the layers, *viz.* bone-muscle interface, muscle-fat interface and fat-skin interface are subjected to continuity of heat flux and temperature.

$$T_j\Big|_{\Gamma_{j3}} = T_i\Big|_{\Gamma_{i2}}, \quad \text{for } j = 1, 2, 3;\ i = j + 1, \tag{6.5a}$$

$$\vec{n} \cdot (k_j \nabla T_j)\Big|_{\Gamma_{j3}} = \vec{n} \cdot (k_i \nabla T_i)\Big|_{\Gamma_{i2}}, \quad \text{for } j = 1, 2, 3;\ i = j + 1, \tag{6.5b}$$

where, k_j, k_i are the thermal conductivities of the two layers across an interface; Γ_{j3}, $(j = 1, 2, 3)$ represent the inner surface of skin, fat and muscle as seen in Fig. 24; Γ_{i2}, $(i = 2, 3, 4)$represent the outer surface of fat, muscle and bone as seen in Fig. 24.

4. The solution of steady state governing equation, $(T_i(r, z), t = 0)$ is used as the initial condition for solving the transient governing equation given by Eq. (6.1).

$$T = T_i(r, z), \quad \text{at } t = 0 \tag{6.6}$$

Table XII. List of parameters varied to study their effect on finger temperature during hyperemia using first order model.

Parameter	Base Value	Variation
β	3	2, 3, 4
τ_h	120 s	60, 120, 180
t_{dw}	45 s	25, 35, 45
h_{air}	6 $W/m^2.K$	3, 6, 9
T_{air}	25 ^oC	21, 23, 25
T_A	37.5 ^oC	37, 37.5, 38

E. Model Results

The first-order model was solved using FEM in COMSOL Multiphysics. For carrying out the parametric study, COMSOL Script along with MATLAB was used. A grid independence test was carried out to find the optimum grid, which consisted of a triangular mesh of 8116 elements. The parameters varied during the study and the variation in their values can be summarized in Table XII.

In Chapter V, a parametric study was performed on the zero-order model, classifying the parameters into 3 groups. The zero-order model is also validated using experiments described in Chapter VIII. Validation of the first order model was not performed, due to non-availability of the required experimental setup as will be discussed in Chapter VIII. Therefore, calculations done using the first order model will be compared to that of the zero-order model.

The parameters varied were classified into 4 groups *v.i.z*: hemodynamic factors (β, τ_h, t_{dw}), environmental factors (h_{air}, T_{air}), physiological factors (T_A, T_i), anthro-

pometric factors (h_1, h_2, h_3, L_1). As in the zero-order model presented in Chapter V, each parameter was varied in turn, keeping all the other parameters constant at their base case values as seen in Tables III and XII. In the first order model, anthropometric factors is an additional group among the factors being considered for the parametric study which affect the finger thermal response; these factors consider changes in layer size (h_j,R_4) and length of the finger (L_1). However their effect will not be presented here as these factors are not present in the zero-order model and at this stage of the research we are interested in comparing zero-order and first order models. The thermal response of the finger was characterized by 4 terms: the maximum rebound temperature, (TR), the time required to achieve TR, (t_{TR}), the maximum drop in temperature (TD), the time required to achieve TD, (t_{TD}) and are illustrated in Fig. 13.

To study the effect of a single parameter over the thermal response; the initial blood perfusion (ω_0) was maintained constant throughout the parametric study.

In the first order model a steady state solution is used as the initial condition for the transient problem. Whenever any parameter other than the hemodynamic factors is varied, the steady state solution changes, thus altering the initial temperature distribution, $T_i(r, z)$. As a result, the parametric study shows a combined effect of the change in the (hemodynamic, physiological, or anthropometric) parameter considered and a change in the initial temperature $T_i(r, z)$. This coupling is a direct characteristic of the first order model. Unlike the zero-order model, where it was possible to force the initial temperature to be a constant in spite of variations in any parameter; in the first order model, this could not be forced upon the model, as the model is more realistic and highly coupled in nature. In the next paragraphs the effect of 6 parameters over TR, TD and T_i is presented and the results are summarized in Table XIII; this table also shows a comparison withe zero-order model (Table VII).

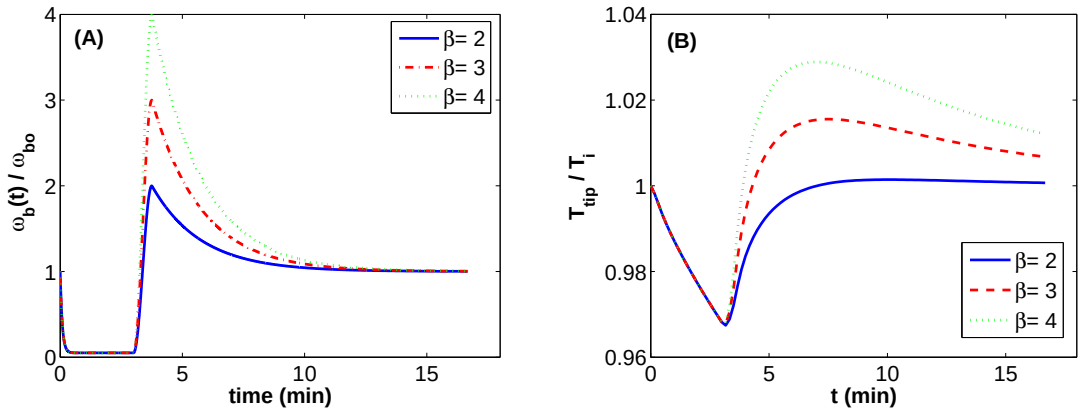

Fig. 25. **(A)** Blood perfusion due to variation in β during reactive hyperemia, **(B)** Effect of variation in β on temperature during reactive hyperemia, calculated using the first order model.

The effect of factors affecting the fingertip temperature can be summarized as follows:

(i) Effect of hemodynamic factors:

(a) Maximum hyperemic blood flow (β): β is found to be strongly correlated to the maximum rebound temperature (TR) as can be seen in Fig. 25, similar to the zero-order model. The proportionality for β is given by:

$$\beta \propto \left[\mathrm{TR}, \frac{1}{t_{\mathrm{TR}}}\right]. \tag{6.7}$$

(b) Rate at which blood flow drops to baseline after hyperemia (τ_h): τ_h is directly proportional to the maximum rebound temperature (TR) as can be seen in Fig. 26, similar to the zero-order model. The proportionality for τ_h is given by:

$$\tau_h \propto [\mathrm{TR}, t_{\mathrm{TR}}]. \tag{6.8}$$

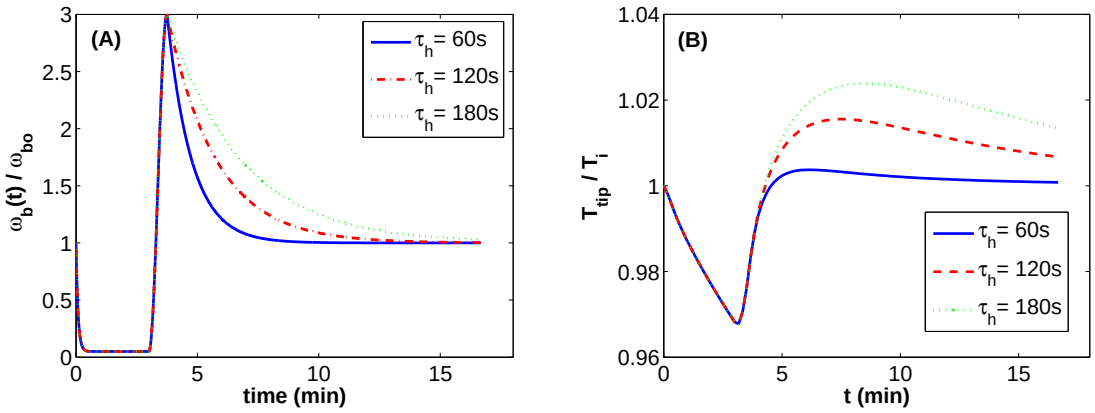

Fig. 26. **(A)** Blood perfusion due to variation in τ_h during reactive hyperemia **(B)** Effect of variation in τ_h on temperature during reactive hyperemia, calculated using the first order model.

(c) Time required to reach maximum hyperemic blood flow (t_{dw}): t_{dw} is found to be the only parameter other than τ_0 which influences the t_{TD}, *i.e.* the time required to reach the lowest drop in temperature, as can be seen in Fig. 27. The proportionality for t_{dw} is given by:

$$t_{dw} \propto \left[\mathrm{TR}, \mathrm{TD}, \frac{1}{t_{\mathrm{TR}}}, \frac{1}{t_{\mathrm{TD}}}\right]. \tag{6.9}$$

(ii) Effect of environmental factors:

(a) External heat convection coefficient (h_{air}): The heat transfer coefficient is found to inversely affect the steady state or initial temperature of the finger, (T_i). Fig. 28, shows the combined effect of variation in h_{air} and T_i. Comparing the proportionality relations for h_{air} and T_i obtained from the zero-order model (Table VII) with Eq. 6.10 , it can be concluded that T_i, enforces a greater influence on the maximum rebound temperature (TR),

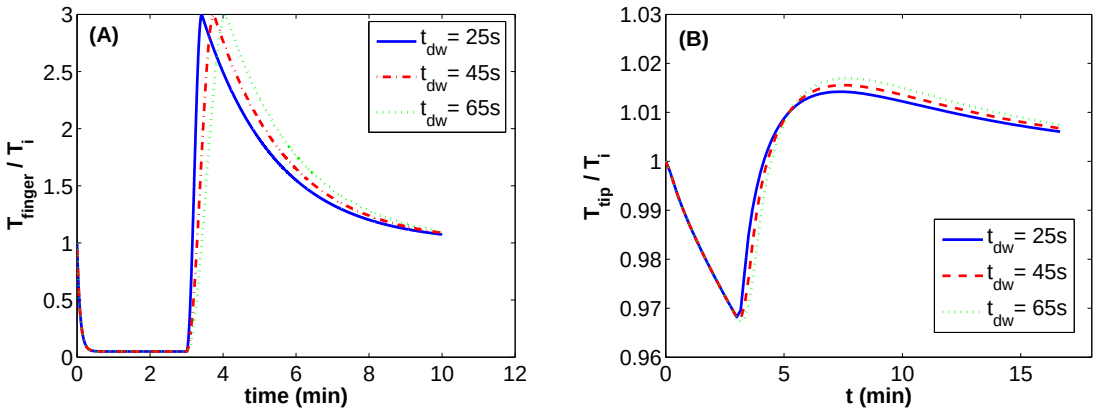

Fig. 27. **(A)** Blood perfusion due to variation in t_{dw} during reactive hyperemia, **(B)** Effect of variation in t_{dw} on temperature during reactive hyperemia, calculated using the first order model.

than h_{air}, whereas maximum temperature drop (TD) is strongly influenced by h_{air} as compared to T_i. The proportionality for h_{air} is given by:

$$h_{air} \propto \left[\mathrm{TR}, \mathrm{TD}, \frac{1}{T_i}\right]. \tag{6.10}$$

(b) Surrounding air temperature (T_{air}): A variation in the ambient temperature is found to be directly proportional to T_i. Fig. 29, shows the combined effect of variation in T_{air} and T_i. Comparing proportionality relations for T_{air} and T_i obtained from the zero-order model (Table VII) with Eq. 6.11, it can be noted that T_i, enforces a greater influence on the rebound temperature (TR), than T_{air}, whereas maximum temperature drop (TD) is strongly influenced by T_{air} as compared to T_i. The proportionality for T_{air} is given by:

$$T_{air} \propto \left[\frac{1}{\mathrm{TR}}, \frac{1}{\mathrm{TD}}, T_i\right]. \tag{6.11}$$

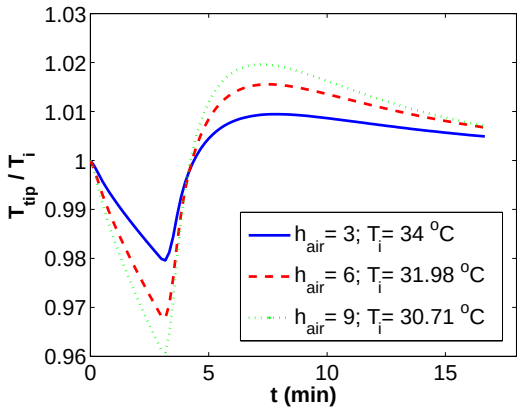

Fig. 28. Effect of variation in h_{air} on temperature during reactive hyperemia, calculated using the first order model.

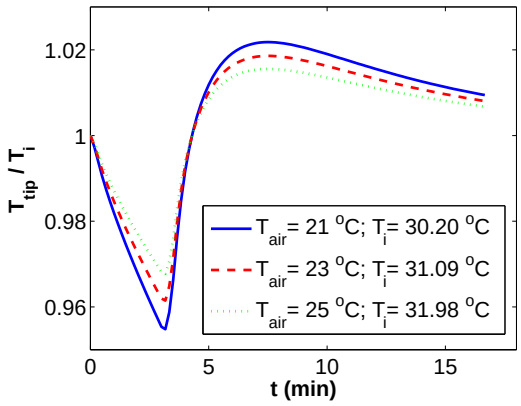

Fig. 29. Effect of variation in T_{air} on temperature during reactive hyperemia, calculated using the first order model.

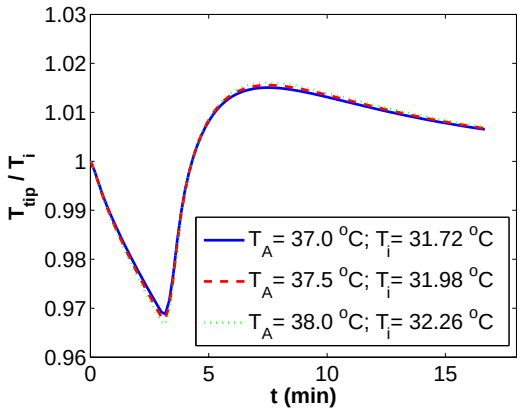

Fig. 30. Effect of variation in T_A on temperature during reactive hyperemia, calculated using the first order model.

(iii) Effect of physiological factors:

(a) Body temperature (T_A): A variation in the body temperature is found to be directly proportional to (T_i). Fig. 30, shows the combined effect of variation in T_A and T_i. Comparing proportionality relations for T_A and T_i obtained from the zero-order model (Table VII) with Eq. 6.12, it can be noted that the effects of T_i and T_A almost cancel each other and the resulting thermal response is very less sensitive to minor changes in body temperature T_A. The proportionality for T_A is given by:

$$T_A \propto [\mathrm{TR}, \mathrm{TD}, T_i]\,. \tag{6.12}$$

The proportionality relations obtained for the first order model are compared with that of the zero-order and coupled zero-order models and are summarized in Table XIII. It can be seen from such comparison that the proportionality relations for the first order model are identical with those of the zero-order model for parameters

Table XIII. Comparison of the proportionality relations for the zero-order, coupled zero-order and first order models. Superscript indicates the model used.

Zero-order	Coupled zero-order	First order
$\beta^0 \propto \left[\mathrm{TR}^0, \frac{1}{t^0_{\mathrm{TR}}}\right]$	-	$\beta^1 \propto \left[\mathrm{TR}^1, \frac{1}{t^1_{\mathrm{TR}}}\right]$
$\tau^0_h \propto \left[\mathrm{TR}^0, t^0_{\mathrm{TR}}\right]$	-	$\tau^1_h \propto \left[\mathrm{TR}^1, t^1_{\mathrm{TR}}\right]$
$t^0_{dw} \propto \left[\mathrm{TR}^0, \mathrm{TD}^0, \frac{1}{t^0_{\mathrm{TR}}}, \frac{1}{t^0_{\mathrm{TD}}}\right]$	-	$t^1_{dw} \propto \left[\mathrm{TR}^1, \mathrm{TD}^1, \frac{1}{t^1_{\mathrm{TR}}}, \frac{1}{t^1_{\mathrm{TD}}}\right]$
$h^0_{air} \propto \left[\frac{1}{\mathrm{TR}^0}, \mathrm{TD}^0, \frac{1}{t^0_{\mathrm{TR}}}\right]$	$h^0_{air} \propto \left[\mathrm{TR}^0, \mathrm{TD}^0, \frac{1}{T^0_i}\right]$	$h^1_{air} \propto \left[\mathrm{TR}^1, \mathrm{TD}^1, \frac{1}{T^1_i}\right]$
$T^0_{air} \propto \left[\mathrm{TR}^0, \frac{1}{\mathrm{TD}^0}, t^0_{\mathrm{TR}}\right]$	$T^0_{air} \propto \left[\frac{1}{\mathrm{TR}^0}, \frac{1}{\mathrm{TD}^0}, T^0_i\right]$	$T^1_{air} \propto \left[\frac{1}{\mathrm{TR}^1}, \frac{1}{\mathrm{TD}^1}, T^1_i\right]$
$T^0_A \propto \left[\mathrm{TR}^0, \frac{1}{t^0_{TR}}\right]$	$T^0_A \propto \left[\mathrm{TR}^0, \mathrm{TD}^0, T^0_i\right]$	$T^1_A \propto \left[\mathrm{TR}^1, \mathrm{TD}^1, T^1_i\right]$

β, τ_h, and t_{dw}; whereas the proportionality relations for the first order model are identical with those of the coupled zero-order model for the parameters h_{air}, T_{air} and T_A.

CHAPTER VII

INVERSE HEAT CONDUCTION PROBLEM (IHCP)

As mentioned in Chapter VI, the boundary condition at the finger base, as well as a function describing axial variation of blood perfusion in the finger are missing. This chapter describes the setting up and solution of an inverse problem that can be used to find one of these unknowns. This work only focuses on the determination of the steady state (or initial) axial blood perfusion function. The mathematical and numerical implementation is described, however the analysis has not been finished due to the unavailability of direct measurements.

A. Need for an Inverse Problem

In the first order model, the finger geometry was approximated by a 2D axis-symmetric tapered cylinder composed of four layers: skin, fat, muscle and bone. The blood perfusion in the different layers varies drastically, with blood perfusion in the skin being the highest, and lowest in the fat layers and absent in the bone layer. Early numerical experiments with the first order model were carried out with a uniform blood flow distribution for the different layers in the finger. However, such an approximation failed to depict the observed variation in the temperature distribution along the finger observed with IR images of finger as can be seen in Fig. 31.

Description of the regional variation of skin perfusion function (ω_{b1}) is not available in the literature. In this work, a inverse heat transfer problem was proposed and solved to determine the axial distribution of blood perfusion in the skin layer. The problem studied was simplified to deal only with the steady state distribution. This gives a good initial approach as the temporal variation of blood perfusion during DTM is known to follow the relationships presented in Chapter IV. We will now

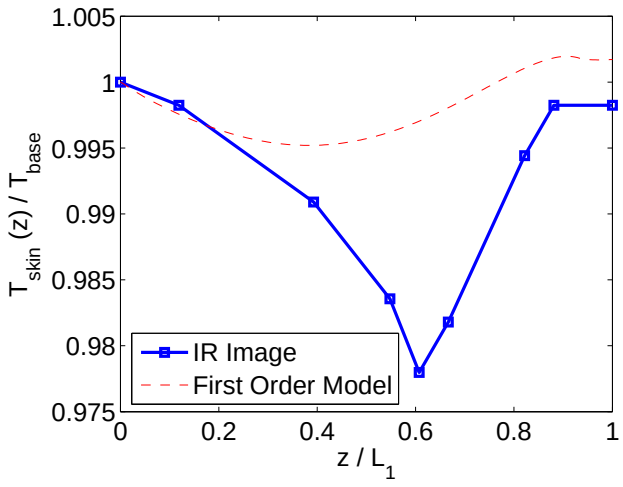

Fig. 31. Comparison of the temperature distribution along the skin surface obtained from IR image of the finger and first order model (assuming a quadratic blood perfusion function).

discuss what exactly is a inverse heat transfer problem.

B. Concept of an Inverse Heat Conduction Problem

In a direct problem, we solve for the temperature distribution in the defined geometry given the boundary conditions, the heat generation and the thermo-physical properties for the system. However in a inverse problem, we solve for the boundary conditions, the thermo-physical properties, or the source term by specifying the temperature or heat flux at certain points. In general terms, in a direct problem, the cause is given and the effect is determined, whereas in a inverse heat transfer problem, the effect (or effects) is given and the cause is determined. As inverse heat transfer problem can be a problem about unknown initial condition, boundary condition, source term, thermo-physical properties and so on.

An inverse problem can be solved by a *parameter estimation* or *function estimation* approach. If some information is available about the form of the function of the

unknown quantity, the inverse estimation is reduced to the estimation of few unknown parameters forming the function. However if prior information is unavailable regarding the functional form of the unknown quantity, the inverse problem is approached by a function estimation approach in an infinite dimensional space of functions.

C. Steps in Setting up the Inverse Problem for Optimizing Axial Skin Blood Perfusion, $(\omega_{b1}(z))$

The blood perfusion in the skin layer was solved as a inverse heat conduction problem (IHCP) using a *function estimation* approach; this method is selected because no prior information is available regarding the form of the function describing the axial blood perfusion distribution is known.

Solving the IHCP for blood perfusion can be stated as finding the unknown functional form for axial blood perfusion distribution $(\omega_{b1}(z))$, such that the temperature on the skin surface, calculated from the direct problem (first order model at steady state), $T_1(r, z)$ matches the temperature on the skin surface observed from an available IR images, $Y(r, z)$ such as Fig. 10. In other words, IHCP can be stated as an optimization problem involving the minimization of the error between the calculated and the observed temperature along the skin surface. The goal of the minimization problem is to achieve the desired skin blood perfusion function $(\omega_{b1}(z))$ by minimizing an objective function, $S\big[\omega_{b1}(z)\big]$, given by:

$$S\big[\omega_{b1}(z)\big] = \frac{1}{2}\sum_{m=1}^{M}\Big\{T_1[r_m, z_m; \omega_{b1}(z)] - Y_m\Big\}^2, \tag{7.1}$$

where, S is the objective functional given by least squares error between calculated and observed temperatures; $\omega_{b1}(z)$ is the unknown blood perfusion function or source function to be optimized; M is the number of points along the skin at which temper-

ature is matched; $T_m(r_m, z_m)$ is the temperature calculated from the first order model by solving the direct problem given in the Chapter VI and Y_m is the observed temperature from IR images, respectively at the specified points (r_m, z_m), for $m = 1, 2, ..., M$ along the skin. It must be noted that IHCP are inherently ill-posed in nature [66]. Further, the direct problem (Eq. 7.2 - 7.5) is nonlinear and therefore, the functional to be minimized may have local minima.

A iterative procedure is used to find the optimum skin blood perfusion function such that the objective functional, S approaches zero. The technique used for iteratively solving the IHCP restate as a minimization problem the *conjugate gradient method with adjoint problem* was used [67]. This method belongs to the class of *iterative regularization techniques*. The iterative regularization represents the class of techniques in no explicit regularization term is added like the *Tikhonov regularization*, but the number of iterations itself act as the regularization parameter [68].

The conjugate gradient method (CGM) is a method in which the search directions are so selected that they are orthogonal to each other. Therefore unlike the steepest descent method, the search is never repeated along the same direction, thus reducing the number of iterations significantly. In fact a linear CGM takes at the most n number of iterations to converge, where $\omega_{b1}(z) \in R^n$ where R^n is an $n-$dimensional space.

The steps required to solve the inverse problem are summarized by the algorithm in Fig. 32. At the start of the procedure, $(\omega_{b1}^0(z))$ is initialized to some intelligent guess value. Next the direct problem (Eq. 7.2 - 7.5) is solved to find the temperature along the skin surface $(T_1(r, z))$. The objective functional (S) is checked to see if it is less than the permissible error. Next an adjoint problem (Eq. 7.26 - 7.29) is solved to calculate the Lagrangian multiplier $(\lambda_j(r, z))$ which is required for finding the gradient of objective functional (∇S) as will be explained later. The conjugation coefficient

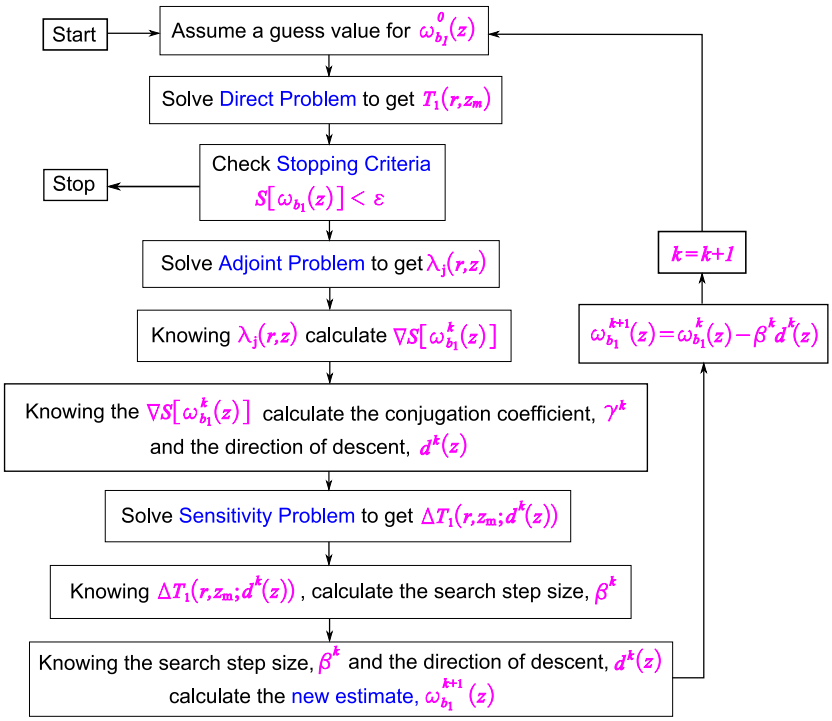

Fig. 32. Algorithm for solving the inverse heat conduction problem to optimize axial skin blood perfusion function ($\omega_{b1}(z)$), using conjugate gradient method with adjoint problem.

(γ^k) is computed using the Fletcher-Reeves expression [68, 66] to calculate the direction of descent ($d^k(z)$) for the next iteration. The search step size (β^k) is calculated for each iteration k, using a simple line search algorithm along $d^k(z)$ which requires the gradient of the objective functional and the solution of the sensitivity problem $\Delta T_1(r,z)$ (Eq. 7.11 - 7.14). Knowing the search step size (β^k) and the direction of descent ($d^k(z)$) a new estimate for the blood perfusion function ($\omega_b^{k+1}{}_1(z)$) is determined, followed by the repetition of entire procedure until the objective functional (S) is minimized.

The IHCP for optimization of axial skin blood perfusion function $\omega_{b1}(z)$ was setup using the steps outlined below:

1. Direct Problem
2. Inverse Problem
3. Sensitivity Problem
4. Adjoint Problem
5. Gradient Equation
6. Iterative Procedure
7. Stopping Criteria

The subsequent sections will now describe each of the steps taken to setup the IHCP.

1. Direct Problem

The direct problem involves solving for the temperature field in all the layers simultaneously at steady state using the first order model. As already described in Chapter VI, the mathematical formulation for the direct problem (at steady state) is given by:

For skin ($j = 1$),

$$\mathscr{C}_1 : \quad k_1 \nabla^2 T_1 + \rho_b C_{p_b} \omega_{b1}(z)(T_A - T_1) + q_{m1} \; = \; 0 \tag{7.2a}$$

$$\vec{n}_{11} \cdot (k_1 \nabla T_1)\big|_{\Gamma_{11}} \; = \; q_{flux_1}, \tag{7.2b}$$

$$\vec{n}_{12} \cdot (k_1 \nabla T_1)\big|_{\Gamma_{12}} \; = \; h_{air}(T_{air} - T_1)\big|_{\Gamma_{12}}, \tag{7.2c}$$

$$T_1\big|_{\Gamma_{13}} \quad = \quad T_2\big|_{\Gamma_{22}}, \tag{7.2d}$$

$$\vec{n}_{13} \cdot (k_1 \nabla T_1)\big|_{\Gamma_{13}} \quad = \quad \vec{n}_{22} \cdot (k_2 \nabla T_2)\big|_{\Gamma_{22}}, \tag{7.2e}$$

For fat ($j = 2$),

$$\mathscr{C}_2 : \quad k_2\nabla^2 T_2 + \rho_b C_{p_b}\omega_{b2}(T_A - T_2) + q_{m2} \;=\; 0 \tag{7.3a}$$

$$\vec{n}_{21} \cdot (k_2 \nabla T_2)\big|_{\Gamma_{21}} \;=\; q_{flux2}, \tag{7.3b}$$

$$T_2\big|_{\Gamma_{22}} \;=\; T_1\big|_{\Gamma_{13}}, \tag{7.3c}$$

$$\vec{n}_{22} \cdot (k_2 \nabla T_2)\big|_{\Gamma_{22}} \;=\; \vec{n}_{13} \cdot (k_1 \nabla T_1)\big|_{\Gamma_{13}}, \tag{7.3d}$$

$$T_2\big|_{\Gamma_{23}} \;=\; T_3\big|_{\Gamma_{32}}, \tag{7.3e}$$

$$\vec{n}_{23} \cdot (k_2 \nabla T_2)\big|_{\Gamma_{23}} \;=\; \vec{n}_{32} \cdot (k_3 \nabla T_3)\big|_{\Gamma_{32}}, \tag{7.3f}$$

For muscle ($j = 3$),

$$\mathscr{C}_3 : \quad k_3\nabla^2 T_3 + \rho_b C_{p_b}\omega_{b3}(T_A - T_3) + q_{m3} \;=\; 0 \tag{7.4a}$$

$$\vec{n}_{31} \cdot (k_3 \nabla T_3)\big|_{\Gamma_{31}} \;=\; q_{flux3}, \tag{7.4b}$$

$$T_3\big|_{\Gamma_{32}} \;=\; T_2\big|_{\Gamma_{23}}, \tag{7.4c}$$

$$\vec{n}_{32} \cdot (k_3 \nabla T_3)\big|_{\Gamma_{32}} \;=\; \vec{n}_{23} \cdot (k_2 \nabla T_2)\big|_{\Gamma_{23}}, \tag{7.4d}$$

$$T_3\big|_{\Gamma_{33}} \;=\; T_4\big|_{\Gamma_{42}}, \tag{7.4e}$$

$$\vec{n}_{33} \cdot (k_3 \nabla T_3)\big|_{\Gamma_{33}} \;=\; \vec{n}_{42} \cdot (k_4 \nabla T_4)\big|_{\Gamma_{42}}, \tag{7.4f}$$

For bone ($j = 4$),

$$\mathscr{C}_4 : \quad k_4\nabla^2 T_4 + \rho_b C_{p_b}\omega_{b4}(T_A - T_4) + q_{m4} \;=\; 0 \tag{7.5a}$$

$$\vec{n}_{41} \cdot (k_4 \nabla T_3)\big|_{\Gamma_{41}} = q_{flux4}, \tag{7.5b}$$

$$T_4\big|_{\Gamma_{42}} = T_3\big|_{\Gamma_{33}}, \tag{7.5c}$$

$$\vec{n}_{42} \cdot (k_4 \nabla T_4)\big|_{\Gamma_{42}} = \vec{n}_{33} \cdot (k_3 \nabla T_3)\big|_{\Gamma_{33}}, \tag{7.5d}$$

2. Inverse Problem

The inverse problem is concerned with the estimation of the unknown strength of the source term $\omega_{b1}(z)$, in this problem, by minimizing the least squares error between the observed and calculated temperature from the direct problem, at several locations $(r = r_m,\ z = z_m),\ m = 1, 2, ..., M$ along the skin surface, and is given by the objective functional $S[\omega_{b1}(z)]$. It is assumed that the unknown function $\omega_{b1}(z) = G^k(z)$; here $G(z)$ belongs to the Hilbert space of square integrable functions in the domain $[0, L_1]$ [68, 67]; here L_1 is the axial length of skin layer as described earlier. Functions in such space satisfy the following property:

$$\int_{z=0}^{L_1} \big[\omega_{b1}(z)\big]^2 dz < \infty. \tag{7.6}$$

No functional form is assumed for $\omega_{b1}(z)$, the only assumption being that it belongs to the Hilbert space $[0, L_1]$.

To minimize the least squares norm of the error given by Eq. 7.1, we equate to zero the gradient of error functional, $S[\omega_{b1}(z)]$ with respect to the unknown blood perfusion functions, $\omega_{b1}(z)$, that is:

$$\nabla S\big[\omega_{b1}(z)\big] = 0, \tag{7.7}$$

where, $\nabla(S[\omega_{b1}(z)])$, is the gradient of the objective functional. However, we cannot find the gradient of the functional, since we have no information regarding the

functional form of the $\omega_{b1}(z)$. Thus to determine the gradient of the functional, the sensitivity function, $\Delta T_j(r,z)$ and the Lagrangian multiplier $\lambda_j(r,z)$ are needed. Therefore we develop two auxiliary problems *sensitivity problem* and the adjoint problem in order to determine these two functions as described in next sections.

3. Sensitivity Problem

The *sensitivity function*, $\Delta T(r,z)$, is the solution of the sensitivity problem and is defined as the directional derivative of the temperature, $T(r,z)$ in the direction of the perturbation of the unknown function [66].

The *sensitivity problem* was obtained by assuming that the temperature $T_j(r,z)$ and temperature dependent properties change by a small amount, when the unknown strength, $\omega_{b1}(z)$ of the source term is perturbed by $\epsilon\Delta\omega_{b1}(z)$. Here ϵ is a really small number. The choice of $\Delta\omega_{b1}(z))$ will be described later in the analysis.

$$\omega_{b1}(z) = \omega_{b1}(z) + \epsilon\Delta\omega_{b1}(z) \tag{7.8a}$$

$$T_{j_\epsilon}(r,z) = T_j(r,z) + \epsilon\Delta T_j(r,z) \tag{7.8b}$$

To find the directional derivative of a variable in the direction of the $\Delta\omega_{b1}(z)$, it is necessary to define a limiting parameter, $\mathscr{O}$:

$$\Delta\mathscr{O} = \lim_{\epsilon\to 0}\frac{\mathscr{O}_\epsilon - \mathscr{O}}{\epsilon} \tag{7.9}$$

where, $\mathscr{O}$ represents a general term in the direct problem or the objective functional. The directional derivative of that term is $\Delta\mathscr{O}$. Applying the liming operator to the objective functional S we get:

$$\Delta S\big[\omega_{b1}(z)\big] = \sum_{m=1}^{M}\iint_{\Omega_1}\left\{\Big\{T_1\big[r_m,z_m\big]-Y_m\Big\}\theta_1(r_m,z_m)\delta\left(r-r_m\right)\delta\left(z-z_m\right)\right\}d\Omega_1 \tag{7.10}$$

where, $\delta(\cdot)$ is Dirac delta function; θ_1 is the directional derivative of skin temperature. The directional derivatives of temperature, $(\Delta T_j(r,z))$ are replaced by $\theta_j(r,z) = \Delta T_j(r,z)$ for ease of writing. Applying the limiting operator to the direct problem (Eq. 7.2 - 7.5), after a few simple manipulations we get the following sensitivity problem:

For skin $(j = 1)$,

$$\Delta\mathscr{C}_1 : \quad k_1\nabla^2\theta_1 + \rho_b C_{p_b}\big[\Delta\omega_{b1}(z)(T_A - T_1) - \omega_{b1}(z)\theta_1\big] \;=\; 0 \tag{7.11a}$$

$$\vec{n}_{11}\cdot(k_1\nabla\theta_1)\Big|_{\Gamma_{11}} \;=\; 0, \tag{7.11b}$$

$$\vec{n}_{12}\cdot(k_1\nabla\theta_1)\Big|_{\Gamma_{12}} \;=\; -h_{air}\theta_1\Big|_{\Gamma_{12}}, \tag{7.11c}$$

$$\theta_1\Big|_{\Gamma_{13}} \;=\; \theta_2\Big|_{\Gamma_{22}}, \tag{7.11d}$$

$$\vec{n}_{13}\cdot(k_1\nabla\theta_1)\Big|_{\Gamma_{13}} \;=\; \vec{n}_{22}\cdot(k_2\nabla\theta_2)\Big|_{\Gamma_{22}}, \tag{7.11e}$$

For fat $(j = 2)$,

$$\Delta\mathscr{C}_2 : \quad k_2\nabla^2\theta_2 - \rho_b C_{p_b}\big[\omega_{b2}\theta_2\big] \;=\; 0 \tag{7.12a}$$

$$\vec{n}_{21}\cdot(k_2\nabla\theta_2)\Big|_{\Gamma_{21}} \;=\; 0, \tag{7.12b}$$

$$\theta_2\Big|_{\Gamma_{22}} \;=\; \theta_1\Big|_{\Gamma_{13}}, \tag{7.12c}$$

$$\vec{n}_{22}\cdot(k_2\nabla\theta_2)\Big|_{\Gamma_{22}} \;=\; \vec{n}_{13}\cdot(k_1\nabla\theta_1)\Big|_{\Gamma_{13}}, \tag{7.12d}$$

$$\theta_2\Big|_{\Gamma_{23}} \;=\; \theta_3\Big|_{\Gamma_{32}}, \tag{7.12e}$$

$$\vec{n}_{23}\cdot(k_2\nabla\theta_2)\Big|_{\Gamma_{23}} \;=\; \vec{n}_{32}\cdot(k_3\nabla\theta_3)\Big|_{\Gamma_{32}}, \tag{7.12f}$$

For muscle ($j = 3$),

$$\Delta\mathscr{C}_3 : \quad k_3\nabla^3\theta_3 - \rho_b C_{p_b}\left[\omega_{b3}\theta_3\right] \;=\; 0 \tag{7.13a}$$

$$\vec{n}_{31}\cdot(k_3\nabla\theta_3)\Big|_{\Gamma_{31}} \;=\; 0, \tag{7.13b}$$

$$\theta_3\Big|_{\Gamma_{32}} \;=\; \theta_2\Big|_{\Gamma_{23}} \tag{7.13c}$$

$$\vec{n}_{32}\cdot(k_3\nabla\theta_3)\Big|_{\Gamma_{32}} \;=\; \vec{n}_{23}\cdot(k_2\nabla\theta_2)\Big|_{\Gamma_{23}}, \tag{7.13d}$$

$$\theta_3\Big|_{\Gamma_{33}} \;=\; \theta_4\Big|_{\Gamma_{42}} \tag{7.13e}$$

$$\vec{n}_{33}\cdot(k_3\nabla\theta_3)\Big|_{\Gamma_{33}} \;=\; \vec{n}_{42}\cdot(k_4\nabla\theta_4)\Big|_{\Gamma_{42}}, \tag{7.13f}$$

For bone ($j = 4$),

$$\Delta\mathscr{C}_4 : \quad k_4\nabla^4\theta_4 - \rho_b C_{p_b}\left[\omega_{b4}\theta_4\right] \;=\; 0 \tag{7.14a}$$

$$\vec{n}_{41}\cdot(k_4\nabla\theta_4)\Big|_{\Gamma_{41}} \;=\; 0, \tag{7.14b}$$

$$\theta_4\Big|_{\Gamma_{42}} \;=\; \theta_3\Big|_{\Gamma_{33}} \tag{7.14c}$$

$$\vec{n}_{42}\cdot(k_4\nabla\theta_4)\Big|_{\Gamma_{42}} \;=\; \vec{n}_{33}\cdot(k_3\nabla\theta_3)\Big|_{\Gamma_{33}}, \tag{7.14d}$$

In the sensitivity problem given above, $\Delta\omega_{b1}(z)$ is the only term needed for solving the above problem. The computation of $\Delta\omega_{b1}(z)$ will be addressed later in the section.

4. Adjoint Problem

In the adjoint problem, Lagrange multipliers, $\lambda_j(r, z)$ are introduced for the minimization of the error functional Eq. 7.1 because the temperature $T_1(r_m, z_m; \omega_{b1}(z))$

appearing in the functional needs to satisfy a constraint, which is the solution of the direct problem given by Eqs. 7.2 - 7.5. Thus the introduction of the Lagrangian multipliers $\lambda_j(r,z)$ transforms the minimization of $S\big[\omega_{b1}\,(z)\,\big]$, under the constraint of the direct (constrained optimization) problem, to a minimization without constraint (unconstrained optimization) problem [67]. The Lagrange multipliers, which are also needed for the calculation of the gradient equation (as will be apparent later in this section), are obtained through the solution of a problem adjoint to the sensitivity problem given by Eqs. 7.11 - 7.14.

We write the Lagrangian by adding each constraint $\mathscr{C}_j$, given by Eqs. 7.2a, 7.3a, 7.4a, and, 7.5a, multiplied by a Lagrangian multiplier $\lambda_j(r,z)$.

$$\mathscr{L}\big[\omega_{b1}(z)\big] \;=\; S\big[\omega_{b1}\,(z)\,\big] \;+\; \sum_{j=1}^{4} \iint\limits_{\Omega_j} \Big\{ \mathscr{C}_j(r,z)\lambda_j(r,z) \Big\} d\Omega_j, \tag{7.15}$$

Next, the stationary points of the Lagrangian equation must be found, this is done by choosing the Lagrangian multipliers such that:

$$\Delta\mathscr{L}\big[\omega_{b1}(z)\big] \;=\; 0, \tag{7.16}$$

where, $\Delta\mathscr{L}$ is the variation of the Lagrangian, it is found by taking the directional derivatives of each components of the Lagrangian.

With the sensitivity problem already defined by Eqs. 7.11 - 7.14, and $\Delta S\big[\omega_{b1}(z)\big]$ defined by Eq. 7.10, the variation of the Lagrangian, $\Delta\mathscr{L}$ can be written as follows:

$$\Delta\mathscr{L}\big[\omega_{b1}(z)\big] \;=\; \sum_{m=1}^{M} \iint\limits_{\Omega_1} \Delta S\big[\omega_{b1}(z)\big] d\Omega_1 \;+ \sum_{j=1}^{4} \iint\limits_{\Omega_j} \Big\{ \Delta\mathscr{C}_j(r,z)\lambda_j(r,z) \Big\} d\Omega_j \tag{7.17}$$

where the variation of the constraints ($\Delta\mathscr{C}_j$) is given by Eqs. 7.11a, 7.12a, 7.13a, and,

7.14a. Writing the variation of each of the terms in the above equation we get:

$$\Delta\mathscr{L}\big[\omega_{b1}(z)\big] \;=\; \iint\limits_{\Omega_1} \lambda_1\Big\{k_1\nabla^2\theta_1 + \rho_b C_{p_b}\big[\Delta\omega_{b1}(z)(T_A - T_1) - \omega_{b1}(z)\theta_1\big]\Big\}d\Omega_1 \;+$$
$$\iint\limits_{\Omega_2} \lambda_2\Big\{k_2\nabla^2\theta_2 - \rho_b C_{p_b}\big[\omega_{b2}\theta_2\big]\Big\}d\Omega_2 \;+\; \iint\limits_{\Omega_3} \lambda_3\Big\{k_3\nabla^3\theta_3 - \rho_b C_{p_b}\big[\omega_{b3}\theta_3\big]\Big\}d\Omega_3 \;+$$
$$\iint\limits_{\Omega_4} \lambda_4\Big\{k_4\nabla^4\theta_4 - \rho_b C_{p_b}\big[\omega_{b4}\theta_4\big]\Big\}d\Omega_4 \;+\; \sum_{m=1}^{M}\iint\limits_{\Omega_1}\Big\{\Big\{T_1\big[r_m, z_m; \omega_{b1}(z)\big] - Y_m\Big\}$$
$$\theta_1(r_m, z_m)\delta\left(r - r_m\right)\delta\left(z - z_m\right)\Big\}d\Omega_1 \quad (7.18)$$

Eq. 7.18 can be rearranged and written more compactly as follows:

$$\Delta\mathscr{L}\big[\omega_{b1}(z)\big] \;=\; \sum_{j=1}^{4}\iint\limits_{\Omega_j} k_j\Big\{\lambda_j\nabla^2\theta_j\Big\}d\Omega_j \;-\; \sum_{j=1}^{4}\iint\limits_{\Omega_j}\Big\{\rho_b C_{p_b}\big[\omega_{bj}\theta_j\lambda_j\big]\Big\}d\Omega_j \;+$$
$$\sum_{m=1}^{M}\iint\limits_{\Omega_1}\Big\{\Big\{T_1 - Y_m\Big\}\theta_1(r_m, z_m)\delta\left(r - r_m\right)\delta\left(z - z_m\right)\Big\}d\Omega_1 \;+$$
$$\iint\limits_{\Omega_1}\Big\{\rho_b C_{p_b}\big[\Delta\omega_{b1}(z)(T_A - T_1)\lambda_1\big]\Big\}d\Omega_1, \quad (7.19)$$

Using second Green's identity [69, 70], we can write the first integral in Eq. 7.19 as:

$$k_j\iint\limits_{\Omega_j}\Big\{\lambda_j\nabla^2\theta_j\Big\}d\Omega_j \;=\; k_j\int\limits_{\Gamma_j}\Big\{\lambda_j\frac{\partial\theta_j}{\partial n}\Big\}d\Gamma_j \;-\; k_j\int\limits_{\Gamma_j}\Big\{\theta_j\frac{\partial\lambda_j}{\partial n}\Big\}d\Gamma_j \;+$$
$$k_j\iint\limits_{\Omega_j}\Big\{\lambda_j\nabla^2\theta_j\Big\}d\Omega_j, \quad (7.20)$$

Note that,

$$\Gamma_j \;=\; \Gamma_{j1} + \Gamma_{j2} + \Gamma_{j3}, \;\text{ for }\; j = 1, 2, 3, \quad (7.21a)$$

$$\text{and, }\; \Gamma_4 \;=\; \Gamma_{41} + \Gamma_{42}, \quad (7.21b)$$

Using Eqs. 7.20 and 7.21 we can write the first term on the right hand side of Eq. 7.19 for (say) the skin layer ($j = 1$) as:

$$k_1 \iint\limits_{\Omega_1} \left\{ \lambda_1 \nabla^2 \theta_1 \right\} d\Omega_j \;=\; k_1 \sum_{i=1}^{3} \int\limits_{\Gamma_{1i}} \left\{ \lambda_1 \frac{\partial \theta_1}{\partial n_{1i}} \right\} d\Gamma_{1i} \;-\; k_1 \sum_{i=1}^{3} \int\limits_{\Gamma_{1i}} \left\{ \theta_j \frac{\partial \lambda_1}{\partial n_{1i}} \right\} d\Gamma_{1i} + k_1 \iint\limits_{\Omega_1} \left\{ \lambda_1 \nabla^2 \theta_1 \right\} d\Omega_1, \tag{7.22}$$

Similarly, terms for fat, muscle and bone layers can be written and substituted in Eq. 7.19. The variation for the Lagrangian (Eq. 7.19) can be simplified further, by making use of the boundary conditions for the sensitivity problem given by Eqs. 7.11 - 7.14, rewritten below for convenience in a compact notation:

$$k_j \frac{\partial \theta_j}{\partial n_{j1}}\bigg|_{\Gamma_{j1}} \;=\; 0; \qquad \text{for } j = 1,2,3,4, \tag{7.23a}$$

$$k_j \frac{\partial \theta_j}{\partial n_{j1}}\bigg|_{\Gamma_{12}} \;=\; -h_{air}\theta_1; \qquad \text{for } j = 1,2,3,4, \tag{7.23b}$$

$$\theta_j\Big|_{\Gamma_{j3}} \;=\; \theta_i\Big|_{\Gamma_{i3}}; \qquad \text{for } j = 1,2,3;\;\; i = j+1, \tag{7.23c}$$

$$k_j \frac{\partial \theta_j}{\partial n_{j1}} \;=\; k_i \frac{\partial \theta_i}{\partial n_{i1}}; \qquad \text{for } j = 1,2,3;\;\; i = j+1, \tag{7.23d}$$

Note here that, $\frac{\partial}{\partial n_{ji}}(\cdot)$ can also be rewritten as:

$$\frac{\partial}{\partial n_{ji}}\big(\,\cdot\,\big) \;=\; \vec{n}_{ji} \cdot \nabla(\cdot), \tag{7.24}$$

where, $\vec{n}$ is the outward normal to Γ_{ji} at a point on Γ_{ji}.

Using Eqs. 7.20, 7.21 and 7.23, Eq. 7.19 can be simplified and written as:

$$\begin{aligned}
\Delta\mathscr{L}\big[\omega_{b1}(z)\big] \;=\; & \iint\limits_{\Omega_1}\Bigg\{k_1\nabla^2\lambda_1 \;-\; \rho_b C_{p_b}\omega_{b1}(z)\lambda_1 \;+\; \sum_{m=1}^{M}\Big\{T_1 - Y_m\Big\}\delta(r-r_m) \\
& \qquad \delta(z-z_m)\Bigg\}\theta_1 d\Omega_1 \;+\; \sum_{j=2}^{4}\iint\limits_{\Omega_j}\Bigg\{k_j\nabla^2\lambda_j \;-\; \rho_b C_{p_b}\omega_{bj}\lambda_j\Bigg\}\theta_j d\Omega_j \;+ \\
& k_1\sum_{i=2}^{3}\int\limits_{\Gamma_{1i}}\Bigg\{\lambda_1\frac{\partial\theta_1}{\partial n_{1i}}\Bigg\}d\Gamma_{1i} \;-\; k_1\sum_{i=1}^{3}\int\limits_{\Gamma_{1i}}\Bigg\{\theta_1\frac{\partial\lambda_1}{\partial n_{1i}}\Bigg\}d\Gamma_{1i} \;+ \\
& k_2\sum_{i=2}^{3}\int\limits_{\Gamma_{2i}}\Bigg\{\lambda_2\frac{\partial\theta_2}{\partial n_{2i}}\Bigg\}d\Gamma_{1i} \;-\; k_2\sum_{i=1}^{3}\int\limits_{\Gamma_{2i}}\Bigg\{\theta_2\frac{\partial\lambda_1}{\partial n_{2i}}\Bigg\}d\Gamma_{2i} \;+ \\
& k_3\sum_{i=2}^{3}\int\limits_{\Gamma_{3i}}\Bigg\{\lambda_3\frac{\partial\theta_3}{\partial n_{3i}}\Bigg\}d\Gamma_{3i} \;-\; k_3\sum_{i=1}^{3}\int\limits_{\Gamma_{3i}}\Bigg\{\theta_3\frac{\partial\lambda_3}{\partial n_{3i}}\Bigg\}d\Gamma_{3i} \;+ \\
& k_4\int\limits_{\Gamma_{4i}}\Bigg\{\lambda_4\frac{\partial\theta_4}{\partial n_{4i}}\Bigg\}d\Gamma_{4i} \;-\; k_4\sum_{i=1}^{2}\int\limits_{\Gamma_{4i}}\Bigg\{\theta_4\frac{\partial\lambda_4}{\partial n_{4i}}\Bigg\}d\Gamma_{4i} \;+ \\
& \iint\limits_{\Omega_1}\Big\{\rho_b C_{p_b}\omega_{b1}(T_A - T_1)\lambda_1\Big\}d\Omega_1
\end{aligned} \tag{7.25}$$

An analysis of the stationary points of $\Delta\mathscr{L}$ gives the adjoint problem associated with the sensitivity problem *i.e.* by choosing the Lagrangian multipliers such that, they satisfy the Eq. 7.16.

For skin ($j = 1$),

$$k_1\nabla^2\lambda_1 - \rho_b C_{p_b}\omega_{b1}(z)\lambda_1 + \sum_{m=1}^{M}\Big[T_1(r_m, z_m) - Y_m\Big] \;=\; 0, \tag{7.26a}$$

$$\vec{n}_{11}\cdot(k_1\nabla\lambda_1)\big|_{\Gamma_{11}} \;=\; 0, \tag{7.26b}$$

$$\vec{n}_{12}\cdot(k_1\nabla\lambda_1)\big|_{\Gamma_{12}} \;=\; -h_{air}\lambda_1\big|_{\Gamma_{12}}, \tag{7.26c}$$

$$\lambda_1\big|_{\Gamma_{13}} = \lambda_2\big|_{\Gamma_{22}} \tag{7.26d}$$

$$\vec{n}_{13}\cdot(k_1\nabla\lambda_1)\big|_{\Gamma_{13}} = \vec{n}_{22}\cdot(k_2\nabla\lambda_2)\big|_{\Gamma_{22}}, \tag{7.26e}$$

For fat ($j = 2$),

$$k_2\nabla^2\lambda_2 - \rho_b C_{p_b}\omega_{b2}\lambda_2 = 0, \tag{7.27a}$$

$$\vec{n}_{21}\cdot(k_2\nabla\lambda_2)\big|_{\Gamma_{21}} = 0, \tag{7.27b}$$

$$\lambda_2\big|_{\Gamma_{22}} = \lambda_1\big|_{\Gamma_{13}}, \tag{7.27c}$$

$$\vec{n}_{22}\cdot(k_2\nabla\lambda_2)\big|_{\Gamma_{22}} = \vec{n}_{13}\cdot(k_1\nabla\lambda_1)\big|_{\Gamma_{13}}, \tag{7.27d}$$

$$\lambda_2\big|_{\Gamma_{23}} = \lambda_3\big|_{\Gamma_{32}}, \tag{7.27e}$$

$$\vec{n}_{23}\cdot(k_2\nabla\lambda_2)\big|_{\Gamma_{23}} = \vec{n}_{32}\cdot(k_3\nabla\lambda_3)\big|_{\Gamma_{32}}, \tag{7.27f}$$

For muscle ($j = 3$),

$$k_3\nabla^2\lambda_3 - \rho_b C_{p_b}\omega_{b3}\lambda_3 = 0, \tag{7.28a}$$

$$\vec{n}_{31}\cdot(k_3\nabla\lambda_3)\big|_{\Gamma_{31}} = 0, \tag{7.28b}$$

$$\lambda_3\big|_{\Gamma_{32}} = \lambda_2\big|_{\Gamma_{23}}, \tag{7.28c}$$

$$\vec{n}_{32}\cdot(k_3\nabla\lambda_3)\big|_{\Gamma_{32}} = \vec{n}_{23}\cdot(k_2\nabla\lambda_2)\big|_{\Gamma_{23}}, \tag{7.28d}$$

$$\lambda_3\big|_{\Gamma_{33}} = \lambda_4\big|_{\Gamma_{42}}, \tag{7.28e}$$

$$\vec{n}_{33}\cdot(k_3\nabla\lambda_3)\big|_{\Gamma_{33}} = \vec{n}_{42}\cdot(k_4\nabla\lambda_4)\big|_{\Gamma_{42}}, \tag{7.28f}$$

For bone ($j = 4$),

$$k_4 \nabla^2 \lambda_4 - \rho_b C_{p_b} \omega_{b4} \lambda_4 \;=\; 0, \tag{7.29a}$$

$$\vec{n}_{41} \cdot (k_4 \nabla \lambda_4)\big|_{\Gamma_{41}} \;=\; 0, \tag{7.29b}$$

$$\lambda_4\big|_{\Gamma_{42}} \;=\; \lambda_3\big|_{\Gamma_{32}}, \tag{7.29c}$$

$$\vec{n}_{42} \cdot (k_4 \nabla \lambda_4)\big|_{\Gamma_{42}} \;=\; \vec{n}_{43} \cdot (k_3 \nabla \lambda_3)\big|_{\Gamma_{33}}, \tag{7.29d}$$

Clearly, with no error, the adjoint problem has zero solution.

5. Gradient Equation

It is convenient to note that, if the Lagrangian multipliers $\lambda_j(r, z)$ satisfy the solution of the adjoint problem then, then:

$$\mathscr{L} \;=\; S[\omega_{b1}(z)] \tag{7.30}$$

$$\Delta\mathscr{L} \;=\; \Delta S[\omega_{b1}(z)] \tag{7.31}$$

Now, using the above identity and noting that in Eq. 7.25, after the terms containing $\Delta T(r, z, t)$ are allowed to vanish, the following integral term is left:

$$\Delta S\big[\omega_{b1}(z)\big] \;=\; \iint\limits_{\Omega_1} \Big\{ \rho_b C_{p_b} \omega_{b1}(z)(T_A - T_1)\lambda_1 \Big\} d\Omega_1 \tag{7.32}$$

By definition [69], directional derivative of S in the direction of the perturbation $\Delta\omega_{b1}(z)$, is the inner product of the gradient of the objective functional and the direction of the perturbations $\Delta\omega_{b1}(z)$, given by $\langle \nabla S \omega_{b1}(z), \Delta\omega_{b1}(z) \rangle$. Now, considering that the unknown function $\omega_{b1}(z)$ belongs to the space of square integrable functions

[68, 71] we can write the inner product as:

$$\Delta S\big[\omega_{b1}(z)\big] \;=\; \int_{z=0}^{L_1} \nabla S\big[\omega_{b1}(z)\big]\Delta\omega_{b1}(z)\,dz \tag{7.33}$$

where, $\nabla S\big[\omega_{b1}(z)\big]$ is the gradient of the functional $S\big[\omega_{b1}(z)\big]$. Comparing Eq. 7.32 and Eq. 7.33, we can write:

$$\nabla S\big[\omega_{b1}(z)\big] \;=\; \int_{r=\mathscr{R}_2(z)}^{\mathscr{R}_1(z)} \rho_b C_{p_b}(T_A - T_1(r,z))\lambda_1(r,z)\,r dr \tag{7.34}$$

6. Iterative Procedure

The unknown function $\omega_{b1}(z)$ is estimated by minimization of the functional $S\big[\omega_{b1}(z)\big]$ given by Eq. 7.1. The minimization of the functional is achieved by an iterative procedure by precise selection of the direction of descent and of the step size for each iteration, k. The iterative procedure of the conjugate gradient method [68, 66] for the estimation of the unknown function $\omega_{b1}(z)$ is given by:

$$\omega_{b1}^{k+1}(z) \;=\; \omega_{b1}(z) - \beta^k d^k(z), \tag{7.35}$$

where, β^k is the *search step size* and $d^k(t)$ is the *direction of descent*, defined as:

$$d^k(z) \;=\; \nabla S\big[\omega_{b1}^k(z)\big] + \gamma^k d^{k-1}(z) \tag{7.36}$$

where, γ^k is the conjugation coefficient. The direction of descent is a conjugation of the gradient direction, $\nabla S(\omega_{b1}(z))$, and the direction of descent of the previous iteration, $d^{k-1}(z)$. Different expressions are available for the conjugation coefficient, γ^k such as the Polak-Ribiere and Flethcher Reeves expression [68, 67]. The conjugation

coefficient γ^k was calculated using the Fletcher-Reeves expression:

$$\gamma^k = \frac{\int_{z=0}^{L_1} \left\{\nabla S\left[\omega_{b1}^k(z)\right]\right\}^2 dz}{\int_{z=0}^{L_1} \left\{\nabla S\left[\omega_{b1}^{k-1}(z)\right]\right\}^2 dz}, \tag{7.37}$$

$$\text{for } k = 1, 2, ...$$

$$\text{with } \gamma^0 = 0 \ for \ k = 0$$

The step search size β^k is determined by minimizing the functional $S\left[\omega_{b1}(z)\right]$ given by Eq. 7.1 with respect to β^k, and is given by:

$$\beta^k = \frac{\int_{z=0}^{L_1} \sum_{m=1}^{M} \left\{T_1\left[r_m, z_m, t; \omega_{b1}^k(z)\right] - Y_m(z)\right\} \theta_1\left[r_m, z_m, t; d^k(z)\right] dz}{\int_{z=0}^{L_1} \left\{\theta_1\left[r_m, z_m, t; d^k(z)\right]\right\}^2 dz} \tag{7.38}$$

7. Stopping Criteria

The iterative procedure given by Eq. 7.35-7.38 is applied until a stopping criteria is satisfied based on the *Discrepancy Principle*. The stopping criteria based on the *Discrepancy Principle* is given by:

$$S\left[\omega_{b1}(z)\right] < \epsilon \tag{7.39}$$

where, $S\left[\omega_{b1}(z)\right]$ is computed with Eq. 7.1. A sufficiently small tolerance of $\epsilon = 0.01$ is specified.

8. Computational Algorithm

The unknown function $\omega_{b1}(z)$ is first initialized to some initial guess value. The computational algorithm for the IHCP using CGM is given by Ozisik, 2002 [66].

(i) Solve the direct problem (Eqs.7.2 - 7.5) and calculate $T(r, z, t)$ based on $\omega_{b1}^k(z)$.

(ii) Check the stopping criteria given by Eq. 7.39. Continue if not satisfied. If the criteria is satisfied then the corresponding $\omega_{b1}^{k}(z)$ is the optimized skin blood perfusion function.

(iii) Knowing $T(r_m, z_m, t)$ and the observed temperature $Y_m(z)$, solve the adjoint problem (Eqs.7.26 - 7.29) and compute $\lambda_j(r, z)$.

(iv) Knowing $\lambda_j(r, z)$, compute $\nabla S\left[\omega_{b1}^{k}(z)\right]$ from Eq. 7.34.

(v) Knowing the gradient $\nabla S\left[\omega_{b1}^{k}(z)\right]$, compute γ^k from the Fletcher-Reeves expression, Eq. 7.37, and the direction of descent $d^k(z)$ from Eq. 7.36.

(vi) We set $\Delta\omega_{b1}^{k}(z) = d^k(z)$ and solve the sensitivity problem (Eqs.7.11 - 7.14) to obtain $\theta_1(r_m, z_m, t; d^k(z))$.

(vii) Knowing $\theta_1(r_m, z_m, t; d^k(z))$, compute the search step size β^k from Eq. 7.38.

(viii) Knowing the search step size β^k and the direction of descent $d^k(z)$, compute the new estimate $\omega_{b1}^{k}(z)$ from Eq. 7.35 and return to Step 1.

D. Implementation Using COMSOL-MATLAB Interfacing

As described in Chapter VI, COMSOL Multiphysics was used to solve the first-order model using FEM. COMSOL Multiphysics is a GUI based FEM software, based on MATLAB code. This allows the software to interact and integrate seamlessly with M code written in MATLAB. This requires MATLAB and COMSOL Multiphysics to be installed on the same machine. This seamless integration allows COMSOL Multiphysics to export the entire model as a structure to MATLAB, where further operations can be performed on it. Also COMSOL can generate a M code for the model developed using the COMSOL GUI.

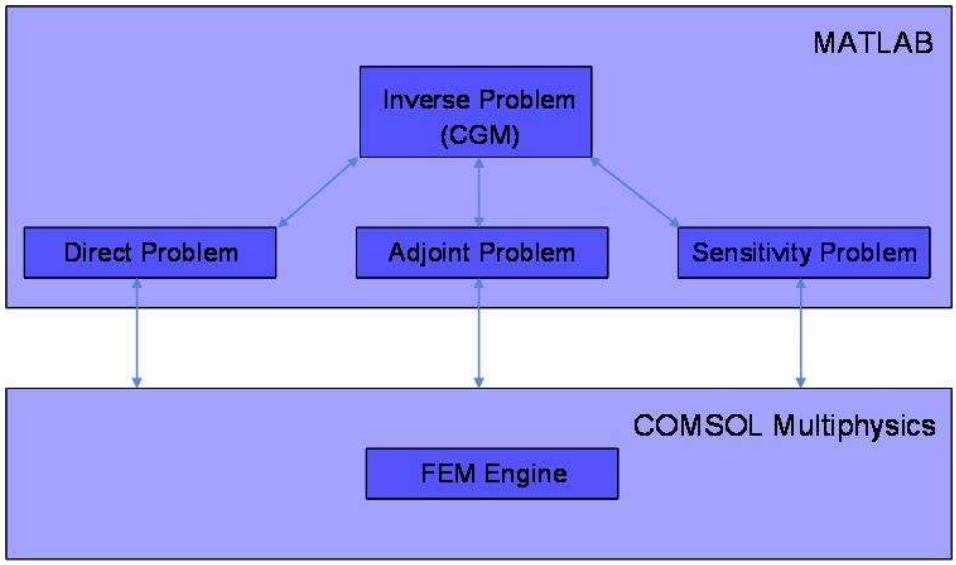

Fig. 33. Interfacing was achieved between MATLAB and COMSOL Multiphysics through COMSOL Script.

Using this seamless integration, it was possible to use the superior FEM capabilities of COMSOL Multiphysics and the flexibility and mathematical functionality of MATLAB as can be seen in Fig. 33. The iterative procedure of the conjugate gradient method was implemented in MATLAB as per the algorithm as shown in Fig. 32 by the function *InverseProb*. *InverseProb* then gets the required data by calling *CalT*, *CalLambda*, and, *CalDeltaT* for solving the Direct, Adjoint and Sensitivity problems respectively, which in turn call the COMSOL Multiphysics FEM engine.

CHAPTER VIII

MODEL VALIDATION

Validation for the zero order model is obtained by substituting the measured finger blood perfusion in the mathematical model, and by comparing calculated and measured temperature. Blood perfusion in the finger, for the case of normal and hyperemic flow, was measured using Venous Occlusion Plethysmography (VOP) as discussed in Chapter III. Validation of the first order model presented in Chapter VI will not be completed during this study, as it requires experimental techniques currently unavailable to us. These techniques are depicted in Fig. 34 and are: **(a)** Laser Doppler Flowmetry (LDF) to measure local perfusion at the skin level, **(b)** Infrared Imaging to measure temperature over the entire skin surface, and **(c)** Ultrasound to measure blood velocity and vessel diameter.

For the validation, eight healthy volunteers were recruited at Texas A&M University, the data obtained is divided in three categories: **(1)** blood perfusion (using plethysmography); **(2)** temperature and heat flux (skin, body and ambient temperature as well as skin heat flux), and **(3)** anatomical parameters (weight, height, finger length, and finger circumference). For the experimental validation, the following protocol was followed:

- **Step 1:** The study required one visit to the laboratory that lasted between 1.5 and 2 hours. During the visit, the parameters indicated in Tables XIV - XV were obtained and calculated. In this visit the volunteer was informed about the experimental methodology and asked to sign the consent form. This time served for the subject to arrive to a thermoneutral condition where skin temperature became stable. Body temperature and room temperature were recorded at the beginning and end of the experiment, and their average values were used in the

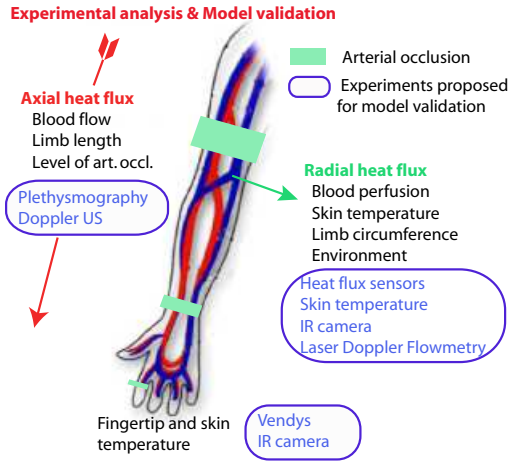

Fig. 34. Experimental techniques necessary for the determination direct determination of skin heat flux, skin perfusion and blood flow in selected arteries.

calculations.

- **Step 2:** The volunteer was seated with the right arm resting on a support placed at the heart level. To reduce errors in blood volume measurement, the arm was immobilized using foam blocks. During equilibration, the cuff and sensors were placed as indicated in Fig. 35.

- **Step 3:** After equilibration, the DTM test was performed by inflating the cuff above systolic pressure (200 mmHg) for up to 3 minutes. Data acquisition for temperature and heat flux was started 5 minutes before occlusion (baseline), and continued for 6 minutes after cuff was released; this allowed to record the temperature variations during hyperemia and until the skin temperature returned to baseline values. Arterial occlusion was performed with a finger cuff (Hokanson, Bellevue, WA) inflated by a Hokanson E20 Rapid Cuff Inflator and AG101 Air Source.

- **Step 4:** The next procedure involved the measurement of normal blood per-

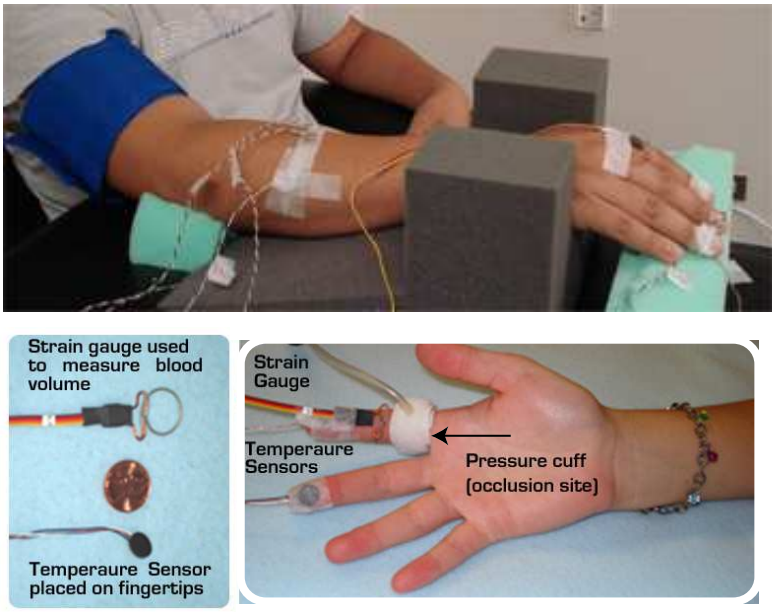

Fig. 35. **(Top)** Positioning of right arm for DTM and VOP experiments, foam blocks are used to reduce unwanted motion; This picture shows occlusion at upper arm level instead of finger level. **(Bottom)** Placement of sensors for experimental validation; sensors used correspond to mercury strain gauge, heat flux sensors with embedded thermocouple and finger cuff.

fusion using venous occlusion plethysmography (VOP) following the normal protocol reported elsewhere [52].

- **Step 5:** Hyperemic blood flow into the finger was measured by performing arterial occlusion as indicated in step 2, and was quickly followed by venous occlusion plethysmography (VOP). This measurement was extended during 2 to 3 minutes following cuff deflation depending on the subject, and provided the required temporal variations in blood volume changes.

A waiting time of 10 to 15 minutes between each study (steps 2, 3 and 4) was considered to allow blood perfusion and skin temperature to return to normal value. All research on human subjects within Texas A&M University is subjected to a formal Institutional Review Board authorization. The protocol for this research was submitted to IRB for consideration and was approved on August 26, 2006. The personnel involved in this research also completed human research subject training and have received certification from ICIT. Subject participation was voluntary and the subjects were able to withdraw from the study at any time. All details regarding the protocol were explained to the subjects as a part of the informed consent form and a information poster and cards were created and displayed in the laboratory. There are no anticipated risks from participation in this study. There may be discomfort during the time the cuff is inflated; discomfort may include numbness, spasms, tingling, bruising and weakness of the arm and hand.

The subjects were instructed not to consume food or caffeinated drinks within 3 hours before the beginning of the experiment. The measurements taken from all subjects are detailed in next four tables beginning with Tables XIV and XV.

Table XIV. Mean physical characteristics for participants in the study

Subject number	Sex	Age (yr)	Height (cm)	Weight (kg)	T_A (^oC)	Resting BP ($S/DmmHg$)
1	M	31	182	200	36.8	135/93
2	M	21	189	178.6	37.4	148/101
3	M	23	174.5	152	37.1	136/84
4	M	22	171.6	148	36.6	139/78
5	M	23	180.5	132	37.3	132/75
6	M	21	180	155	36.95	123/68
7	F	23	160.5	132	36.6	124/75
8	F	32	148.7	118	37.5	128/74

A. Measurement of Thermal Response

Thermal measurements were performed using type T thermocouples and heat flux sensors connected to an Omega OMB-DAQ-56 Data Acquisition system. The measurements were obtained following the same procedure used by the VENDYS^{TM} system developed by Endothelix. VENDYS^{TM} is a sensitive digital thermal monitoring device, that allows to non-invasively measures vascular responsiveness. Parameters including TR (maximum temperature rebound post-deflation) and TD (maximum temperature fall during cuff inflation), were measured, together with the heat flux at the skin level due to environmental conditions. Description of these parameters in a DTM test are given in Fig. 4 in the introductory chapter of this thesis.

The heat flux at the skin surface was determined using heat flux meters with an embedded T thermocouple (Concept Engineering, CT); heat flux sensors are flat

Table XV. Finger dimension and strain gauge location for subjects participating in the study

Subject Number	Finger Circumf. (base) (cm)	Finger Circumf. (SG location) (cm)	Finger length (base-tip) (cm)	SG location (tip) (cm)
1	7.2	6.6	8.2	4.8
2	6.7	5.0	9.5	4.0
3	6.5	6.0	7.9	4.0
4	6.7	6.0	9.0	4.0
5	6.0	5.0	7.4	3.9
6	6.7	5.0	8.5	4.0
7	6.0	5.0	8.0	3.9
8	6.0	5.0	7.5	3.4

plate transducer designed to measure heat flow through a surface where the plate is applied. The flow of heat from or to the surface in consideration creates a small temperature difference between the upper and lower surfaces of the meter. These surfaces are in thermal contact with a special, miniature, high temperature thermopile, which generates a direct current signal from the temperature difference and serves to estimate the surface heat flux. These devices are widely used in medical and physiological measurements of heat flow [42, 72, 33], and in this experiment were used to determine heat flux at different locations of the arm, hand and fingers in the experiment performed. These sensors were attached to the skin surface using surgical tape (Micropore).

B. Blood Volume Measurement

Plethysmography denotes the techniques related to the measurement and recording of changes in organ volume. In this study, we employed strain gauge plethysmography (SGP), which uses a thin rubber tube filled with Mercury or Indium-Gallium. The gauge is placed around the limb or digit of interest. As the volume of the limb changes due to varying blood volume, the tube is stretched and the electrical resistance increases. This electrical information is processed and displayed as a waveform (Fig. 36). Common applications of SGP include measuring arterial blood flow into the limbs and digits (also called arterial inflow, or venous occlusion plethysmography (VOP), venous capacitance, and maximum venous outflow to detect deep venous thrombosis in the legs, and peripheral arterial disease.

Normally arterial and venous flow in a limb are equal on average during the cardiac cycle. Venous occlusion plethysmography (VOP) measures arterial inflow by abruptly stopping venous outflow with a proximal cuff inflated to a value above venous

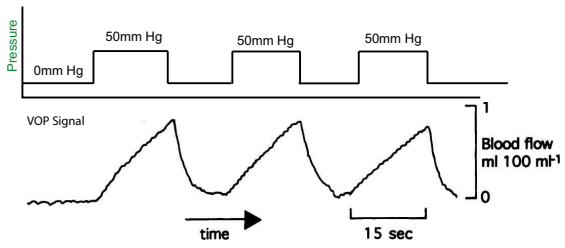

Fig. 36. Pressure cuff variation during venous occlusion plethysmography (VOP) and corresponding waveform indicating percentile change of strain gauge circumference or finger volume. Figure adapted from [73].

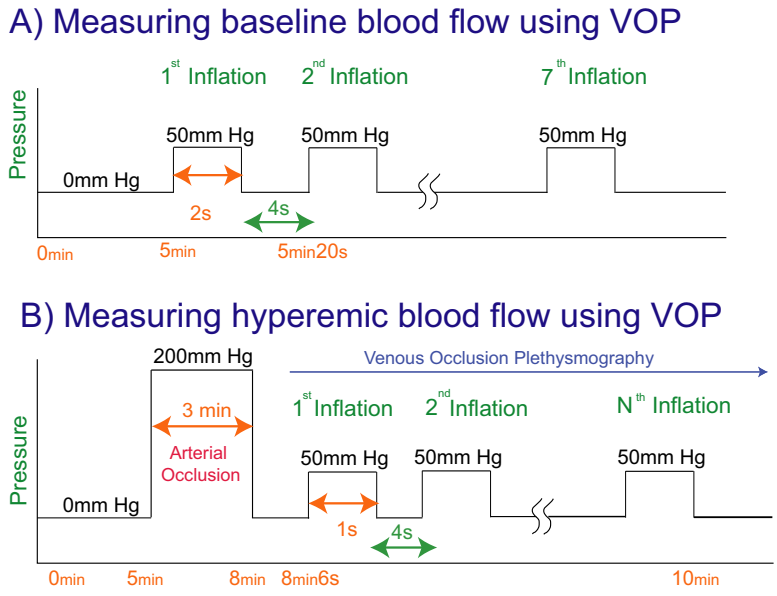

Fig. 37. Representation of pressure of the pneumatic cuff used to perform arterial and venous occlusion during **(A)** normal VOP and **(B)** hyperemic VOP. Arterial occlusion is performed at 200 mmHg and venous occlusion at 50 or 60 mmHg.

pressure, but below arterial pressure (typically about 50 to 60 mmHg). This causes the volume of the limb to increase due to arterial inflow; the strain gauge is used to measure the volume change in the limb. The rate of change of the volume, in percent per minute, is equivalent to the arterial flow rate at the moment of venous occlusion. Plethysmography is based on the assumption that flow is similar throughout the region under consideration. There are two timed stages during VOP as indicated in Fig. 37 and enumerated below:

- **Inflation or venous occlusion** characterized by arterial blood accumulation while the cuff is inflated to 50 mmHg or a value higher than the venous pressure. An inflation time of 2 and 1 seconds was used during Step 4 and Step 5 respectively.

- **Venous draining** or time from the beginning of one measurement to the beginning of the next measurement; during this time, the limb empties all the accumulated blood, and it becomes ready for the next occlusion. A reading interval of 6 and 5 seconds was used during Step 4 and Step 5 respectively.

In this study, finger plethysmography was performed using a set of Hokanson strain gauges with circumferences between 4.5 and 7.0 cm. The strain gauges were connected to a Hokanson EC6 Plethysmograph; and the occlusion was created at finger level using the E20 Hokanson Rapid Cuff Inflator and the NIVP3 software to control cuff inflation and deflation and balance the strain gauge.

C. Experimental Data

For each subject the type of data recorded is shown in Fig. 38 and corresponds to:

- DTM plot showing the temperature history of the fingertip temperature in

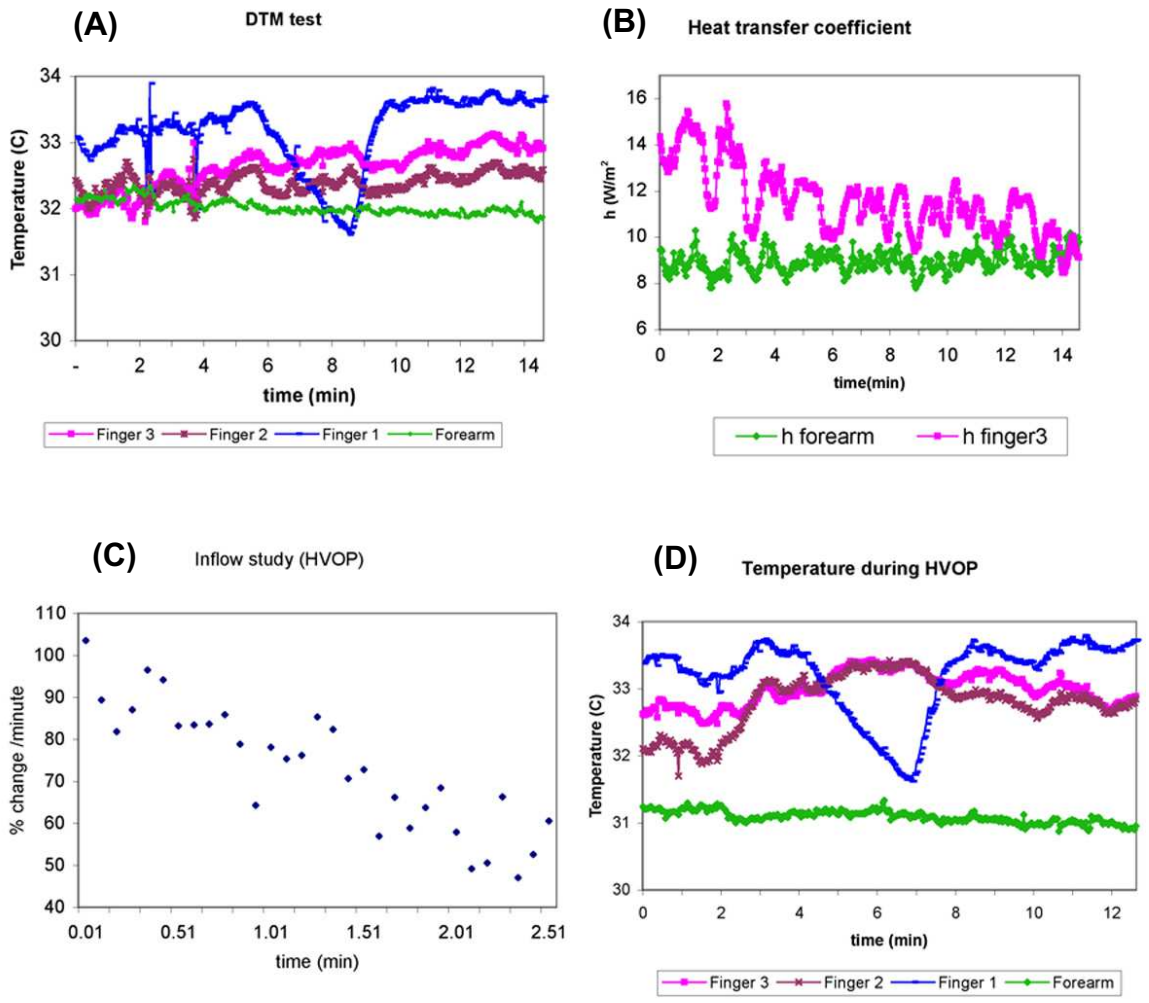

Fig. 38. General set of measurements obtained during validation experiments: **(A)** temperature during DTM test, **(B)** heat transfer coefficient (h) calculated using measured skin heat flux and temperature, **(C)** inflow studies (VOP or HVOP) to determine blood perfusion or alterations in fingertip volume during hyperemia, and **(D)** temperature alterations during inflow studies. The data presented corresponds to Subject 1.

the occluded finger or *finger 1* (index finger of right hand), baseline or un-occluded finger or *finger 2* (ring finger of right hand), contra-lateral finger or *finger 3* (index finger of left arm), and temperature at middle forearm (right arm between wrist and elbow).

- Plot of heat transfer coefficient h calculated using the heat flux measured with the HF sensors at the skin level and the skin temperature. The values plotted are: h_{finger_3}, and $h_{forearm}$.

- Fingertip and arm temperature variation in during normal (VOP) and hyperemic (HVOP) venous occlusion plethysmography.

- Recording of blood volume variation during hyperemia.

From the recorded data the following trends are observed:

- The DTM data show very little TR value in comparison to the values reported with VENDYS^{TM}, the reason of this difference is variations in arm posture and consequently blood perfusion. The protocol followed in these experiment was to place the arm at heart level, where as the normal protocol followed with the reported DTM studies [7, 19], involve the hand placed over the lap (*i.e.* below heart level). The temperature variation, as well as the corresponding posture is indicated in Fig. 39.

- It was observed that the fingertip temperature was reduced during VOP experiments while determining normal and hyperemic VOP. The reason of this reduction is the increment in the blood volume stored in the venous plexus during the procedure. As indicated in Chapter III, when blood volume in the venous plexus increases, cooling occurs. This has a deleterious effect as it will

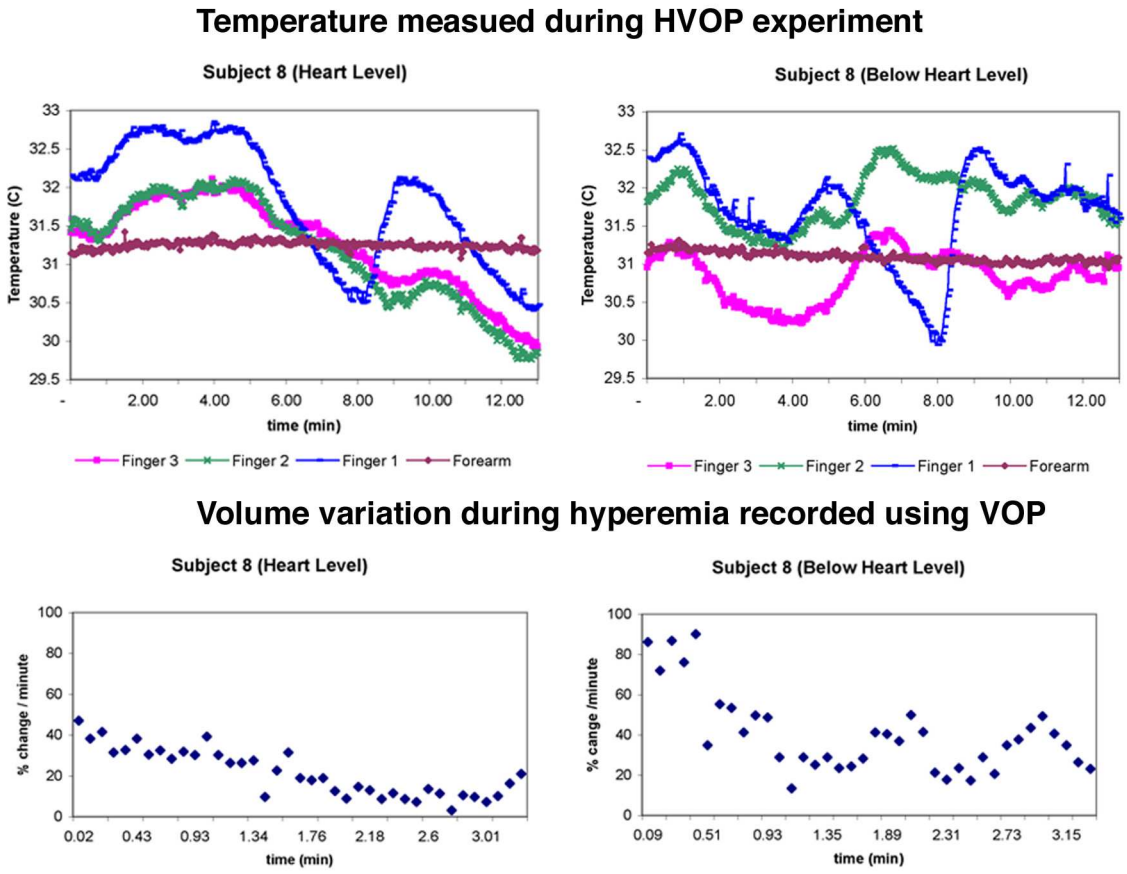

Fig. 39. Variation in fingertip temperature during DTM test performed at heart level and 10 cm below heart level.

produce vasoconstriction and reduce the hyperemic response producing an error in the measurement. This is an important effect that will be discussed with more detail in the next section dealing with experimental errors.

- The heat transfer coefficient calculated from direct measurements of skin temperature and heat flux in *finger 3* (contra-lateral finger) and *forearm*, show little variation during the DTM experiment. The average values for each subject for the arm and *finger 2* or *finger 3*, are in the range of 6 and 10 $W/m^{2o}C$ and 2 to 20 $W/m^{2o}C$, respectively. The heat flux in the occluded finger was not measured because of imperfect contact and the thermal inertia of the heat flux sensor, which can be reduced by using smaller sensors; currently the diameter of the heat flux sensors used was 9.5 mm. For future experiments, smaller heat flux sensors with embedded T thermocouple will be used instead, and they will be placed in the 3 fingers studied, as well as dorsal and palmar surfaces of the hand instead of the arm. Heat flux at the skin level seems to be a very sensitive parameter to posture, skin temperature and blood perfusion; more importantly it can be used to characterize the thermal state of a subject (vasoconstriction, vasodilation and thermo-neutral).

- Blood perfusion during hyperemia was measured during 20 to 40 inflow/outflow cycles, that corresponded to a time lapse of 1.7 min to 3.5 min, respectively. It was observed that the blood perfusion measured using VOP during hyperemia converged, to the value recorded in the normal case. For this reason in future experiments normal blood perfusion will be determined with an average of the last 3 measurements of blood volume; this will reduce 18 minutes of experiment time. During hyperemia the percentile blood change per minute recorded decays as time passes. An exponential drop is assumed and MATLAB was used to

estimate a correlation for such behavior.

D. Experimental Observations and Error Sources

During the experiments, the most challenging effect was that of the effect of initial temperature, the thermal condition (vasoconstriction or vasodilation) and the presence of "cold finger". The factors observed to affect the thermal response to hyperemia *i.e* TR and TD value were:

- Initial temperature and thermal equilibration: A thermo-neutral condition is achieved when the skin temperature reaches a constant value and no heat is gained from or lost to the environment. It is convenient to mention that finger temperature oscillates. The experiment was performed in a closed room with ambient temperature between 21 and 25 ^oC. Arriving to thermo-neutral condition required that the subject spent between 30 to 60 minutes inside the room without performing any major physical activity. During this time consent form and medical data questionnaire were filled out and anthropometric measurements were performed. The duration of the stabilization time was observed to be subject dependent. During our trials, several cases were observed where the subjects showed continuous heating or cooling of the fingers beyond the natural skin temperature oscillations even after a stabilization period of 45 minutes.

  In several experiments it was observed that the presence of heating and cooling of the fingers and the value of the skin temperature at the beginning of the experiment (initial temperature T_i) were very significant for the determination of the thermal effect of hyperemia or the magnitude of the TR value. Presence of cooling or heating seems to mask the temperature changes due to hyperemia. If the fingers are getting cold and the DTM test is performed, the TR value

recorded will be less than it should be if the subject reached a thermo-neutral condition, and the experiment will provide a false positive; the opposite effects is observed when the fingers are getting warmer as the experiment progresses. When warming up or cooling down is present, the same effect is observed in all fingers independently of the natural temperature differences between them. Before occlusion (baseline) and after the occlusion is terminated, the un-occluded fingers (control hand and control finger in hand where occlusion is performed) keep showing the original tendency (warming up or cooling down), taking the difference between the temperature in the occluded finger and the un-occluded finger during reperfusion (after pressure cuff performing the occlusion is released) will allow us to isolate the contribution of finger cooling or warming. Note that: **(1)** observing the difference between the temperature of the occluded finger and the control finger during baseline measurements will allow us to estimate the normal temperature differences between the fingers; and **(2)** observing the difference between the temperature in the occluded finger and the control finger after the cuff deflation, will provide the true hyperemic response by removing the environmental effect.

- Temperature of the room: Temperature of the room is lower than outside ambient temperature and below 22^oC. Arriving to a cooler environment, produces vasoconstriction and a reduction in skin temperature. Vasoconstriction reduces the hyperemic flow and its thermal effects (*i.e.* TR value). The temperature at each finger is slightly different due to size variations (volume, surface area), and hand posture.

- Positioning of the arm where DTM was performed: Posture alters two things: **(1)** the thickness of the boundary layer around the fingers as seen in Fig. 40,

Fig. 40. Diagram showing natural convection boundary layer over a subject in different postures.

and therefore the heat transfer coefficient; and **(2)** the finger blood perfusion, more specifically the volume of venous blood or the rate at which venous blood is drained from the finger. To look at the effect of posture, finger temperature and blood perfusion, 1 subject was used to monitor the changes in temperature and blood flow at 3 different arm positions (Fig. 39). The positions corresponded to the arm placed 10 cm over the heart level, at heart level and 10 cm below heart level. It was seen that the temperature of the fingers is continuously reduced when the arm is positioned at heart level and above, and the TR value measured during DTM is also reduced as arm height increases; there are few published studies dealing with posture and its effect on finger blood perfusion. The main effect of postural changes regarding blood perfusion is the variation in the volume of venous blood accumulated in the fingers [74, 75, 76]; this effect can be seen in Fig. 41, which shows variation in temperature and change in finger blood volume during hyperemia using VOP.

- Thermal effect of VOP: Venous occlusion plethysmography technique depends on the successful occlusion of veins draining the region of interest. During ve-

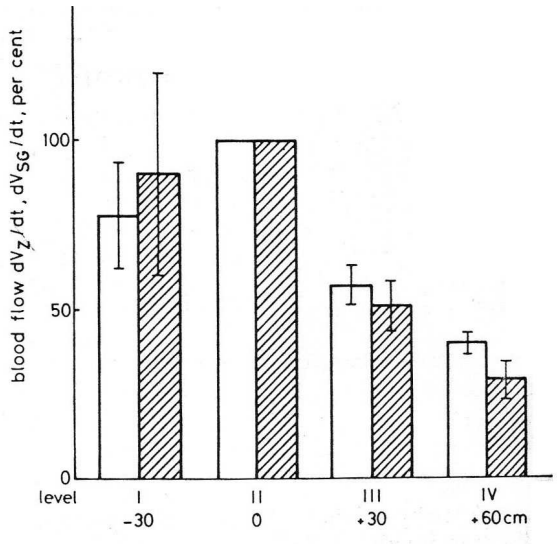

Fig. 41. Blood volume change in the middle finger (using SGP and impedance) following alterations in the arm levels relative to the heart. The volume changes shown correspond are calculated as differences between the volume measured at position IV (60 cm above the heart) and positions I, II and III. Taken from [51].

nous occlusion, blood is accumulated in the veins, and vein diameter together with venous pressure increase; as a result the arterio-venous pressure (which controls the volume of blood feeding the region of interest) decreases [52]. During VOP, the increase in venous pressure and vein diameter are controlled by changing the inflow time (time the veins are occluded). During measurement of normal blood perfusion using VOP, it was observed that the fingertip temperature dropped between 0.5 and 1 ^oC after application of 7 to 10 inflow cycles (2 seconds of cuff inflation and 4 seconds for venous drainage) depending on the subject. This temperature change is the result of variations of the venous blood volume. Fig. 42 shows the comparison of finger temperature measured during DTM and HVOP studies; this figure shows the clear presence of vasoconstriction. It should be noted that the normalized temperature $T_{finger}/\bar{T}_{start}$

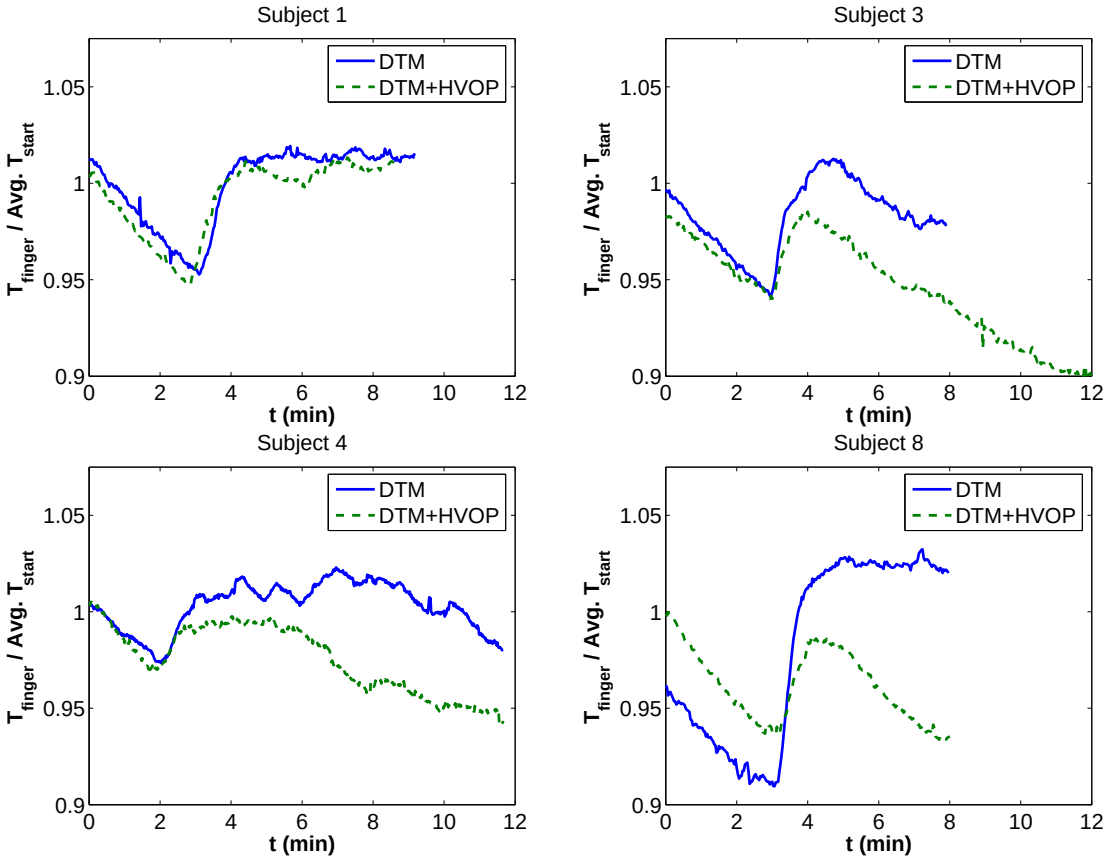

Fig. 42. Comparison of finger temperature measured during DTM with the temperature measured (normalized by the average baseline temperature before the start of occlusion) when DTM and HVOP are performed simultaneously for subjects 1, 3, 4 and 8. A drop in finger temperature can be observed when DTM and HVOP are performed simultaneously.

sometimes is not 1 at $t = 0$. This is because at the start of the experiment T_{finger} may be different than $\bar{T}_{start}$; magnitude of such difference is given by δT_{start} in Table XVI.

Other parameters that affect are the occlusion pressure, and the position of the finger with respect to the heart level. To reduce the temperature alteration due to VOP, a different technique to look at blood perfusion changes is necessary, such as LDF.

E. Comparison of Experimental Measurements and Model Results

To perform the comparison between measured and calculated temperature, the temporal variation of blood perfusion $\omega_b(t)$ as shown in Fig. 11 in Chapter IV is necessary. The variation of $\omega_b(t)$ can be divided into 2 stages, as seen in Fig. 11: *Stage I* is occlusion, and *Stage II* is reperfusion. *Stage II* can further be divided into: *Stage IIA* characterized by hyperemia and *Stage IIB* characterized by return to baseline. Blood perfusion (ω_b) is known to be linearly related to x [58, 77], and the proportionality constant is calculated using finger circumference and location of strain gauge (Table XV). To obtain a relationship for $\omega_b(t)$ during DTM, the data for the percentile circumference change per unit time (x), obtained during VOP for *Stage IIB* (using NIVP3, Fig. 38) is exported to MATLAB and an regression analysis was carried out.

Several fits were considered: **(1)** cubic polynomial, **(2)** Gaussian fit, and **(3)** exponential fit of the form

$$x(t) = a_1 \exp(-b_1 t). \tag{8.1}$$

Exponential fitting produced the highest values of R^2 and adjusted R^2 as well as the lowest value of SSE. To improve the quality of the fitted curve and data, smoothing was performed using Robust Loess quadratic fit. Fig. 43 shows the experimental data (percentile variation in volume per unit time) and fitted lines for several subjects. The square markers correspond to the experimental measurements, the solid line indicates the fitted curve using the coefficients shown in Table XVII, and the dotted lines indicate the confidence interval. In the cases presented, the fitted line shows good agreement with the experimental data.

The data obtained from the experiments was fed into the zero-order model. The zero-order model requires two types of data: **(1)** Parameters related to modeling of reactive hyperemia (Eqs. 4.1 - 4.2) (τ_0, t_{occ}, t_{dw}, τ_h, $\alpha = \omega_s/\omega_0$, $\beta = \omega_{max}/\omega_0$,

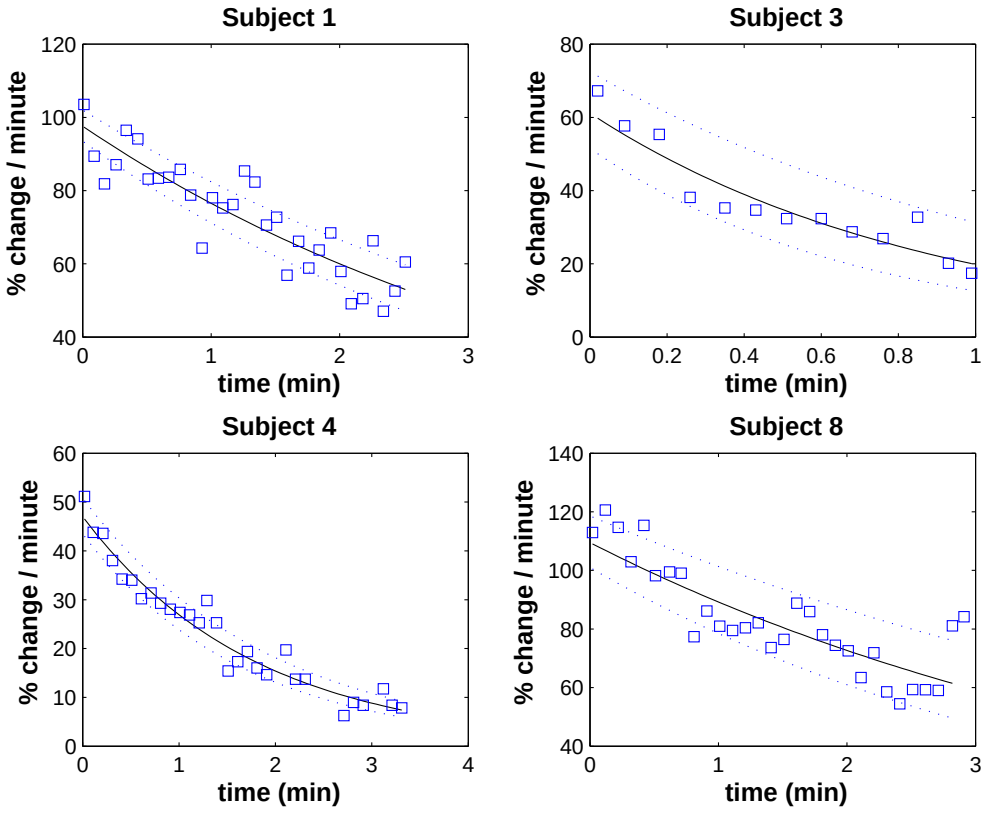

Fig. 43. Plots indicating volume changes per unit time (minute) in the finger during reactive hyperemia, measured using VOP on different subjects. Values for the exponential fit are given in Table XVII.

Table XVI. Table showing input parameters for zero-order model. Parameters were determined from DTM and VOP experiments.

Subject Number	$\bar{h}_{finger}$ $(W/m^{2o}C)$	$\bar{h}_{arm}$ $(W/m^{2o}C)$	T_{air} (^oC)	T_A (^oC)	$t_{occlusion}$ (min)	Baseline (min)
1	11.55	8.95	22.33	36.8	3	5.40
2	12.06	9.58	25.00	37.4	3	5.0
3	17.07	9.80	23.75	37.1	3	5.0
4	13.30	7.58	22.50	36.6	2	5.0
5	1.35	6.93	23.50	37.3	3	5.0
6	16.20	6.72	22.75	36.95	3	5.0
7	20.54	8.43	23.50	36.6	2	6.0
8	13.81	6.64	24.00	37.5	3	5.0

Subject Number	$\bar{T}_{start} \pm \delta T_{start}$ (^oC)	T_{min} (^oC)	t_{min} (min)	T_{max} (^oC)	t_{max} (min)
1	33.17 ± 0.95	31.61	3.10	33.81	5.63
2	34.90 ± 0.22	33.00	3.03	35.20	6.97
3	32.83 ± 0.54	30.92	3.03	32.24	4.40
4	35.27 ± 0.30	34.33	2.02	35.94	5.30
5	23.56 ± 0.24	23.44	3.13	24.10	4.93
6	33.07 ± 0.87	30.09	3.07	33.46	4.60
7	31.79 ± 0.57	30.99	2.37	32.37	6.02
8	32.25 ± 1.07	29.33	3.03	33.29	5.17

The quantities showing a bar at the top correspond to time averages; *baseline* indicates the duration of baseline reading or time waited before occlusion, $t_{occlusion}$ is the time that the arterial occlusion lasted, t_{min} and t_{max} represent times measured after occlusion started.

Table XVII. Table showing input parameters for zero-order model for selected subjects. Parameters were determined from DTM and VOP experiments. Note that the coefficients a_1, and b_1 describe the relationship for percentile change in circumference per unit time $x(t)$ given in Eq. 8.1.

Subject Number	$x_0 \pm \delta x_0$[a] $(\%/min)$	$a_1 \pm \delta a_1$ $(\%/min)$	$b_1 \pm \delta b_1$ $(1/min)$	R^2
1	40.40 ± 4.75	97.61 ± 1.05	0.2432 ± 0.0298	0.91
3	12.60 ± 4.00	61.13 ± 1.19	1.1260 ± 0.2850	0.87
4	9.82 ± 1.96	47.04 ± 1.08	0.5582 ± 0.0431	0.96
8	64.43 ± 4.50	109.51 ± 1.08	0.2049 ± 0.0475	0.73

[a] x_0 was obtained by VOP performed under baseline condition.

$\zeta = \omega_f/\omega_0$) **(2)** Parameters related to the governing equation for the zero-order model (Eq. 5.1) (ρ, C_p, ρ_b, C_{p_b}, h_{air}, T_{air}, T_A, T_i, A, V). The values and expression used for these parameters are summarized in Table XVIII.

To calculate the blood perfusion term $\omega_b(t)$ needed in the zero order model, Eqs. 4.1 and 4.2 are used, along with the values for the parameters stated above. Finally, to determine ω_o used in Eqs. 4.1 and 4.2, two different procedures can be done: **(1)** use Eq. 5.2 given in Chapter V for the steady state blood perfusion ω_o and substitute the values of heat transfer coefficient, fingertip area, body temperature, air temperature and initial or start temperature shown in Table XVIII; or **(2)** use the value for the percentile change per unit time x_o recorded using VOP (Table XVII). It is important to note that the blood perfusion calculated using x_o corresponds to the volume of blood from the fingertip to the location where the strain gauge is placed; the blood perfusion required in the zero order model is in the fingertip only, so a correction factor given by the ratio of volumes should be considered. This ratio is

Table XVIII. Summary of the parameters required by the zero-order model.

Parameters	Units	Expression	Refer
$\alpha = \omega_s/\omega_i$	-	0.05	(Table III)
$\beta = \omega_{max}/\omega_i$	-	a_1/x_0	(Table XVII)
$\zeta = \omega_f/\omega_i$	-	1	(Table III)
τ_0	s	5	(Table III)
τ_h	s	$1/b_1$	(Table XVII)
t_{occ}	s	$t_{occlusion}$	(Table XVI)
t_{dw}	s	45	(Table III)
ρ	kg/m^3	1085	(Table IV)
C_p	$J/kg.^oK$	3680	(Table IV)
ρ_b	kg/m^3	1069	(Table IV)
C_{p_b}	$J/kg.^oK$	3650	(Table IV)
h_{air}	$W/m^2.^oK$	$\bar{h}_{finger}$	(Table XVI)
T_{air}	^oC	T_{air}	(Table XVI)
T_A	^oC	T_A	(Table XVI)
T_i	^oC	$\bar{T}_{start}$	(Table XV)
A	m^2	$2\pi R^{\mathrm{a}} H^{\mathrm{b}}$	(Table XV)
V	m^3	$\pi R^2 H$	(Table XVI)

[a] R is radius of the finger at the location of the strain gauge.

[b] H is the length of the finger from the tip of the finger till the location of the strain gauge.

given by R/ℓ, where ℓ is the distance between the location of the strain gauge and the fingertip, and R the radius assuming a cylindrical finger.

The uncertainty associated with blood perfusion ($\omega_b(t)$) is a function of the uncertainty of ω_o, ω_{max}, ω_s, ω_f, β and was calculated using the deviations of the coefficients x_o, a_1 and b_1 given in Table XVII, and has the following form:

$$\delta\omega_o = \omega_o \left(\frac{\delta h_{finger}}{h_{finger}} + \frac{\delta A}{A} + \frac{(T_A - T_{air})\delta T_{start}}{(T_{air} - T_{start})(T_A - T_{start})} \right); \tag{8.2}$$

$$\delta\omega_b^I(t) \;=\; \left[\frac{(1-\alpha)\omega_b^I(t)}{\omega_o - \omega_s} \right] \delta w_o, \;\; \text{for} \;\; t \leq t_{occ}, \tag{8.3}$$

$$\delta\omega_b^{IIA}(t) \;=\; \left[\frac{\omega_b^{IIA}(t) - \omega_s}{\omega_{max} - \omega_s} \right] \delta w_{max} + \left[\frac{\omega_b^{max}(t) - \omega_{IIA}}{\omega_{max} - \omega_s} \right] \delta w_s,$$
$$\text{for} \;\; t_{occ} < t \leq (t_{occ} + t_{dw}), \tag{8.4}$$

$$\delta\omega_b^{IIB}(t) \;=\; \left[\frac{\omega_b^{IIB}(t) - \omega_f}{\omega_{max} - \omega_f} \right] \delta w_{max} + \left[\frac{\omega_{max} - \omega_b^{IIB}(t)}{\omega_{max} - \omega_f} \right] \delta w_f + b_1 \left[\omega_b^{IIB}(t) - \omega_f \right] \delta w_f,$$
$$\text{for} \;\; t > (t_{occ} + t_{dw}). \tag{8.5}$$

In equation (8.2), A represents the surface area of the fingertip, which is calculated using the finger dimensions of Table XV. The error in calculation of h_{finger}, A and V were assumed to be 30%, 20% and 20% respectively. Using equations 8.2-8.5, together with δh_{finger} and δA, and δV the uncertainty in the thermal response obtained using the zero-order model was calculated.

Figure 44 shows the fingertip temperature calculated using Eq. 4.1 - 4.2 for $\omega_b(t)$ and Eqs. 8.3 - 8.5 for $\delta\omega_b(t)$ and the parameters of Tables XIV. These curves are

calculated for subjects 1, 3, 4 and 8, and represent the prediction for the zero order model. These plots also show an upper and lower temperature calculated using the upper and lower uncertainties of the different parameters considered. Fig. 44 also shows the comparison of the measurement in each subject and the temperature calculated using the zeroth order model. These figures, show a good agreement between model predictions and measurements for subjects 3 and 4; the predictions for subjects 1 and 8 show a difference in the slope of the temperature drop during the occlusion period. For the analysis of the zero order model presented in Chapter V, we observed that the heat transfer coefficient h, as well as the initial temperature T_i have a strong effect over such temperature drop and associated slope. During the experiments, both subject 1 and 8, showed a h that was varying with time during the baseline and occlusion, as seen in Fig. 38 for subject 1. For the calculations an average value for h was used during the whole experiment (as indicated in Table XVI); however, it can be seen that such value underestimates the h coefficient during baseline and occlusion. Consequently, for better agreement, we need either to use in the model the time variation measured for h during the experiment, or approximate a function for it as done for $x(t)$ or $\omega_b(t)$.

The other significant difference while comparing model results and temperature measurements for subjects 1 and 8, is during stage IIB or hyperemia. Figure 42 shows that between the time DTM test and hyperemic VOP test was performed, the initial temperature was varied, as well as the hyperemic response. In subject 1, the maximum hyperemic response occurs at different times, and in subject 8 it has significantly different magnitude.

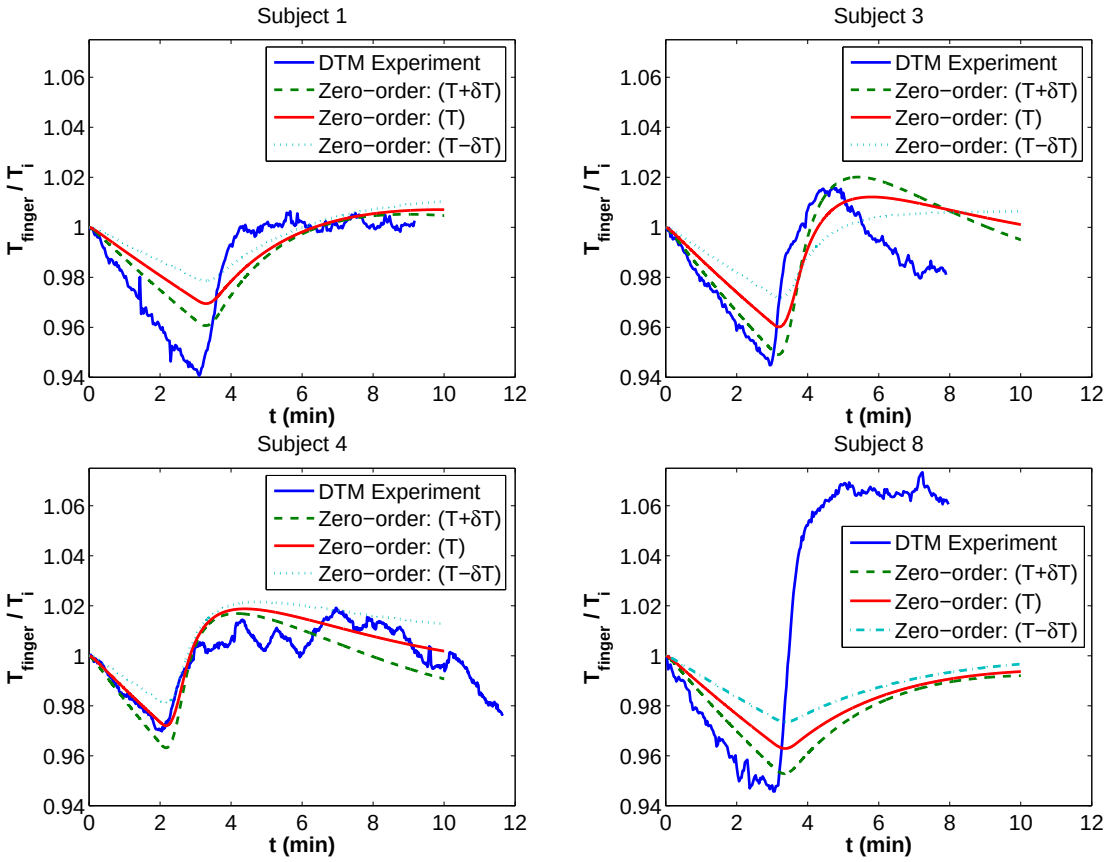

Fig. 44. Comparison of measured and calculated finger temperature changes during DTM for subjects 1, 3, 4 and 8. Calculations correspond to solutions using the zero order model by feeding the temporal variations in blood perfusion during stage IIB or hyperemia estimated experimentally. In these plots maximum and minimum temperatures are calculated using the upper and lower values of the concerned parameters.

CHAPTER IX

CONCLUSIONS AND FUTURE STUDIES

For this project, one of our aims was the creation of an index to characterize vascular reactivity and arterial health; such index is needed to include the factors contributing to fingertip temperature. Creation of an *index* is fundamental to establish the predictive nature of any clinical test. First we needed to prove a relationship between vascular reactivity (β) and temperature as well as other parameters. We have shown the different parameters contributing and we have created a way of quantifying their effect using mathematical models.

Two different mathematical models, together with a function describing the temporal variation of blood perfusion were used to analyze the temperature change during the DTM test. The models created allowed us to look at the effect of environmental parameters, such as ambient temperature and heat transfer coefficient; and the effect of body temperature, initial fingertip temperature and finger dimensions. The results were summarized in tables XIII, where the relationship between temperature rebound (TR) and temperature drop (TD) and the different parameters studied (β, h_{air}, t_{dw} and τ_h) are presented.

Further analysis is needed to completely understand the effect of the initial temperature as it affects several other parameters like heat transfer coefficient and skin perfusion. Initial temperature is an indication of the thermal state, i.e. if the finger is at a stationary temperature (thermo-neutral state), the presence of temperature oscillations and their period, if the subject is experiencing vasoconstriction (temperature is dropping) or vasodilation (temperature is increasing). Only by fully understanding of this relationship, the DTM can be used with confidence in the monitoring the risk of cardiovascular disease.

Both thermal models described herein were able to reproduce the trend of the temperature response observed experimentally at the fingertip. The parametric studies performed with the zeroth order model served to separate the contribution of environment and blood flow over the temperature curves measured during brachial artery occlusion. We observed that the skin temperature (T_i), body temperature ((T_A)) and heat transfer coefficient (h_{air}) affect more drastically the temperature drop TD reached during occlusion, the slope for the temperature drop; and the digit temperature after hyperemic blood flow. On the other hand, the quantities characterizing the hyperemic blood flow (β, τ_h and t_{dw}) affect primarily the rebound temperature value TR. These relationships indicate that T_i and T_A, should be used as normalizing factors.

Even though the zero order model shows phenomenological agreement, it shows significant limitations when predictions are compared with direct measurements; such variations are the result of inapplicability of the model because the Biot number calculated using the values for h_{finger} and finger size is outside of the lumped range. For this reason the first order model was proposed; for full application of the first order thermal model, several parameters are unknown, such as variation of blood perfusion at the skin level along the finger length and a heat flux boundary condition at the finger base; an inverse heat conduction problem has been defined. The first order model reproduces the same physical behavior observed by the zero order model.

The results obtained at this point indicate the need to further extend a mathematical model, as it has the clear capability to analyze the thermal effects of vascular reactivity.

Future studies proposed: The future studies require a parallel development of theoretical and experimental work.

- Perform a sensitivity analysis using the zero and first order model.
- Perform IR imaging at stationary or thermo-neutral state to obtain temperature measurements necessary for the determination of the axial perfusion function using the inverse problem defined herein.
- Propose and solve the inverse heat conduction problem to determine the heat flux at the hand/finger interface.
- Creation of a three dimensional model of heat transfer based in a layered geometry using the axial perfusion function obtained in previous items.
- Validate perfusion function using Infrared Imaging and Laser Doppler Flowmetry (LDF).
- Introduce significant vasculature at the finger level and evaluate the effect of countercurrent heat exchange in addition to the blood perfusion term considered in the bioheat equation.

In addition, the ultimate goal of this research is to include factors of thermoregulation and neural response, for which we need to keep investigating the alterations of blood volume in the finger with posture and temperature, the cooling observed during VOP, and to create a correlation between heat transfer coefficient and blood perfusion. The results of this research will be applicable to justify the use of DTM, its predictive value and its adoption in clinical setting and most importantly in home monitoring as a predictive tool.

REFERENCES

[1] P. Perrone-Filardi, A. Cuocolo, G. Brevetti, A. Silvestro, G. Storto, S. Dellegrottaglie, L. Corrado, M. Cafiero, R. Camerino, M. Polimeno, A. Zarrilli, G. Caiazzo, A. Maglione, A. Petretta, and M. Chiariello, "Relation of brachial artery flow-mediated vasodilation to significant coronary artery disease in patients with peripheral arterial disease," *Am J Cardiol*, vol. 96, no. 9, pp. 1337–1341, 2005.

[2] P. V. Targonski, P. O. Bonetti, G. M. Pumper, S. T. Higano, Jr. Holmes, D. R., and A. Lerman, "Coronary endothelial dysfunction is associated with an increased risk of cerebrovascular events," *Circulation*, vol. 107, no. 22, pp. 2766–8, 2003.

[3] G. Brevetti, A. Silvestro, V. Schiano, and M. Chiariello, "Endothelial dysfunction and cardiovascular risk prediction in peripheral arterial disease: additive value of flow-mediated dilation to ankle-brachial pressure index," *Circulation*, vol. 108, no. 17, pp. 2093–8, 2003.

[4] F. Charbonneau, "Use of measures of endothelial function to stratify risk," *Can J Cardiol*, vol. 17, no. Suppl A, pp. 18A–21A, 2001.

[5] G. Noll and T. F. Luscher, "The endothelium in acute coronary syndromes," *Eur Heart J.*, vol. 19, pp. C30–8, 1998.

[6] R. A. Vogel, M. C. Corretti, and G. D. Plotnick, "A comparison of brachial artery flow-mediated vasodilation using upper and lower arm arterial occlusion in subjects with and without coronary risk factors," *Clin Cardiol.*, vol. 23, no. 8, pp. 571–5., 2000.

[7] K. Gul, T. Naghavi, S. Kaul, M. Jamieson, P. K. Shah, and M. Naghavi, "Digital thermal monitoring before, during and after brachial artery occlusion: a novel and simple method for measuring endothelial function and vascular reactivity," *Submitted to Circulation Journal*, 2005.

[8] M. J. Mullen, R. K. Kharbanda, J. Cross, A. E. Donald, M. Taylor, P. Vallance, J. E. Deanfield, and R. J. MacAllister, "Heterogeneous nature of flow-mediated dilatation in human conduit arteries in vivo: relevance to endothelial dysfunction in hypercholesterolemia," *Circ Res*, vol. 88, no. 2, pp. 145–51, 2001.

[9] D. Behrendt and P. Ganz, "Endothelial function. from vascular biology to clinical applications," *Am J Cardiol*, vol. 90, no. 10C, pp. 40L–48L, 2002.

[10] H. Brunner, J. R. Cockcroft, J. Deanfield, A. Donald, E. Ferrannini, J. Halcox, W. Kiowski, T. F. Luscher, G. Mancia, A. Natali, J. J. Oliver, A. C. Pessina, D. Rizzoni, G. P. Rossi, A. Salvetti, L. E. Spieker, S. Taddei, and D. J. Webb, "Endothelial function and dysfunction. part ii: Association with cardiovascular risk factors and diseases. a statement by the working group on endothelins and endothelial factors of the european society of hypertension," *J Hypertens*, vol. 23, no. 2, pp. 233–246, 2005.

[11] Y. Higashi and M. Yoshizumi, "New methods to evaluate endothelial function: method for assessing endothelial function in humans using a strain-gauge plethysmography: nitric oxide-dependent and -independent vasodilation," *J Pharmacol Sci*, vol. 93, no. 4, pp. 399–404, 2003.

[12] T. Hori, T. Matsubara, T. Ishibashi, K. Higuchi, S. Ochiai, M. Takemoto, S. Imai, I. Nakagawa, K. Ozaki, K. Hatada, T. Mezaki, K. Tsuchida, A. Nasuno, M. Nishio, and Y. Aizawa, "Relationship between endothelial dysfunction

and nitric oxide production in young male smokers," *J Cardiol*, vol. 38, no. 1, pp. 21–28, 2001.

[13] A. L. Moens, I. Goovaerts, M. J. Claeys, and C. J. Vrints, "Flow-mediated vasodilation: a diagnostic instrument, or an experimental tool?," *Chest*, vol. 127, no. 6, pp. 2254–2263, 2005.

[14] S. G. West, "Effect of diet on vascular reactivity: an emerging marker for vascular risk," *Curr Atheroscler Rep*, vol. 3, no. 6, pp. 446–55, 2001.

[15] K. E. Sorensen, I. B. Kristensen, and D. S. Celermajer, "Atherosclerosis in the human brachial artery," *J Am Coll Cardiol*, vol. 29, no. 2, pp. 318–322, 1997.

[16] J. P. Lekakis, C. M. Papamichael, C. N. Vemmos, A. A. Voutsas, S. F. Stamatelopoulos, and S. D. Moulopoulos, "Peripheral vascular endothelial dysfunction in patients with angina pectoris and normal coronary arteriograms," *J Am Coll Cardiol*, vol. 31, no. 3, pp. 541–546, 1998.

[17] M. Hashimoto, M. Eto, M. Akishita, K. Kozaki, J. Ako, K. Iijima, S. Kim, K. Toba, M. Yoshizumi, and Y. Ouchi, "Correlation between flow-mediated vasodilatation of the brachial artery and intima-media thickness in the carotid artery in men," *Arterioscler Thromb Vasc Biol*, vol. 19, no. 11, pp. 2795–800, 1999.

[18] C. J. Hartley, A. K. Reddy, S. Madala, M. L. Entman, L. H. Michael, and G. E. Taffet, "Noninvasive ultrasonic measurement of arterial wall motion in mice," *Am J Physiol Heart Circ Physiol*, vol. 287, no. 3, pp. H1426–32, 2004.

[19] E. Kozlemeny, "Examination of flow mediated dilation with thermometry in case of patients with high cardiovascular risk," *Cardiologia Hungarica*, vol. 35,

pp. 11–16, 2005.

[20] N. Kharalkar and J. W. Valvano, "Analysis of a thermal method for assessing endothelial dysfunction," *Biomed Sci Instrum*, vol. 40, pp. 86–92, 2004.

[21] H. H. Pennes, "Analysis of tissue and arterial blood temperatures in the resting human forearm," *J Appl Physiol*, vol. 1, no. 2, pp. 93–122, 1948.

[22] J. A. Stolwijk, "Mathematical models of thermal regulation," *Ann N Y Acad Sci*, vol. 335, pp. 98–106, 1980.

[23] W. Wulff, "Energy conservation equation for living tissue," *IEEE Trans Biom Eng*, vol. 21, no. 6, pp. 494–495, 1974.

[24] W. Wulff, "Alternatives to the bio-heat transfer equation," *Ann N Y Acad Sci*, vol. 335, pp. 151–4, 1980.

[25] M. M. Chen and K. R. Holmes, "Microvascular contributions in tissue heat transfer," *Ann N Y Acad Sci*, vol. 335, pp. 137–50, 1980.

[26] S. Weinbaum and L. M. Jiji, "A new simplified bioheat equation for the effect of blood flow on local average tissue temperature," *J Biomech Eng*, vol. 107, no. 2, pp. 131–139, 1985.

[27] L. M. Jiji, S. Weinbaum, and D. E. Lemons, "Theory and experiment for the effect of vascular microstructure on surface tissue heat transfer–part ii: model formulation and solution," *J Biomech Eng*, vol. 106, no. 4, pp. 331–41, 1984.

[28] G. Kastberger and R. Stachl, "Infrared imaging technology and biological applications," *Behav Res Methods Instrum Comput*, vol. 35, no. 3, pp. 429–439, 2003.

[29] S. Weinbaum, L. X. Xu, L. Zhu, and A. Ekpene, "A new fundamental bioheat equation for muscle tissue: part i–blood perfusion term," *J Biomech Eng*, vol. 119, no. 3, pp. 278–88, 1997.

[30] J. W. Baish, "Formulation of a statistical model of heat transfer in perfused tissue," *J Biomech Eng*, vol. 116, no. 4, pp. 521–7, 1994.

[31] S. Konz, C. Hwang, B. Dhiman, J. Duncan, and A. Masud, "An experimental validation of mathematical simulation of human thermoregulation," *Comput Biol Med*, vol. 7, no. 1, pp. 71–82, 1977.

[32] C. K. Charny, S. Weinbaum, and R. L. Levin, "An evaluation of the weinbaum-jiji bioheat transfer model for simulations of hyperthermia," *Adv Heat Mass Transfer Biotechnol - ASME*, pp. 1–10, 1999.

[33] D. Fiala, K. J. Lomas, and M. Stohrer, "A computer model of human thermoregulation for a wide range of environmental conditions: the passive system," *J Appl Physiol*, vol. 87, no. 5, pp. 1957–1972, 1999.

[34] A. R. Laptook, E. L. Lain, and R. J. T. Corbett, "Brain temperature reduction during ischemia," *Pediatr Res*, vol. 43, no. Supplement 2, pp. 181A, 1998.

[35] A. R. Laptook and R. J. Corbett, "The effects of temperature on hypoxic-ischemic brain injury," *Clin Perinatol*, vol. 29, no. 4, pp. 623–649, vi, 2002.

[36] P. R. Wainwright, "The relationship of temperature rise to specific absorption rate and current in the human leg for exposure to electromagnetic radiation in the high frequency band," *Phys Med Biol*, vol. 48, no. 19, pp. (19):3143–55., 2003.

[37] G. M. J. Van Leeuwen, J. J. W. Langendijk, B. J. A. M. Van Leersum, A. P. M. Zwamborn, S. N. Hornsleth, and A. N. T. J. Kotte, "Calculation of change in brain temperatures due to exposure to a mobile phone," *Phys Med Biol*, vol. 44, pp. 2367–2379, 1999.

[38] S. R. Upreti and A. A. Jeje, "A noninvasive technique to determine peripheral blood flow and heat generation in a human limb," *Chem Eng Sci*, vol. 59, no. 21, pp. 4415–4423, 2004.

[39] S. Perrey, M. E. Tschakovsky, and R. L. Hughson, "Muscle chemoreflex elevates muscle blood flow and o2 uptake at exercise onset in nonischemic human forearm," *J Appl Physiol*, vol. 91, no. 5, pp. 2010–2016, 2001.

[40] C. E. Smith, "A transient, three-dimensional model of the human thermal system," Ph.D. dissertation, Kansas State University, Manhattan, KS, 1991.

[41] S. Weinbaum, L. M. Jiji, and D. E. Lemons, "Theory and experiment for the effect of vascular microstructure on surface tissue heat transfer–part i: anatomical foundation and model conceptualization," *J Biomech Eng*, vol. 106, no. 4, pp. 321–330, 1984.

[42] M. B. Ducharme and P. Tikuisis, "Role of blood as heat source or sink in human limbs during local cooling and heating," *J Appl Physiol*, vol. 76, no. 5, pp. 2084–2094, 1994.

[43] H. Sari, M. Gartner, A. Hoeft, and V. Candas, "Glove thermal insulation: local heat transfer measures and relevance," *Eur J Appl Physiol*, vol. 92, no. 6, pp. 702–705, 2004.

[44] A. Shitzer, L. A. Stroschein, R. R. Gonzalez, and K. B. Pandolf, "Lumped-parameter tissue temperature-blood perfusion model of a cold-stressed fingertip," *J Appl Physiol*, vol. 80, no. 5, pp. 1829–34, 1996.

[45] W. J. Song, S. Weinbaum, D. Lemons, and L. M. Jiji, "A combined macro and microvascular model for whole limb heat transfer," *J Biomech Eng*, vol. 110, no. 4, pp. 259–68, 1988.

[46] M. Zhu, S. Weinbaum, and D. E. Lemons, "A three-dimensional variable geometry countercurrent model for whole limb heat transfer," *J Biomech Eng*, vol. 114, no. 3, pp. 366–76, 1992.

[47] L. Zhu, L. X. Xu, Q. He, and Weinbaum, "A new fundamental bioheat equation for muscle tissue—part ii: Temperature of sav vessels," *J Biomech Eng*, vol. 124, no. 1, pp. 121–132, 2002.

[48] N. Charkoudian, "Skin blood flow in adult human thermoregulation: how it works, when it does not, and why," *Mayo Clin Proc*, vol. 78, pp. 603–612, 2003.

[49] J. M. Johnson, G. L. Brengelmann, J. R. Hales, P. M. Vanhoutte, and C. B. Wenger, "Regulation of the cutaneous circulation," *Fed Proc*, vol. 45, pp. 2841–2850, 1986.

[50] T. Mendez, J. Figueroa, V. Kuriachan, R. Mohebpour, O. Ley, and C. Quick, "Creation of a two-dimensional heat transfer model to study thermoregulation in the bat wing," Houston, TX: Houston Society of Engineering Medicine and Biology, Feb 2006.

[51] Y. Yamamoto and P. A. Oberg, "Measurement of digital blood flow using the laser doppler, impedance and strain-gauge methods," *Med Biol Eng Comput*,

vol. 28, no. 2, pp. 113–8, 1990.

[52] G. E. Burch, *Digital Plethysmography, Introducing a Method for Recording Simultaneously the Time Course of the Rate of Blood Flow Into and Out of the Finger Tip*, New York, NY: Grune & Stratton, 1954.

[53] L. B. Rowell, *Human Cardiovascular Control*, New York, NY: Oxford University Press, 1993.

[54] J. M. Johnson, "Nonthermoregulatory control of human skin blood flow," *J Appl Physiol*, vol. 61, no. 5, pp. 1613–22, 1986.

[55] Y. He, H. Liu, and R. Himeno, "A one-dimensional thermo-fluid model of blood circulation in the human upper limb," *Int J Heat Mass Transfer*, vol. 47, no. 12/13, pp. 2735–2745, 2004.

[56] F. H. Netter, *Atlas of Human Anatomy*, Summit, NJ: Ciba-Geigy, 1989.

[57] J. W. Rohen, C. Yokochi, and E. Lutjen-Drecoll, *Color Atlas of Anatomy: A Photographic Study of the Human Body*, Philadelphia: Lippincott Williams & Wilkins, 2002.

[58] N. Benjamin, A. Calver, J. Collier, B. Robinson, P. Vallance, and D. Webb, "Measuring forearm blood flow and interpreting the responses to drugs and mediators," *Hypertension*, vol. 25, no. 5, pp. 918–923, 1995.

[59] O. Ley and Y. Bayazitoglu, "Brain temperature calculation during stroke and various cooling modalities," *Submitted to Ann Biomed Eng*, 2004.

[60] G. B. Tee, A. H. Rasool, A. S. Halim, and A. R. Rahman, "Dependence of human forearm skin postocclussive reactive hyperemia on occlusion time," *J Pharmacol Toxicol Methods*, vol. 50, no. 1, pp. 73–8., 2004.

[61] D. I. Abramson, A. Kahn, H. Rejal, G. A. Turman, Jr. Tuck, S., and C. J. Fleischer, "Relationship between a range of tissue temperature and local oxygen uptake in the human forearm. ii. changes observed after arterial occlusion in the period of reactive hyperemia," *J Clin Invest*, vol. 37, no. 7, pp. 1039–1048, 1958.

[62] B. K. Siesjo, "Chapter 11," in *Brain Energy Metabolism*, pp. 324–344. New York, NY: John Wiley and Sons, 1978.

[63] A. F. Mills, *Heat Transfer*, Upper Saddle River, NJ: Prentice Hall, 1999.

[64] W. M. Kays, M. E. Crawford, and B. Weigand, *Convective Heat and Mass Transfer*, New York, NY: McGraw-Hill Higher Education, 2004.

[65] O. Ley and Y. Bayazitoglu, "Effect of physiology on the temperature distribution of a layered head with external convection," *Int J Heat Mass Transfer*, vol. 46, pp. 3233–3241, 2003.

[66] M. N. Ozisik and H. R. B. Orlande, *Inverse Heat Transfer: Fundamentals and Applications*, New York, NY: Taylor and Francis, 2000.

[67] Y. Jarny, M. N. Ozisik, and J. P. Bardon, "A general optimization method using adjoint equation for solving multidimensional inverse heat conduction," *Int J Heat Mass Transfer*, vol. 34, no. 11, pp. 2911–2919, 1991.

[68] O. M. Alifanov, *Inverse Heat Tranfer Problems*, Berlin: Springer-Verlag, 1994.

[69] F. B. Hildebrand, *Advanced Calculus for Applications*, Englewood Cliffs, NJ: Prentice-Hall, 1976.

[70] R. A. Khachfe and Y. Jarny, "Numerical solution of 2-d nonlinear inverse heat conduction problems using finite-element techniques," *Numer Heat Transfer, Part B*, vol. 37, no. 1, pp. 45–67, 2000.

[71] F. S. Gayzik, P. S. Elaine, and L. Tahar, "Experimental validation of an inverse heat transfer algorithm for optimizing hyperthermia treatments," *J Biomech Eng*, vol. 128, no. 4, pp. 505–515, 2006.

[72] M. B. Ducharme and P. Tikuisis, "In vivo thermal conductivity of the human forearm tissues," *J Appl Physiol*, vol. 70, no. 6, pp. 2682–2690, 1991.

[73] A. W. Stanton, B. Holroyd, J. W. Northfield, J. R. Levick, and P. S. Mortimer, "Forearm blood flow measured by venous occlusion plethysmography in healthy subjects and in women with postmastectomy oedema," *Vasc Med*, vol. 3, pp. 3–8, 1998.

[74] N. Olsen, O. U. Petring, and N. Rossing, "Exaggerated postural vasoconstrictor reflex in raynaud's phenomenon," *British Medical Journal*, vol. 294, no. 6581, pp. 1186–8, 1987.

[75] B. S. L. Kidd and R. V. McCready, "Effect of change in posture on the blood flow through the fingers and toes," *J Appl Physiol*, vol. 12, no. 1, pp. 121–124, 1958.

[76] Y. A. Mengesha and G. H. Bell, "Forearm and finger blood flow responses to passive body tilts," *J Appl Physiol*, vol. 46, no. 2, pp. 288–92, 1979.

[77] R. J. Whitney, "The measurement of volume changes in human limbs," *J Physiol*, vol. 121, no. 1, pp. 1–27, 1953.

VITA

Name: Chinmay Deshpande

Address: B 807 Ruturang Apt, S/No. 41, Kothrud, Pune, Maharashtra 411051, India

Email: mailtochinmay@gmail.com

Phone: (001) 979-204-4547

Education: M.S. Mechanical Engineering, Texas A&M University, USA, May 2007

B.E., Mechanical Engineering, University of Pune, India May 2004